CURRENT VARIABILITY AT THE OFFSHORE EDGE OF THE LABRADOR CURRENT

by

Arthur A. Allen

Submitted in partial fulfillment of the requirements
for the Degree of Master of Science at Dalhousie
University, December 1979

Examiners:

[redacted]

David A. Huntley

[redacted]

Christopher J.R. Garrett

[redacted]

Anthony J. Bowen

[redacted]

Ross M. Hendry

[redacted]

Peter J. Wangersky

DALHOUSIE UNIVERSITY

Date December 20, 1979

Author Arthur A. Allen

Title Current Variability at the Offshore Edge of the Labrador Current

Department or School Oceanography

Degree M.Sc. Convocation Spring Year 1980

Permission is herewith granted to Dalhousie University to circulate and to have copied for non-commercial purposes, at its discretion, the above title upon the request of individuals or institutions.

Signature of Author

TABLE OF CONTENTS

LIST OF FIGURES

of the sections. Volume transports are in 10^6 m^3/s. Positive is southwards.

(b) The geostrophic velocity (cm/s) at the surface based on zero velocity at 1000 dbars for the station pairs which bracketed 108 - the open circles; and the 12-hour averages of low-passed filtered component of velocity normal to hydrographic section from 108,160 - the dots connected by lines. Positive values are southwards.

(c) The distance (km) offshore from Station 24 of the + 5 cm/s isotact at the surface based on the geostrophic velocities (zero velocity at 1000 dbars). The horizontal lines represent the time (and stations) over which the values were determined, and the vertical bars are the error margins.

Page

Page

ABSTRACT

A current meter array was in place on the lower continental slope off Hopedale, Labrador, during March 1976. The array, combined with 27 hydrographic stations, provided information on the spatial and temporal variability at the offshore edge of the Labrador Current and estimates of volume transport.

The data set revealed a current regime that contained the southward flowing surface (30-50 cm/s) and bottom (20-40 cm/s) boundary currents and a rather unexpected persistent northward surface flow (10-30 cm/s) offshore. Moreover, large amplitude, low-frequency fluctuations (± 23 cm/s) dominated the mean currents, producing complete reversals in the direction of the flow. Simple theoretical models were applied to the observed phenomena to establish the basic dynamics of the current regime.

The major fluctuations in the velocity field were apparently due to weakly bottom-trapped topographic Rossby waves of 8-10 day periods positively interacting with the baroclinic surface currents. The bottom flow was also affected by the presence of bottom-trapped topographic Rossby waves between 4 and 8 day periods, and possibly baroclinic instabilities at 2-3 day periods. Other variability, at higher and lower frequencies, was also investigated.

Geostrophic velocity sections were adjusted to the current meters in an attempt to establish volume transports. However, the large variations in the velocity field due to the low-frequency variability caused large uncertainties in the volume transport estimates. The role of the low-frequency variability to the dynamics and the effects it has on the determination of the volume transports have important implications regarding past and future studies of the Labrador Current system.

ACKNOWLEDGEMENTS

I would like to thank my committee, Drs. Allyn Clarke, David Huntley, Chris Garrett, and Tony Bowen who maintained the high levels which I have strived to achieve in this work.

The many conversations with Allyn Clarke greatly improved my understanding of physical oceanography.

In addition, I would like to thank the staff of the Bedford Institute and the members of the Ocean Circulation Division in particular for their generous help throughout my entire project.

I would like to acknowledge Ed Horne's patience with my numerous and frequent questions when I was learning to use the Bedford Institute's computer.

Pat Williams typed the texts speedily, accurately, and smoothly.

Financial support for my studies was provided by a Dalhousie Fellowship and by my parents.

Finally, I would like to thank Mary Lewis and my parents for their moral support and encouragement.

CHAPTER 1 - INTRODUCTION

The Labrador Sea (see Fig. 1.1) has long been recognized as an important region. Between the time of the Challenger Expedition (1873-1876) and the early portion of the 20th century, Scandinavian, British, American, and Canadian researchers began to study the physical oceanography of the Labrador Sea region. A complete account of the early works in the Labrador Sea and Canadian eastern Arctic is given in Dunbar (1951). Physical oceanographic activity in the Labrador Sea increased after the formation of the International Ice Patrol in 1914 in response to the sinking of the Titanic by an iceberg. In order to predict the movement of icebergs into the busy North Atlantic shipping lanes the U.S. Coast Guard has conducted a number of cruises for the Ice Patrol to the Labrador Sea and Grand Banks area. Undoubtedly, the most significant of these U.S. Coast Guard cruises were the Marion and General Greene expeditions during the summers of 1928, 1931, 1933-1935. The results of these five expeditions were brought together by Smith, Soule, and Mosby (1937). Most of our present day knowledge of the physical oceanography of the Labrador Sea stems directly from their work. The U.S. Coast Guard continues to conduct cruises to the Labrador Sea and Grand Banks area for the International Ice Patrol.

The development of fisheries on the Labrador shelf has increased interest in the area. Dunbar (1951) summarizes the hydrographic cruises before 1950, conducted mainly by Canadian scientists interested in

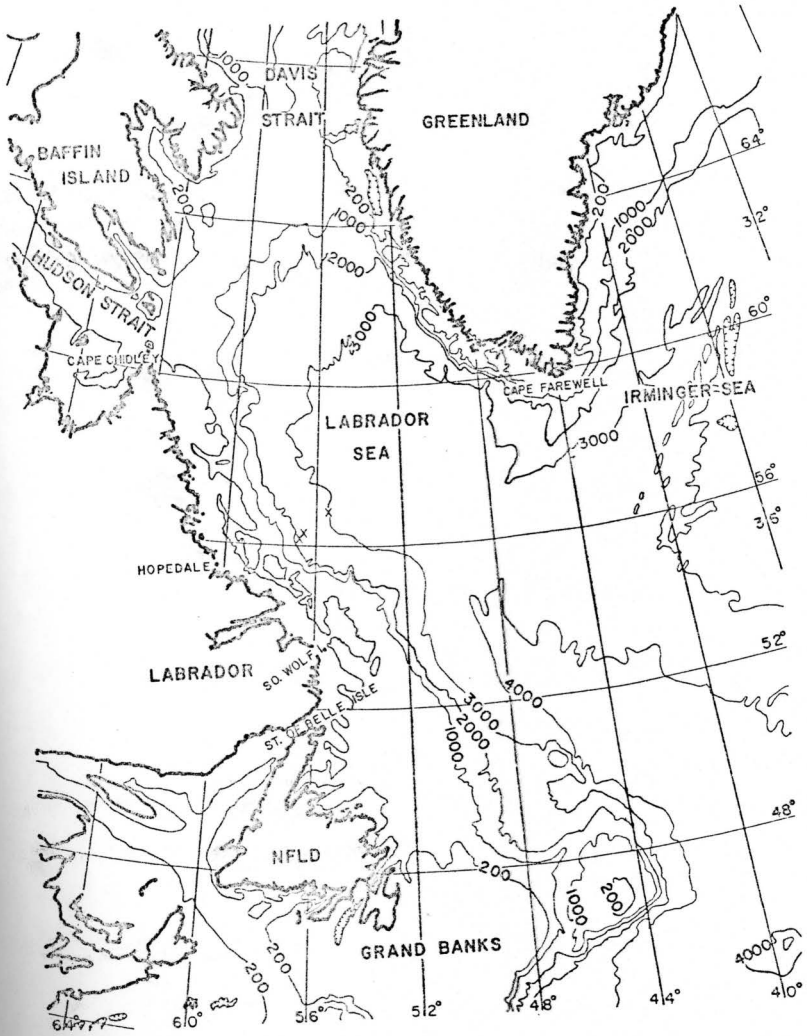

Figure 1.1 - Location map of the Labrador Sea region, redrawn from Canadian Bathymetric Chart 800-A. Contours are in meters. X's are the positions of the current meter moorings.

fishery related problems. Several hydrographic cruises, similar to the Ice Patrol cruises, have been carried out under the auspices of the International Commission for the Northwest Atlantic Fisheries (ICNAF) after the Second World War.

Canadian scientists from the Bedford Institute of Oceanography conducted cruises to the Labrador Sea in the 1960's to investigate the formation of deep water masses. More recently, the exploration for hydrocarbon reserves on the Labrador shelf and slope, and the expansion of the contiguous economic zone to 200 n miles by Canada has meant a renewed interest in the physical oceanography of the Labrador Sea by Canadian scientists.

Physical oceanographers have recognized over the past decade that the oceans are dominated by time-dependent motions. The hydrographic cruises of the past have provided a good description of the permanent surface currents. While previous investigators were aware of variability among their sections, they didn't have the means to investigate the variability. The development over the past decade of the technology of deep-sea current meter moorings capable of recording for very long periods (weeks to months) has been primarily responsible for the study of the time-dependent motions in the oceans. Therefore, due to recent advances in the field of physical oceanography and the increasing importance of the Labrador Sea to Canada, scientists from the Ocean

Circulation Division of the Bedford Institute of Oceanography initiated a large program in the Labrador Sea. The major aims of the entire program are to understand the surface and deep currents of the Labrador Sea in light of the recent developments in physical oceanographic theory and technology; to understand mechanisms of and form estimates of the volumes of deep water masses formed locally in the Labrador Sea. The understanding of these two aspects of the Labrador Sea is critical before prognostic models can be developed regarding the biology and fisheries of the Labrador Sea, the movement and transport of sea ice and icebergs along the Labrador Coast, and the currents and water masses.

Cruise 76002 of the CSS Hudson during February-March, 1976 served as a test cruise for the main portion of the Labrador Sea program which occurred in the winter of 1977-78. The major aims of Hudson 76002 were to provide initial estimates of the winter time volume transport and variability of the offshore branch of the Labrador Current; and to locate and characterize deep convection event(s) associated with the wintertime formation of indigenous deep water. In order to achieve these goals, modifications to pre-existing techniques had to be made in order to operate in the very mobile sea ice conditions of the harsh Labrador Sea winter.

Phase I of Hudson 76002 was the portion of the cruise studying the offshore branch of the Labrador Current. By combining a current meter array with a hydrographic survey, measurements of the currents and the spatial and temporal variations could be obtained. This information along with the experience gained in operating in the hostile Labrador Current region was essential in designing the more extensive program of 1977-78. A deep convection event located during the first phase was returned to in the second phase. Neutrally-buoyant floats, vaned to measure vertical velocities, were tracked in the deep convection event. This provided a test of the floats and combined with hydrographic data provided sufficient detail of the event to allow study of the dynamics involved.

A great deal of effort has gone into the collection and analysis of hydrographic data in the Labrador Sea over the past 100 years. While the mean conditions in the Labrador Sea have been well established by the hydrographic work, the study on the unsteady, time-dependent motions in the Labrador Sea have been outside the scope of previous investigators' studies and out of reach of their instruments. This thesis proposes that unsteady processes in the offshore branch region of the Labrador Current are as important as the steady processes to the dynamics of the area. Using the current meter and hydrographic data collected during Hudson 76002 the steady and unsteady behaviour of the current regime during March 1976 on the continental slope of Labrador are investigated.

Chapter Two reviews the nature of the data collected by Hudson 76002 for the study of the offshore branch of the Labrador Current. A review of the general results from previous investigators in the Labrador Sea introduces the third chapter on the steady conditions. The trends in the current meter records and the characteristics of the water masses are then discussed. The geostrophic currents were determined from the hydrographic data and estimates of volume transports were made for the purpose of comparison with previous estimates. Variation in the flow among the repeated hydrographic sections concludes the third chapter, but the variation is discussed further in Chapter Four.

The fourth chapter is the investigation of the unsteady processes. The tidal and inertial motions recorded by the current meters are discussed first. Then the features of the low-frequency variability are characterized by several separate approaches; repeated horizontal sections, cross-correlation of current meter records, and the investigation of current ellipses. Following which are the application of topographic Rossby waves, baroclinic instability, and continental shelf wave theories to the variability observed in the Labrador Current. The theories predict that certain parameters, conditions, and interactions are associated with each process. Therefore, it is possible to establish which process was or was not present by comparing

the observations with the theories. By identifying the physical processes and interactions that were present on the Labrador slope during March 1976 we can gain an understanding of the system. From this insight, further work can be planned for the investigation of specific processes, past work can be re-evaluated in terms of what is now known, and the development of finer diagnostic and prognostic models can be achieved.

CHAPTER 2 - DATA COLLECTION

The current meter array was designed to cover the offshore branch of the Labrador Current. The current meter measurements were combined with a hydrographic survey in order to provide estimates of volume transport, along with spatial and temporal variability of the current.

2.1 Current Meters

The current meter array consisted of three subsurface current meter moorings which were in a line across the lower continental slope off Hopedale Saddle, see Fig. 1.1. The mooring array was in place from March 5 to April 1, 1976. Each mooring was designed in the following configuration: a streamlined subsurface float with 1250 lbs. of buoyancy at 100 m, a current meter 10 m below the float, and another current meter 150 m below the first. A third current meter was located 100 m above the anchor, with an acoustic release 50 m above the anchor. Reserve buoyancy packages were located along the mooring line. The current meters were on swivels in line with the mooring wire. Anodes were used to protect the mooring wire from corrosion. All current meters were Aanderaa meters which recorded integrated rate, instantaneous direction and temperature at 10-minute intervals. In addition, the upper meters had pressure and conductivity sensors for sampling depth and salinity.

The mooring laying procedure was roughly as follows. The desired depth of the current meters was predetermined, so that the mooring wire could be measured and cut before the cruise. Once in the mooring area the local bathymetry was then charted during the night by surveying the

area with Raytheon echosounders. The following morning the mooring was laid. The ship steamed into the wind (or into the seas, or along a lead in the ice) maintaining the minimum speed necessary for steerage while the mooring was constructed. The subsurface float was launched over the stern of the ship and the instruments were placed in line as the wire was played out behind the ship. When the mooring was fully constructed some 2-3 km of it was trailing the ship. The last piece over the side of the ship was the anchor, which would sink the mooring onto the isobath along which the ship had been steaming.

The innermost mooring (107). Figure 2.1a was laid at 56°21.7'N 56°46.1'W in 2440 m of water. The mooring was laid out in a lead in the ice. The mooring sank twenty minutes after deployment when the swivel to the subsurface float broke. The reserve buoyancy packages enabled the mooring to be recovered on 1 April. From the bottom current meter, a rate signal and temperature record were recoverable from a depth no greater than 100 m above the bottom.

The central mooring (108) Figure 2.1b was laid in 2580 m of water at 56°32.5'N 56°22.2'W on 4 March and recovered on 1 April, 1976. This mooring was laid about 100 m too shallow, and as a consequence the subsurface float was on the surface. The uppermost current meter's record was lost because the recording magnetic tape wasn't over the recording head. The second meter was at 160 m and the third was at 2480 m. Both returned complete records. The temperature record and therefore salinity record from the current meter at 160 m contains considerable

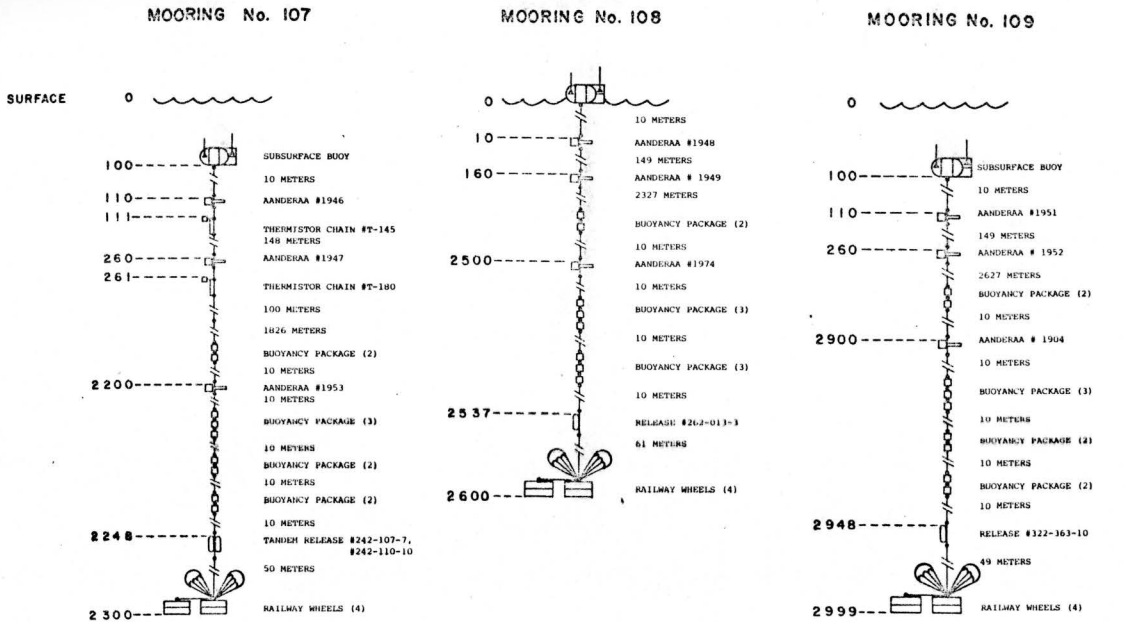

Figure 2.1 - Mooring configuration designs.

instrument noise during the last portion (year days 76-92) of the record.

Hereafter, individual meters will be referred to by a two number code indicating mooring and depth respectively; e.g. (108,160) refers to the meter at depth 160 m on the central mooring #108.

The outermost mooring (109) was laid at 56°49.2'N 55°18.9'W in 3003 m of water. Deployment was on 5 March and recovery on 1 April 1976. Current meters were at 40 m, 190 m, and 2900 m. The direction record from 109,40 remained nearly constant between 245° and 270° during the entire deployment period. Thus the direction record was clearly suspect, for this problem (of the direction sticking) has occurred in other Aanderaa current meter records. Hendry and Hartling (1979) have shown that this problem is due to a strong magnetic field in the case coating. The velocity from this current meter was, therefore, not used.

The record from 109,190 was complete and without instrument noise.

The record from 109,2900 was complete for the first 2.9 days, but during the next 15.8 days the record failed to reset. Thus, the middle portion of the record was lost. However, the meter recorded properly during the last 9.9 days of the mooring period. These data were recoverable. The meter counts the number of revolutions of the rotor from the end of the last 10-minute interval. When the meter fails to reset itself, the counts continue to accumulate over the succeeding 10-minute

intervals until the meter does reset itself, at which time the accumulated counts produce a spike in the rate record. The time clock in the instrument was checked before deployment and after recovery to be sure it was working precisely to eliminate the clock as a possible source of error. Thus the record is extractable from the start until the first spike and from the last spike until the end of the record.

There are discrepancies between the pressure sensor depth and the mooring configuration depth for the upper current meters on Mooring 109, (see Table A). Several explanations were investigated in an attempt to explain the +70 m differences in the depth. Were the depths used to construct the charts of the local bathymetry determined properly? What is the accuracy and precision of the pressure sensors? How accurately can the longest piece of wire for the mooring be measured? Does the wire stretch and how much?

The chart constructed for laying the mooring was checked by the raw depths and times for the echosounder which were kept on magnetic tape. Thus, the raw depths in fathoms from the Hudson's Raytheon echosounder for an assumed sound velocity of 800 fm/s, were converted to meters (1.828 m/fm) and then corrected according to Matthew's (1939) tables. The sound velocities for the Labrador Sea region given by Matthews were checked against the sound velocities derived by the U.S. Naval Oceanographic Tables (Bialek, 1966) for the hydrographic station 25 and were found to be 2-4 m/s slower. Thus the charts were constructed properly and the depths given are accurate to within 4-6 m.

TABLE A

DEPTH OF CURRENT METERS

MOORING #	CM #	CONFIGURATION DEPTH (m)	PRESSURE SENSOR DEPTH (m)	ACTUAL DEPTH (m)
107	1953	2340	--	2340
108	1974	2480	--	2480
108	1949	160	160	160
109	1904	2900	--	2900
109	1952	260	190	190
109	1951	110	40	40

The pressure sensors range was 0-1000 psi (0-680 dbars) and is accurate to 1% of the range (6.8 dbars), NOIC (1975). The pressure sensors were calibrated prior to and after the cruise and were offset to zero at the surface during the periods of deployment and recovery when the instruments were on board. The correction from pressure to depth was a 0.5% reduction magnitude in the 0-200 dbar range for the closest CTD station to the mooring. The pressure difference of the upper two current meters on Mooring #109 are consistent with the mooring configuration separation distance, thus indicating that the pressure sensors were precise. Therefore, it was concluded that the sensors recorded the proper pressure at the instruments.

The bottom current meters were placed 100 m above the anchors and didn't have pressure sensors, thus their depths are taken to be 100 m off the bottom. Current Meter #1953 was the bottom meter on Mooring #107 which collapsed upon deployment. Its depth was taken to be between its configuration depth (2340 m) and the bottom (2440 m) because the collapse may have been only partial due to reserve buoyancy on the mooring.

The designs for moorings 108 and 109 specified lengths of wire 2327 m and 2627 m long, respectively. To measure the wire, two meter wheels in series are used as the wire is reeled off the spool and onto another spool. There are no further checks on the length of wire.

The stretch in the mooring wire would be in the 0.1 to 0.3% range (Reiniger, personal communication) for the loadings encountered while in place. Thus a shallowing of the meters of the order 2-7 m is possible from wire stretching, which isn't significant compared to the discrepancies noted. Thus, the measuring of the very long length of wire appears to be the most likely area where error of this magnitude could occur. Therefore, the possibility of 2-3% error in the measuring processes should be investigated for substantial descrepancies can occur in the deep-sea moorings.

Surface gravity waves can enter the velocity records through the action of mooring motion. Gould and Sambuco (1975) have demonstrated that current measurements made on taut surface moorings have higher current velocities than subsurface moorings. Saunders (1976) showed comparisons of vector averaging current meters (VACM's), with drogues and Aanderaa current meters near the surface. The Aanderaa current meters were recording high velocities because they could not follow the reversal in flow associated with the surface waves. Also the Savonius rotor on the Aanderaa current meters is pumped up by vertical motions past the meter.

Vertical motions are caused directly by the surface waves and by the vertical motion in the mooring line at depth (up to 2000 m) induced by the surface waves. Gould and Sambuco found that the surface mooring current measurements were 1.5 to 2.0 times higher than nearby current measurements on a subsurface float mooring, for depths between 100 and 2000 m for all frequencies.

While 108,160 was below the direct effect of surface waves, estimated to be approximately 100 m by Panicker, Schultz, and Schmit (1974), it was within the range of mooring line induced motions. However, the mooring position was close the the edge of the ice field. While the central portion of the Labrador Sea during March 1976 contained high wave energy, near the ice field short fetch and attenuation by the ice significantly reduced the wave energy. Therefore, while there may be some energy in the velocity records from surface waves motions at 108,160 it is thought to be minimal and not significantly increasing the energy level of the currents measured.

The usable current meter records are as follows: a rate signal and temperature record from 107,2340, Figure 2.2: velocity (i.e. rate and direction), temperature and pressure from 108,160, Figure 2.3; velocity and temperature from 108,2480, Figure 2.4; rate, temperature, and pressure from 109,40, Figure 2.5; velocity, temperature, and pressure from 109,190, Figure 2.6; and velocity and temperature from the first 2.9 days and the last 9.9 days from 109,2900, Figure 2.7. Serious errors in the salinity measurements that include temperature and pressure effects, drift during deployment, and nonrepeatability of calibration offsets, precluded the use of the salinity records of the current meters. See Smith, Foote, and Boyce (1978) for a complete analysis of the Aanderaa salinity measurement problem. The loss of such a large percentage of the current meter measurements was disappointing. However, the current meters that did produce clean records contain valuable information on the nature of the offshore branch of the Labrador Current.

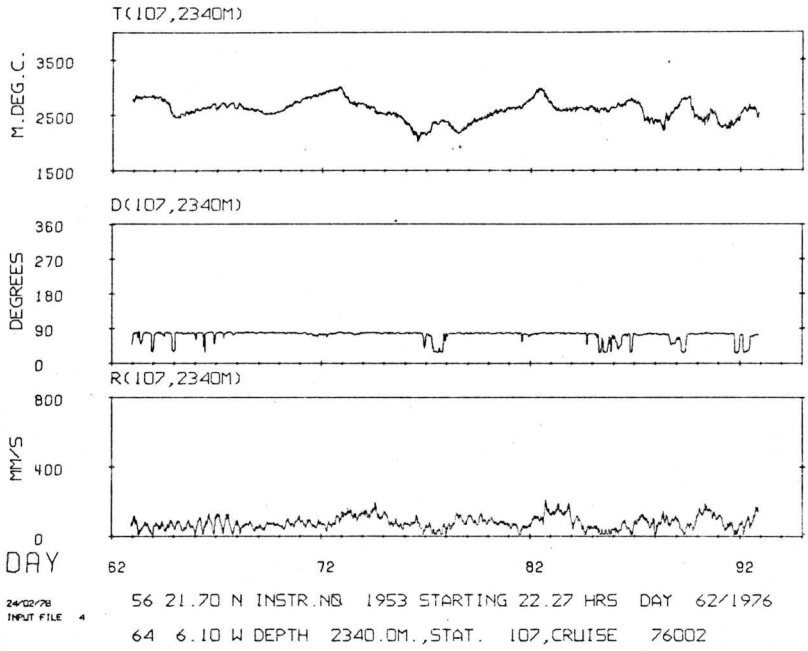

Figure 2.2 - The unfiltered data records from Current Meter 107,2340.

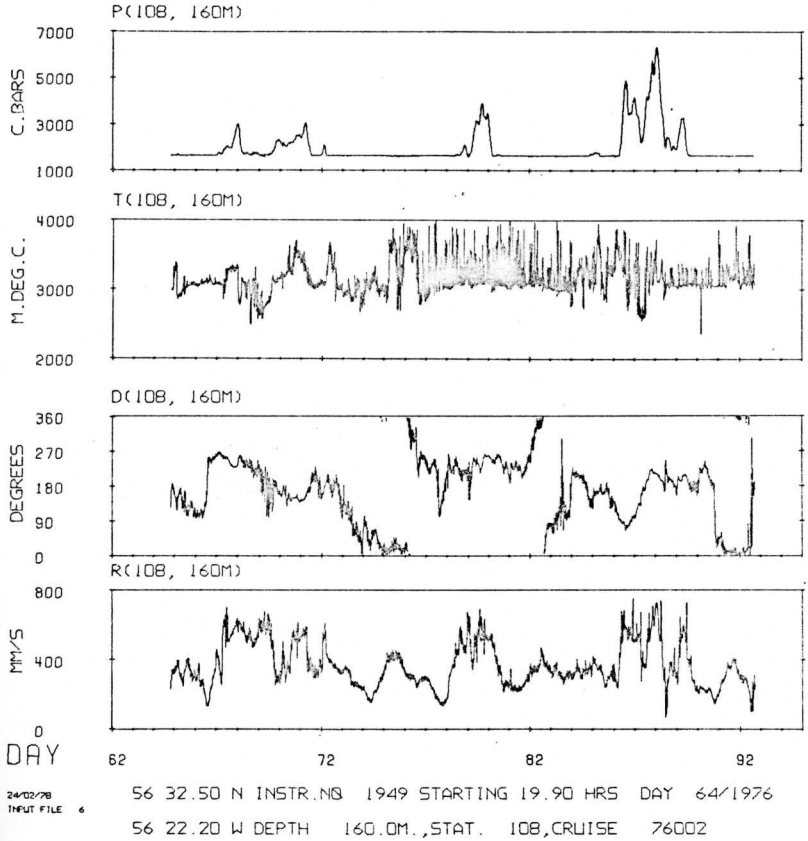

Figure 2.3 - The unfiltered data records from Current Meter 108,160.

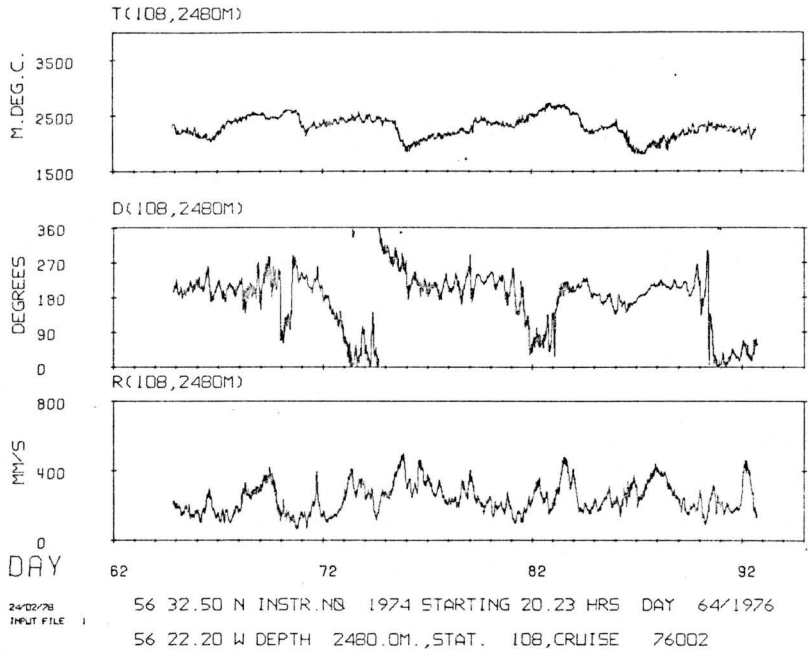

Figure 2.4 - The unfiltered data records from Current Meter 108,2480.

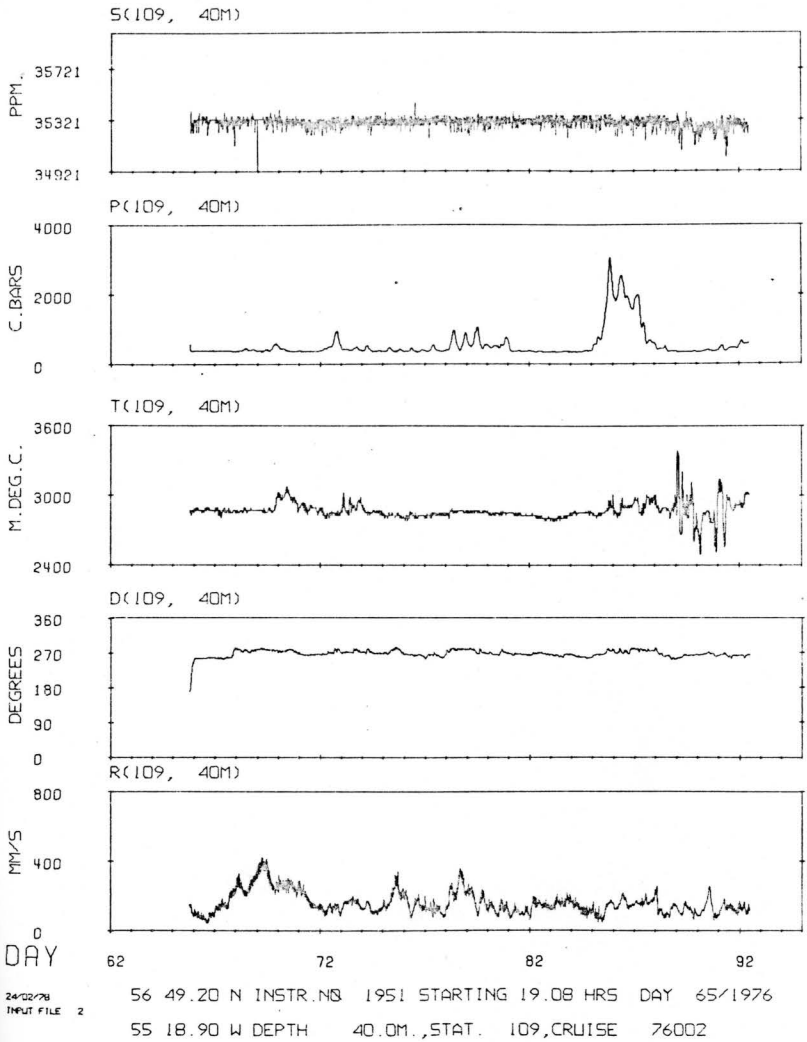

Figure 2.5 - The unfiltered data records from Current Meter 109,40.

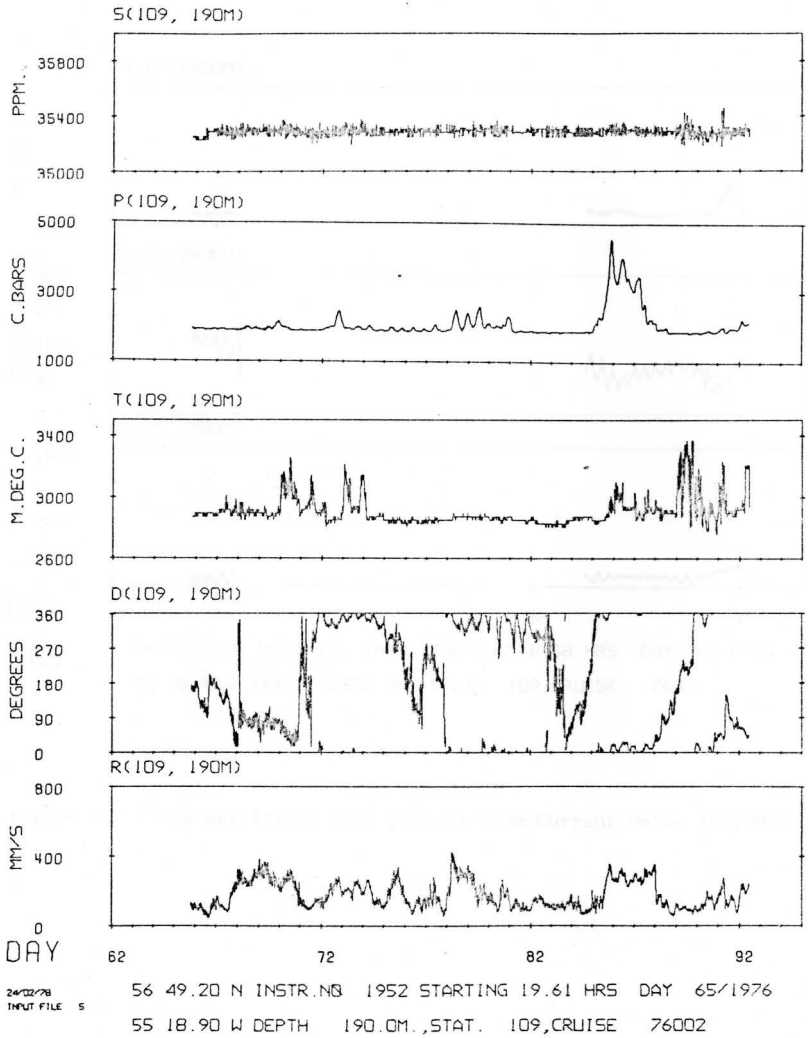

Figure 2.6 - The unfiltered data records from Current Meter 109,190.

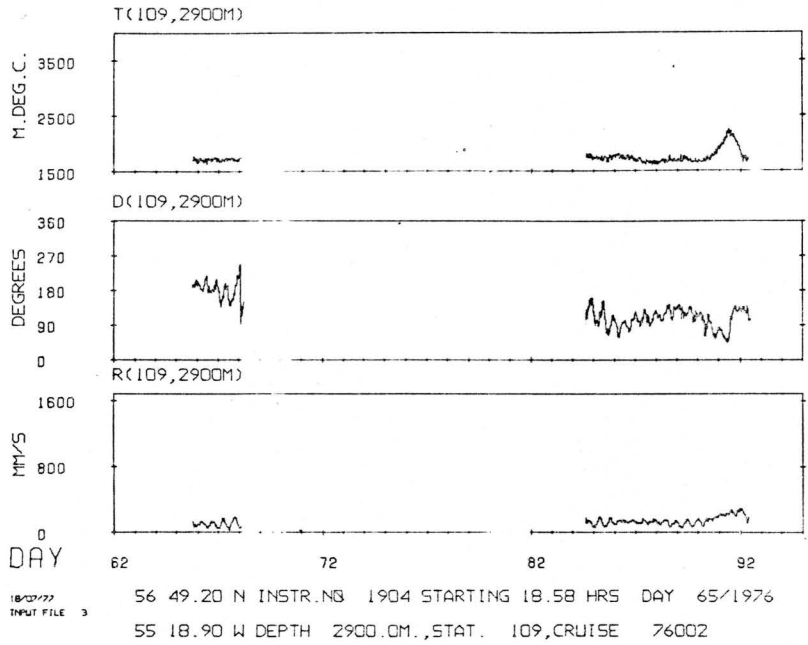

Figure 2.7 - The unfiltered data records from Current Meter 109,2900.

2.2 Hydrographic Survey

A hydrographic survey was done during the first period (Year days 63-69) of the current meter array to provide water mass and density structure information. Twenty-seven stations were observed to 1000 m, 2000 m, or the bottom. The stations comprised roughly five lines along and two lines perpendicular to the mooring line (see Fig. 2.8). The depth range of the CTD was limited to 2000 m, thus for a complete station a Knudsen bottle cast from 2000 m to within 50 m of the bottom was done following the CTD cast. Two of the transverse lines had complete profiles by combining the CTD cast with a bottle cast.

The Guildline Mark III analog CTD was precalibrated at the Bedford Institute in February, 1976 over the full ranges of pressure, temperature, and salinity. The pressure range was 0-2000 dbars and the error didn't exceed 0.15% of the range (3 dbars). The laboratory calibration reduced the error in temperature to less than 0.005°C and in salinity to less than 0.005 °/$_{oo}$. The data were collected by the CTD at 5 Hz with a lowering rate of 50-60 meters per minute. Thus the resolution in pressure is approximately 0.2 dbars. The noise level of the unsmoothed traces was 0.003°C in temperature and 0.003 °/$_{oo}$ in salinity. At the start of each downtrace there was an offset in conductivity that would slowly diminish as the cast proceeded. This problem is thought to be due to not keeping the conductivity cell wet between casts because of the below freezing temperatures in the hydrographic winch room. Since the offset could be either positive

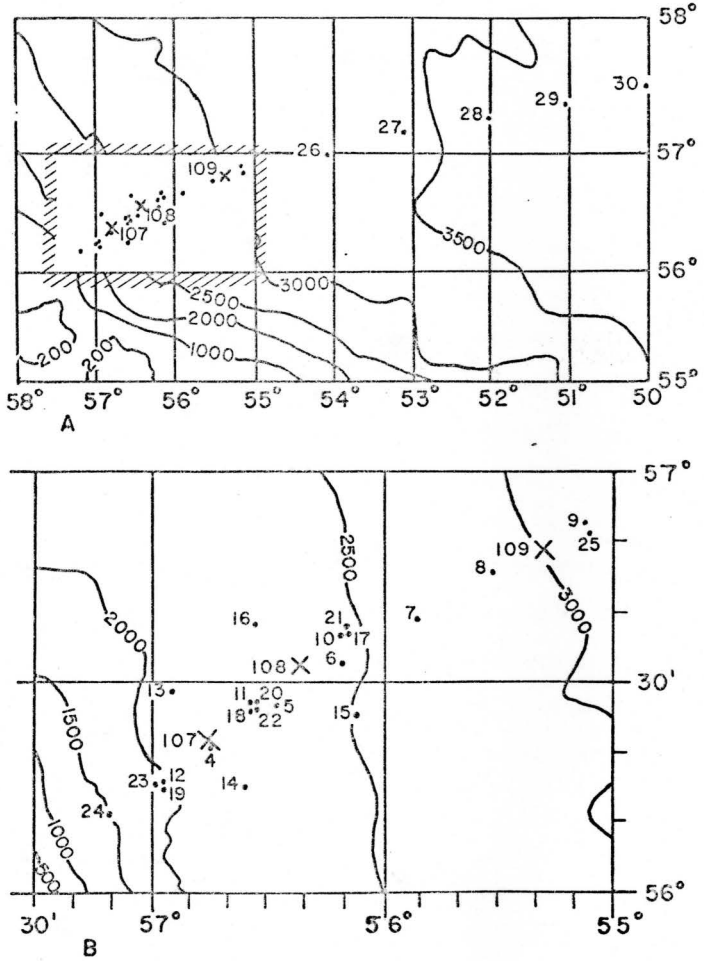

Figure 2.8 - Hydrographic stations (dots) and current meter moorings (X's) positions. The depth contours (meters) are approximate. Figure b is an enlargement of the hatched area in Figure a.

or negative, and lasted as deep as 200 m, the uptraces were used for analysis instead of the downtraces. The raw voltages from the CTD were passed through a Meridian multi-conductor slip-ring at the winch to a Volke digital voltmeter. The digitized voltages were then logged on the HP2100 computer.

Calibration of the CTD was done with water samples collected during the upcast of each station by 10 Niskin bottles on a rosette sampler designed at the Bedford Institute. Onboard salinity determinations were done with a Guildline Autosal laboratory salinometer. The average difference between 58 pairs of randomly drawn duplicate samples was 0.002 °/₀₀. The salinometer was calibrated with standard sea water at the beginning and at the end of each run, and at intermediate intervals of 15-30 samples. The error of the salinity determinations was less than 0.003 °/₀₀, the resolution was 0.0002 °/₀₀. A pair of protected and a single unprotected deep-sea reversing thermometers on alternate Niskin bottles were used for the temperature and pressure calibration. The resolution of the thermometers was 0.01°C. The average difference between 142 pairs of protected thermometers was 0.011°C.

Standard computer programs at the Bedford Institute were used to process the CTD data. Excessive erroneous points were cleaned first by limiting the range of acceptable raw voltages for the three channels. Each station was then split into up and downtraces. Then the raw parameters were converted to physical units; temperature (°C), conductivity (mmho/cm), and pressure (dbars). Flat spots in the traces were

then removed. A flat spot is a region in the trace where the pressure hasn't changed more than 1.3 dbars over nine data points, which means the lowering rate is less than 0.7 m/s. Flat spots occurred when the CTD was stopped for a water sample or when its passage through the water was momentarily slowed due to ship's motion acting opposite to the CTD being winched in or out. The reason for the flat spot removal was that the conductivity cell must be moving in order to flush properly, and to maintain a steady time constant between the conductivity cell and the thermistor, for the determination of salinity, thus all points less than the required flushing rate were removed. Spikes were then removed by setting the maximum allowable difference for single points from the mean curve. The data were then smoothed by a seven-point running mean filter which smoothed the data over approximately 1.2-1.4 dbars. In order to reduce the file sizes, the data were then forward linearly decimated. The allowed differences between the measured value and the interpolated value were 0.01°C for temperature and 0.01 mmho/cm for conductivity.

Salinity was determined by A. Bennett's (1976) formula. Potential temperature was derived by Fofonoff and Froese's (1958) formula and σ_θ was derived by Fofonoff and Tabata's (1958) formula. The final resolution of the CTD profiles was 0.01°C in temperature, 0.01 mmho/cm in conductivity, 0.01 $^{\circ}/_{\circ\circ}$ in salinity, and 3 dbars in pressure. The criteria used to process the CTD data are summarized below.

TABLE B

SUMMARY OF CTD PROCESSING CRITERIA

CHANNEL	TEMPERATURE	CONDUCTIVITY	PRESSURE	SALINITY
RANGE (VOLTS)				
LOWER LIMIT	-0.2	-3.75	-0.1	N.A.
UPPER LIMIT	3.5	3.75	3.5	N.A.
FLAT SPOT REMOVAL	N.A.	N.A.	1.3 dbars/9 points	N.A.
SPIKE REMOVAL				
ALLOWABLE CHANGE	0.012°C	0.02 mmho/cm	1.3 dbars	N.A.
SMOOTHING				
NO. OF POINTS	7	7	7	N.A.
FORWARD LINEAR DECIMATING				
ALLOWABLE CHANGE	0.01°C	0.01 mmho/cm	N.A.	N.A.
FINAL RESOLUTION OF				
THE PROFILES	0.01°C	0.01 mmho/cm	3 dbars	0.01 °/$_{oo}$

The portion of the CTD trace where a water sample was collected was located so that comparison between the CTD and bottle samples could be made. The traces of temperature and salinity indicated that there was no offset in CTD values when the CTD was stopped for a water sample, therefore the portion of the CTD trace just before the bottle was fired could be used in the comparison. Typically, however, when a CTD is stopped for a water sample, an offset occurs in some manner due to instrument wake and flushing effects, unsteady time constant, and heating of the water in the conductivity cell. Therefore, when the CTD is stopped for a water sample, that portion of the trace is removed because it is a flat spot. In order to retrieve the lost lines the following method was used. Using the final version of the bottle data as a guide the appropriate flat spots that correspond to the water samples were located and identified. A program was developed to convert the raw voltages to temperature, pressure, and salinity, recovering the original CTD values. To mimic the response times of the bottles, an average was done over the last 100 points of the CTD trace just before the bottles

were tripped. The CTD was raised just after the tripping of the bottles, terminating the flat spot. Thus, for deep bottles where they are well separated, the part of the CTD trace that corresponds to the water sample is readily identifiable and recoverable.

The difference (Bottle value-CTD value = offset) between the edited bottle data and the CTD were used for calibrating the CTD. The mean and standard deviation for the correction for each station were computed separately. The corrections were applied for temperature, salinity with and without a correction factor for the compression of the conductivity cell with pressure. A single offset for temperature (-0.004°C, std. dev. 0.055, for 220 calibration points) was used for the entire cruise. The wide scatter in the temperature differences is due almost entirely to the low precision of the reversing thermometers rather than to any real variation in the CTD's thermistor with time or depth. However, separate corrections for each station for the salinity, corrected for pressure effects on the cell, were used. In this region of homogeneous water with very low salinity gradients there were in effect up to ten salinity calibration points for the very small range of salinity values encountered at each station. Thus, the 7.0 (average) 2.4 (std. dev.) salinity calibration points per station were capable of distinguishing separate offset values for each station, which were assumed to have been due to real changes in the conductivity cell from station to station. The offsets ranged from -0.004 °/$_{oo}$ to -0.038 °/$_{oo}$ and averaged -0.023 °/$_{oo}$. The average standard deviation of the salinity offsets for the individual stations was 0.003 °/$_{oo}$.

CHAPTER 3 GENERAL PHYSICAL OCEANOGRAPHIC FEATURES DURING MARCH, 1976

3.1 Background

The original and still most comprehensive work on the physical oceanography of the Labrador Sea was done by E. Smith, F. Soule, and O. Mosby (1937). They reported on the results of the Marion and General Greene expeditions during the summers of 1928, 1931, 1933-35 to the Labrador Sea and Davis Strait areas, to collect salinity data at depth from a series of hydrographic stations in lines running from the coast across the shelf. Velocity profiles and dynamic topography, derived by the geostrophic method from the calculated density field, enabled them to describe the prevailing circulation and water mass distribution in the Labrador Sea from Davis Strait to the Grand Banks region. Their work is the foundation of our knowledge of the water masses and surface currents in the Labrador Sea.

More recently, the U.S. Coast Guard has occupied a standard hydrographic section from South Wolf Island, Labrador to Cape Farewell, Greenland once a summer from 1948 to 1969, Moyhiman and Anderson (1971). Also Kollmeyer, McKill, and Corwin (1967) conducted a cruise to the Cape Chidley area to investigate the flow into and out of Hudson Strait from hydrographic data.

Erika Dan, under charter to the Woods Hole Oceanographic Institution, conducted a hydrographic survey in the Labrador Sea area during February-April, 1962. This survey, along with others from the North Atlantic, was compiled into an atlas by Worthington and Wright (1970) Swallow and Worthington (1969) tracked five neutrally-buoyant floats for periods of 12-72 hours in conjunction with the Erika Dan survey. Two floats were 200 km southwest of Cape Farewell and three were 400 km east of the Strait of Belle Isle. The floats at depths of 1650-2400 m were combined with the geostrophic velocities to estimate the deep volume transport in the Labrador Sea.

The Atlantic Oceanographic Laboratory, Bedford Institute, conducted four cruises during 1965-1967 to the Northwest Atlantic and the Labrador Sea. Temperature, salinity, oxygen, and silica data were collected at depth and compiled into an atlas by Grant (1968). Lazier (1973) used the the March-May, 1966 Hudson data from the Labrador Sea along with hydrographic data from Weather Ship Bravo (56°30'N 51°00'W) to investigate the renewal of the water mass indigenous to the Labrador Sea.

Between 1953 and 1977 hydrographic data were collected in the Labrador Sea from a number of cruises for the International Commission for the Northwest Atlantic Fisheries (ICNAF). A bibliography of the physical oceanographic works, including the ICNAF publications, up to 1977 was compiled by Dobson and Jordon (1978). Dunbar in 1951 reviewed the work which had been done up until that time in the Labrador Sea, Baffin Bay,

Hudson Bay, and the neighboring straits and sounds. Both Dunbar (1951) and Smith, Soule, and Mosby (1937) include reviews of the early historical explorations to the Labrador Sea area.

From these oceanographic studies it appears that the surface circulation in the Labrador Sea consists of a broad cyclonic gyre with strong currents around its periphery, see Fig. 3.1. These surface currents are the West Greenland Current to the east, the Labrador Current to the west, and the North Atlantic Current across the southern boundary.

The West Greenland Current flows northwards along the west coast of Greenland. Near 61°N it bifurcates; one branch continues north along the coast through Davis Strait into Baffin Bay, the other branch crosses the northern end of the Labrador Sea. The West Greenland Current transports two water masses into the Labrador Sea. Warm (>4°C) and saline (34.9-35.0°/$_{oo}$) water from the Irminger Sea is located offshore and below the surface and cold (<3°C), low-salinity (<34.0°/$_{oo}$) water from the East Greenland Current which is located inshore at the surface.

The Baffin Land Current flowing south along the coast of Baffin Island carries cold, low-salinity (<-1.0°C, 33.0-33.5°/$_{oo}$) water into Hudson Strait according to the dynamic topographic charts of Kollmeyer et al (1967). This mixes in the Strait with the cold, fresh (<1.0°C, <33.0°/$_{oo}$) outflow of Hudson Bay (Campbell, 1958) and perhaps some outflow from the Canadian Archipelago. The resulting mixture (<1.0°C, <33.5°/$_{oo}$) flows out of Hudson Strait and then southwards along the Labrador Shelf.

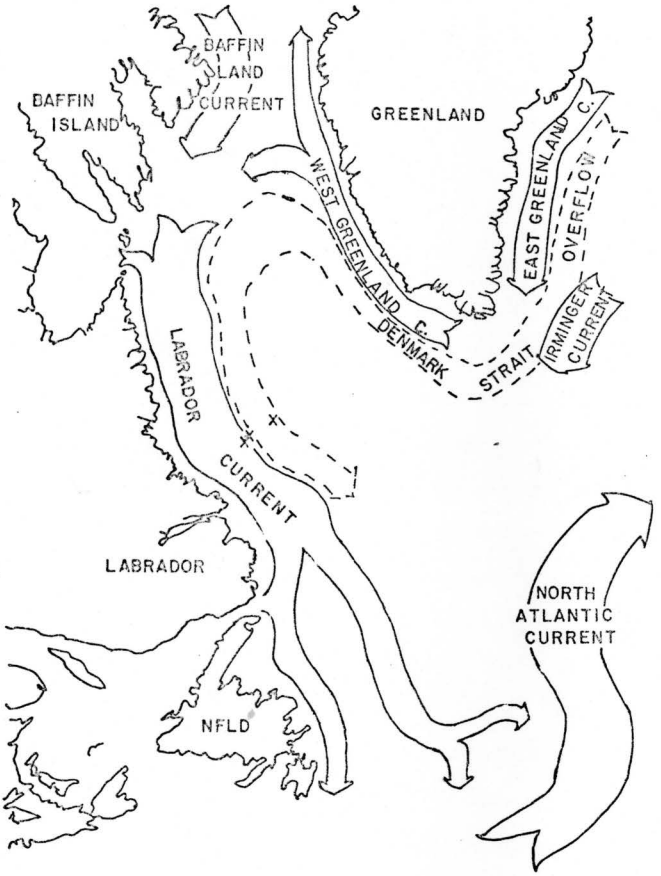

Figure 3.1 - The surface (solid lines) and bottom (dashed lines) currents of the Labrador Sea region. X's are the positions of the current meter moorings.

Near Cape Chidley, Labrador the cold, low-salinity outflow of Hudson Strait is augmented on its offshore side by the extension of the West Greenland Current to form the Labrador Current. Water from the West Greenland Current extension includes a large portion of water which is a remnant of warm, saline Irminger Sea Water. The T-S diagrams from the Labrador Current of Smith, Soule, and Mosby (1937) and a 17-year mean from an annual U.S. Coast Guard section (Kollmeyer et al, 1967) show that the Labrador Current consists of these two water masses and a mixture between them. The warmed surface layer during the summer and the deeper waters over the slope are excluded from both T-S diagrams. Geostrophic sections occupied by Smith, Soule, and Mosby (1937) indicate that the Labrador Current forms two southward flowing current cores, referred to as an inshore branch located at the coast and an offshore branch at the shelf break. They reasoned that the banding was due to either the separate sources of the Labrador Current or the shelf topography (a system of marginal troughs and offshore banks) or both. Thus, the Labrador Current transports southward cold, fresh (<1.0°C, <33.5°/$_{oo}$) water inshore and remnants of relatively warm (3.0-4.0°C), saline (>34.8°/$_{oo}$) Irminger (Atlantic) Water, offshore.

The offshore velocity core is associated with the sharp temperature-salinity gradient between the cold, fresh waters of the Labrador Current and the warmer, saltier water offshore. A slight temperature and salinity maximum at depths of 400-800 meters can be found in the sections of Smith, Soule, and Mosby (1937) and Lazier (1973). This is the remnant of Irminger Sea Water. These investigators indicate that this water flows south as part of the offshore branch of the Labrador Current. The 2.0°C isotherm

at 100 m seems to be a reasonable indicator of the position of the temperature gradient and the associated velocity maximum. The March, 1976 mooring array and hydrographic survey were located over the continental slope, apparently just offshore of the velocity core of the offshore branch of the Labrador Current.

The North Atlantic Current flows northeastwards past the southern boundary of the Labrador Sea. This boundary is an important mixing region between the cold polar waters and warm southern waters. Large meanders in the dynamic topographic charts of Smith, Soule, and Mosby (1937) and Lazier (1973) are evidence of this mixing.

Below 2000 meters, the circulation would also appear to consist of a cyclonic gyre dominated by boundary currents. Geostrophic velocities of 5 cm/s based on zero velocity at 2000 m from Smith, Soule, and Mosby (1937) show an inflow into the Labrador Sea centered at 3000 m on the Greenland side and a corresponding outflow on the Labrador side. Swallow and Worthington's (1969) floats indicated speeds of 10 cm/s and were consistent with a deep cyclonic circulation in the Labrador Sea.

In the central part of the Labrador Sea, Smith, Soule, and Mosby (1937) identified three water masses; intermediate, deep, and bottom, see Fig. 3.2. Lee and Ellett's (1965, 1967) names for the three water masses are Labrador Sea Water, Northeast Atlantic Deep (NEAD), and Northwest Atlantic Bottom (NWAB), respectively. Worthington in his 1976 monograph refers to the origin of the water masses. Thus, NEAD is refered to as the

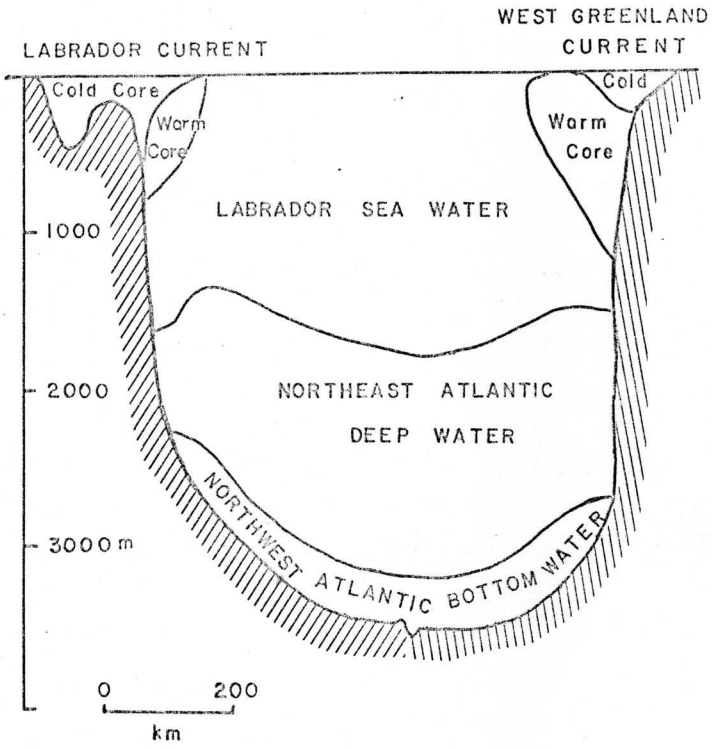

Figure 3.2 - The water masses of the Labrador Sea looking northwards. The cold and warm portions of the Labrador and West Greenland Currents are also shown. This cross-section is based on Grant's (1968) atlas - stations 30-41.

Iceland-Scotland Overflow, NWAB is Denmark Strait Overflow and Labrador Sea Water remains the same. The nomenclature of Lee and Ellett will be used here.

Labrador Sea Water occupies the central portion of the Labrador Sea from the surface down to mid depths, 1500-2000 dbars. This homogeneous water mass is produced locally in the Labrador Sea by winter cooling of the surface layers which sink during deep-convection events to intermediate depths (Lazier, 1973 and Clarke, in preparation). Smith, Soule, and Mosby (1937) reported values of 3.17°C and 34.88°/$_{oo}$ for the Labrador Sea Water. This extended from below the summer thermocline (300 m) to 2100 m in July, 1934. Lazier (1973) defines Labrador Sea Water by the 27.7-27.8 potential density contours. He reports potential temperature values of 3.4°C and salinity of 34.9°/$_{oo}$ for Labrador Sea Water at 1500 m in March-May, 1966. This concurs with the early cruise of the Erika Dan in 1962 (3.3 - 3.4°C, 34.9°/$_{oo}$) and Worthington and Metcalf's (1961) definition of Labrador Sea Water (3.4°C, 34.89°/$_{oo}$).

Below the Labrador Sea Water the warmer saltier NEAD Water is located. Smith, Soule, and Mosby (1937) found temperatures of 3.0-3.2°C with salinities of 34.92 - 34.94°/$_{oo}$ across the Labrador Sea at depths of 2000 - 2500 meters. Lee and Ellett (1967) using data from the International Geophysical Year (1957-58), characterized the NEAD Water in the Labrador Sea from an inflection point in the T-S diagram near 2500 m at 3.0°C and 34.94°/$_{oo}$. The Erika Dan sections in 1962 and the Hudson sections in 1966 showed the same T-S characteristics for the NEAD Water. Both of these

surveys included dissolved oxygens. The NEAD Water is easily distinguished by its low oxygen content (<6.5 ml/l) when compared with the overlying Labrador Sea Water and the NWAB Water below. The lower oxygens indicate that this water mass has not been in contact with the surface as recently as either the Labrador Sea Water or the NWAB Water. The isotherms and isohalines between 1500 and 2000 m are gentle in the central portion of the Labrador Sea. The lack of strong slopes to the isotherms and isohalines indicate a minimum in current at this level. Swallow and Worthington (1969) suggested a velocity minimum at 1200 m based on geostrophic velocity profiles adjusted to their float velocities.

In the lowest 1000 meters of the Labrador Sea the isotherms slope upwards from the center. Two to three hundred meters off the bottom the temperature-salinity gradient sharpens. This gradient which intersects the continental slope below 2000 m marks the upper boundary of the core of the NWAB Water. From Erika Dan and Hudson cruises it is apparent that the NWAB Water is characterized by temperatures between 1.4 and 2.0°C with salinities of 34.90 - 34.92°/$_{oo}$. Dissolved oxygen content was greater than 6.6 ml/l within 200-300 meters of the bottom. This water mass can be traced directly from its origins in the Denmark Strait into the eastern side of the Labrador Basin next to Cape Farewell, Greenland, on the potential temperature-salinity charts of Worthington and Wright's 1970 atlas. The NWAB Water fills the very bottom of the basin and flows out along the western side of the Labrador Basin. The slopes of the isotherms and the flow indicated by the θ-S charts are both consistent with a deep cyclonic

circulation in the Labrador Sea. The confinement of the oxygenated core of the NWAB Water up against the lower continental slope suggests the presence of a bottom boundary current.

3.2 Mean Currents

In March, 1976, a hydrographic section across the offshore branch of the Labrador Current was occupied twice. On these sections one sees the cold (<2°C) water of the Labrador Current in the upper 300 meters (Fig. 3.3, Sta. 4; Fig. 3.5, Sta. 23-24). The salinity of this water is less than 34.8 °/$_{oo}$ (Fig. 3.4, 3.6). Section 4-9 did not extend far enough inshore to enter the core of the Labrador Current, thus the temperatures are not as low as -1.5°C with associated low salinities. Just offshore of this at depths of 300-1000 meters is a warm saline core (>3.0°C, >34.86°/$_{oo}$) which is certainly remnants of the Irminger (Atlantic) Water.

The homogeneous Labrador Sea Water is present at Stations 6 through 9 and Stations 25 through 30 in Figures 3.3, 3.4, 3.5, and 3.6 From the surface down to 1500 m the potential temperature was completely within the 2.9 - 3.0°C range. The salinity was nearly constant at 34.84°/$_{oo}$. The resulting potential density for the upper 1500 m during March, 1976 was 27.78 - 27.79. The Labrador Sea Water was 0.4°C warmer and 0.06°/$_{oo}$ saltier in March of 1966 than 1976, but the potential density had not changed.

The core of the NEAD Water can be located by the temperature layer greater than 3.3°C situated in the greater than 34.93°/$_{oo}$ salinity layer. In the central Labrador Sea this layer is at 2000 - 2500 m. (Fig.

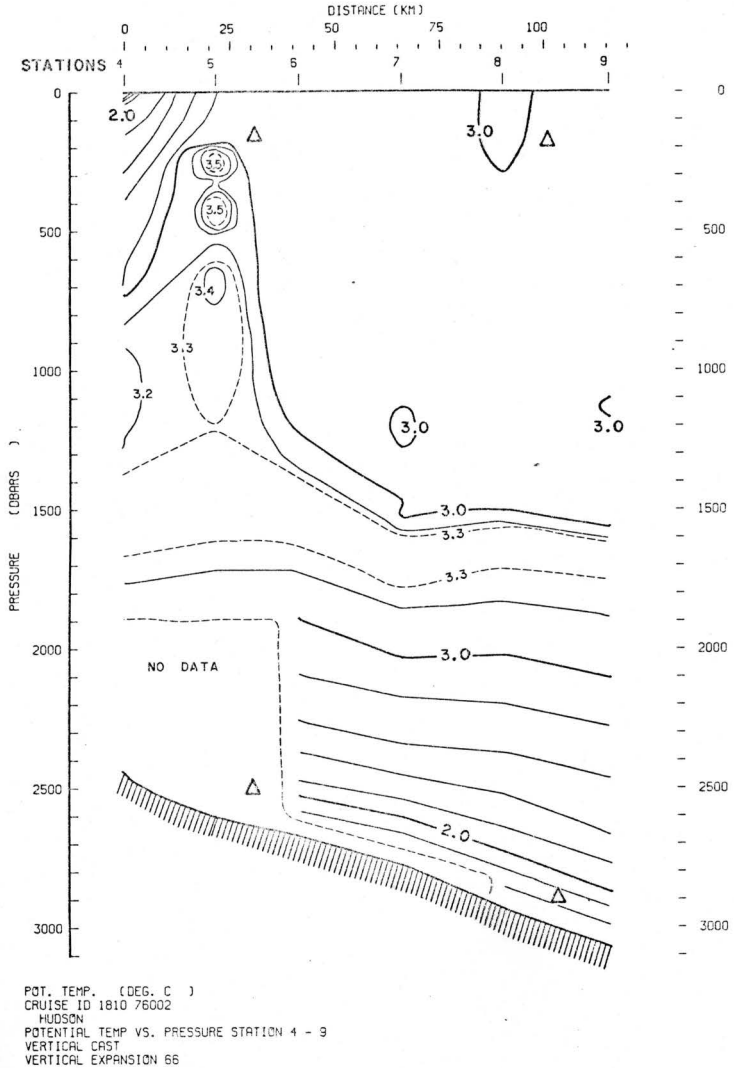

Figure 3.3 - Cross-section of potential temperature (^{o}C) for stations 4-9.

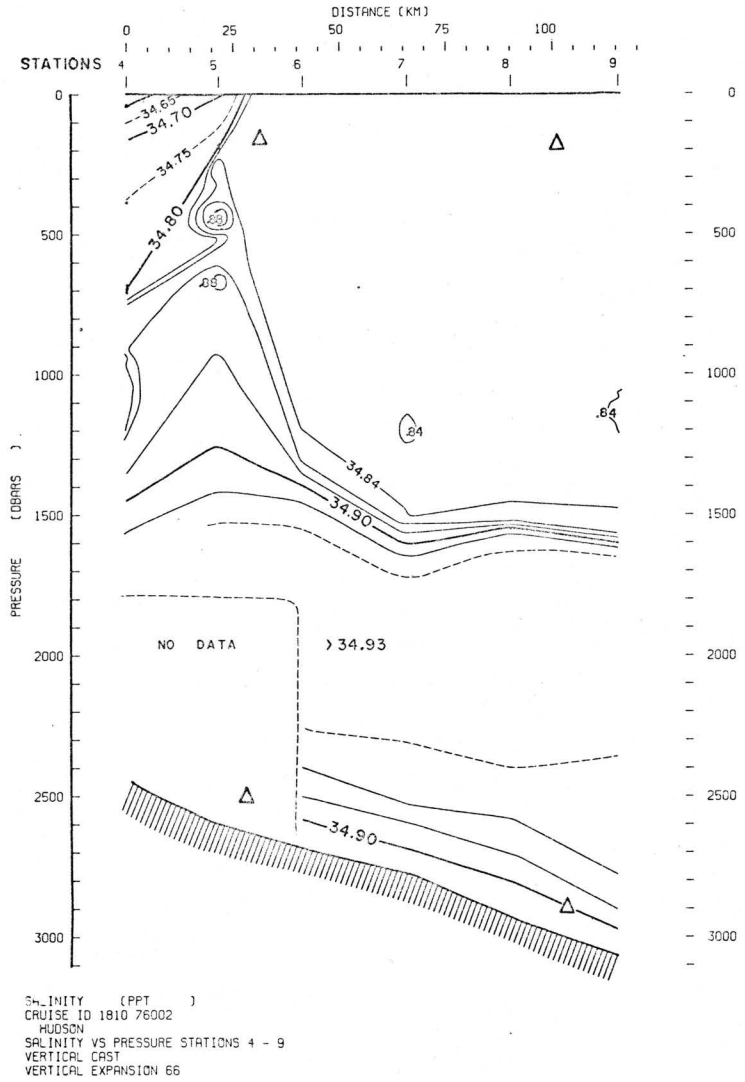

Figure 3.4 - Cross-section of salinity ($^{o}/_{oo}$) for stations 4-9.

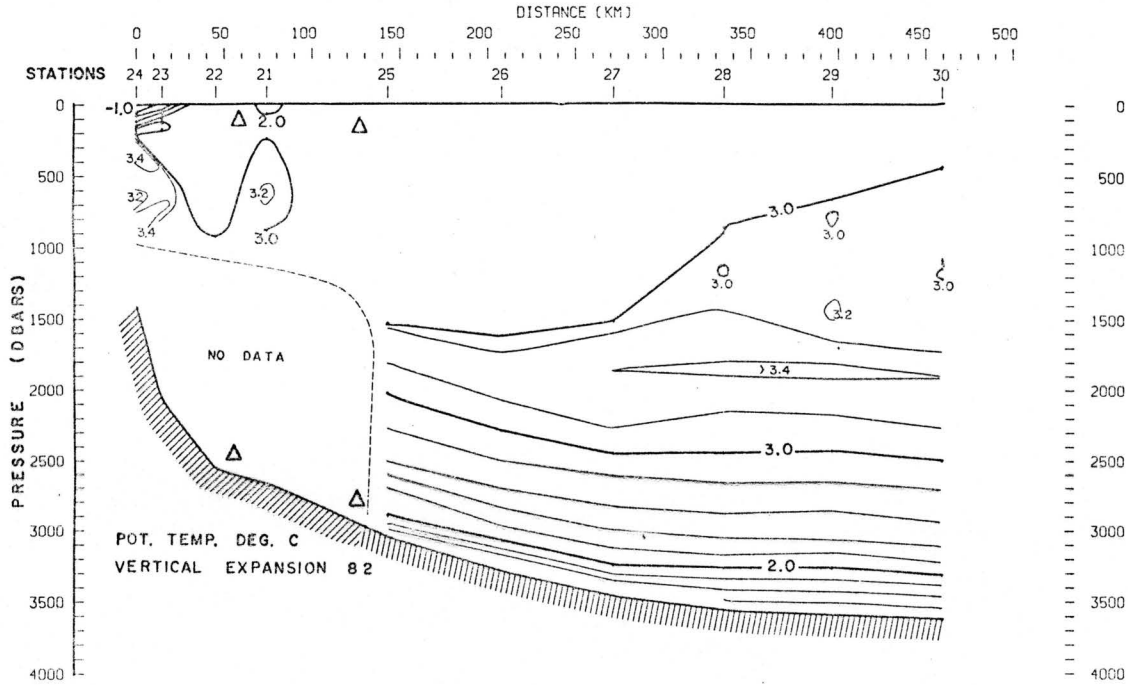

Figure 3.5 - Cross-section of potential temperature (^{o}C) for stations 24-21, 25-30.

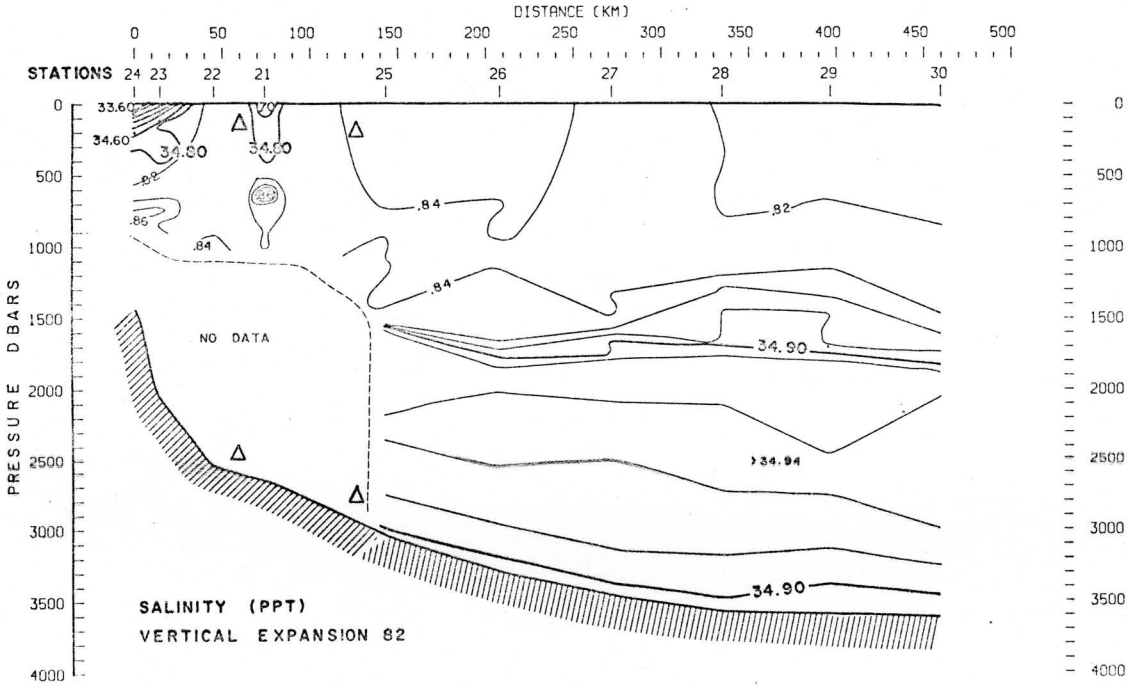

Figure 3.6 - Cross-section of salinity ($^{o}/_{oo}$) for stations 24-21, 25-30.

3.5, 3.6 Sta. 27-30). This layer gently slopes up inshore to approximately 1500 meters (Fig. 3.3 Sta. 4-6). This is consistent with cyclonic circulation if the strength of the circulation is increasing with depth. Swallow and Worthington (1969) chose the boundary between the Labrador Sea Water and the NEAD Water as their reference level for geostrophic calculations, justified by a zone of weak motion at 1000 m and a change in the T-S curve at 1200 m. Therefore, the core of the NEAD Water is thought to be in or near a zone of minimum velocity.

Along the bottom the core of the NWAB Water is only slightly modified from its original values at the Denmark Strait. The θ-S values in March, 1976 (1.4-2.0°C, <34.90°/$_{oo}$) were the same as previous years. The colder water was found deeper (more offshore), see Fig. 3.3 Sta. 6-9, Fig. 3.5 Sta. 25-30. The slope of the isotherms and isohalines are quite consistent with deep cyclonic circulation.

Moorings 108 and 109 were located between Stations 5 and 6 and Stations 8 and 9, respectively; and Stations 21-22 and 21-25, respectively. The hydrographic sections (Fig. 3.3) suggest that the upper current meters should be in Labrador Sea Water. The temperature records from the current meters (Fig. 2.3, 2.5, 2.6) suggest that this is so. Current Meter 108,160 though degraded by instrument noise, was in 3°C water for a large percentage of its time. The warm intrusions, (3.4-3.6°C) for example at Day 70, are undoubtedly due to remnants of Atlantic Water moving past the instrument. 109,190 also has these warm intrusions above a background

level of approximately 3°C. There were two negative anomalies (Day 69, 2.7°C and Day 87, 2.6°C) in the temperature record of 108,160, and a negative anomaly (2.6-2.8°C) at 109,40 during Day 90; however, none were recorded at 109,190. The only water colder than 2.9°C in the upper layers is water from the cold core of the Labrador Current. This indicates that the boundary cold core of the Labrador Current extended offshore as far as 108,160, with cold water being found at the surface as far offshore as 109,40.

The currents at 108,160 were predominately southward in the range 20-60 cm/s, although several northward reversals lasting for periods of a couple of days occurred; for example, see Fig. 2.3, days 74-75, 82, 91-92. The peak southward velocities at 108,160 were of the same magnitude as those derived by Smith, Soule, and Mosby (1937) for the velocity core (30-70 cm/s) centered on the sharp temperature gradient. The lack of 2°C water at 108,160 is evidence that the center of the temperature gradient and its associated velocity maximum did not extend offshore as far as 108,160. This indicates that the absolute velocity profiles for the offshore branch of the Labrador Current derived by Smith, Soule, and Mosby (1937) were possibly too low. The adjustment necessary to match the velocity profiles of Smith, Soule, and Mosby (1937) to the velocities of 108,160 is 10 to 30 cm/s. 108,160 was placed near the boundary of the offshore branch of the Labrador Current which evidently transports southwards a considerable volume of both Atlantic Water remnants and Labrador Sea Water.

The flow at 109,190 was predominately northwards, see Fig. 2.6, The progressive vector diagrams (PVD's), Figure 3.7, show that the flow is first southwards and then swings offshore (eastwards) during days 68 to 70. For the last 2/3 of the 26.7 day record, from Day 71 until Day 91, the flow was northwards at an average rate of 9.8 cm/s. There was, therefore, for much of March, 1976, a substantial northward flow offshore of the Labrador Current.

Weak, northerly flows just offshore of the Labrador Current are present in some of the velocity profiles of Smith, Soule, and Mosby (1937). They describe the northward flows as local and temporary currents. The overall pattern of the surface currents are best shown in the PVD's, Fig. 3.7. This pattern suggests the passage of a cyclonic eddy-like feature southwards between the two moorings. The offshore flow during days 67-70 would occur when the locus of the eddy was north of the array. As the eddy moved between the two moorings a southward flow would occur inshore and a northward flow offshore at 109,190. This feature would have to be local (of the O(50 km)) enough not to entrain water from the cold core of the Labrador Current, since no such water was found at 109,190. This type of feature would appear to be both local and temporary in hydrographic sections. Evidence of this scale feature at the surface can be seen in satellite imagery in the thermal gradient between the cold Labrador Current and the 3°C Labrador Sea Water. Fig. 3.9 is the infrared imagery from NOAA 5 satellite for 3 September 1977. The eddy-like feature enclosed in the box is approximately

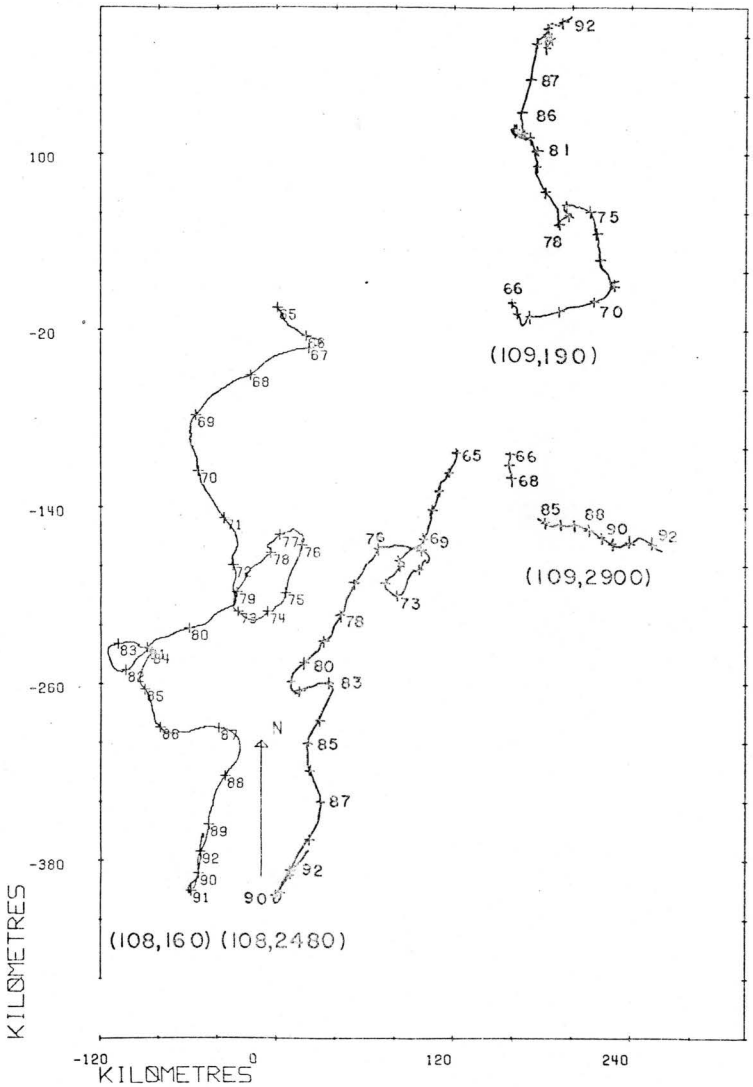

Figure 3.7 - Progressive vector diagrams for the current meters 108,160; 108,2480; 109,180; and 109,2900. The hatch marks are year-days. The starting point of 108,160 is at the origin, the others are separated by arbitrary distances.

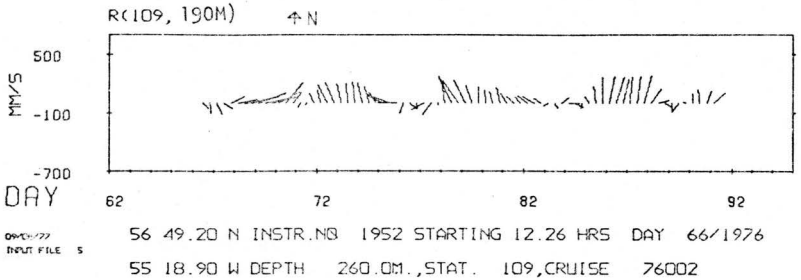

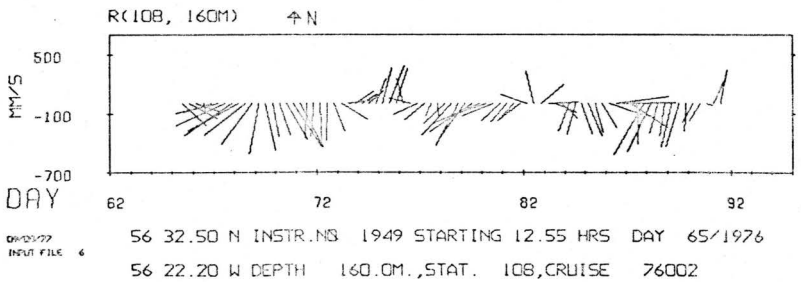

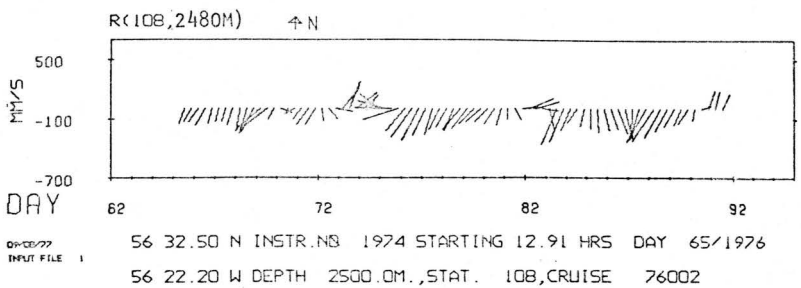

Figure 3.8 - "Stick-diagrams" showing low-pass filtered eight-hour vectors from current meters 109,190; 108,160; and 108,2480.

Figure 3.9

Infrared NOAA5 satellite imagery from 3 September, 1977 of the Labrador Sea region. The boxed area surrounds the feature at the edge of the Labrador Current referred to on pages 45,49. The sides of the box are approximately 90 km. The photograph and the box are both aligned north-south. Clouds (white areas) cover southwestern Labrador, the eastern portion of the Labrador Sea, the Davis Strait region and portions of Greenland. The colder (lighter) waters of the Labrador Current and Hudson Strait are plainly visible.

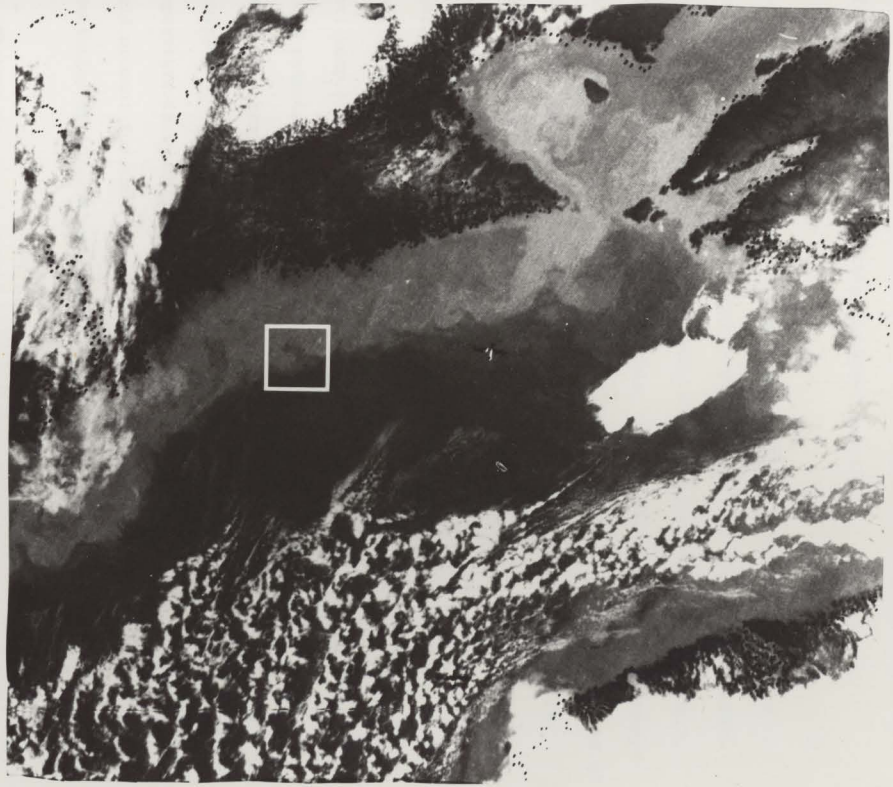

50 km in diameter. The location of this feature is at the shelf break, 200 km off Nain, Labrador. Although this gradient is 200 km inshore of the mooring array, perhaps these same scale features are present further offshore in the region of Atlantic Water remnants.

From the hydrographic sections (Fig. 3.3) it is evident that the bottom current meters were placed in or near the core of the NWAB Water. The temperature records from 109,2900; 108,2480; and 107,2340 (Fig. 2.7, 2.4, and 2.2 respectively) confirm this. At 109,2900 the potential temperature was steady at 1.5°C, with a single deviation to 2.4°C at the end of the record, (potential temperature; the temperature record values were adjusted to potential temperature using the nearby CTD profiles). The steadiness of the record is suggestive of an isothermal bottom boundary layer. Up the slope at 108,2480 the water was warmer, (mean pot. temp. 2.3°C) and exhibited pronounced fluctuations between 1.6°C and 2.5°C (pot. temp.) at a few days period. Still further upslope, 107,2340 had a mean potential temperature of 2.6°C with similar fluctuations (2.0°-2.9°C, pot. temp.) as those at 108,2480. The vertical (or horizontal) excursion of the isotherms necessary to produce an 0.9°C fluctuation in temperature is approximately 200-300 meters (or 100-200 km). Motions that could account for the major fluctuations in temperature at 108,2480 and by association at 107,2340 are dealt with in Section 4.4.

The two deep current meters which returned velocity records, 108,2480 and 109,2900, support the suggestion of deep cyclonic circulation. The average southward flow over the 27.9 day period at 108,2480 was 11 cm/s. The speed ranged from 10-50 cm/s. There were three periods of northward reversals which lasted a couple of days. Further offshore

at 109,2900 the flow was southwards for the first 2.9 days with an average velocity of 9.5 cm/s. The flow was southeastwards (downslope) during the last 9.9 days (days 85-92) of the record. The middle portion of the record was lost due to instrument malfunction. The flow at 109,2900 was without the large fluctuations that were evident at 108,2480, see Figures 2.7 and 2.4. This would indicate that the velocity core of the deep flow was up on the slope nearer 108,2480 than 109,2900. The mean velocities (11 cm/s) reported here are close to previous velocity estimates of Smith, Soule, and Mosby (1937) - 5 cm/s; and those of Swallow and Worthington (1969) - 10 cm/s. However, the range of velocities indicate that a peak of 40-50 cm/s is not uncommon. Thus, it seems likely that the circulation is along the bottom and somewhat concentrated in the region of the 2600 m isobath, and that this is the flow of the waters from the Denmark Strait Overflow into and out of the Labrador Sea as Worthington (1976) has depicted it.

The general picture that emerges is a stronger offshore branch of the Labrador Current which transports considerable quantities of Atlantic Water remnants and Labrador Sea Water. Further offshore, a northward surface flow was found, perhaps the results of local dynamics. A velocity minimum is thought to occur at mid depths (1000-1500 m). Below that, the deep flow and isotherms are consistent with deep cyclonic circulation.

3.3 Geostrophic Currents

Pond and Pickard (1978) give the equations of motion for an incompressible fluid on a plane at a constant latitude on the rotating earth as:

$$\frac{Du}{Dt} = -\frac{1}{\rho}\frac{\partial p}{\partial x} + 2\Omega(\sin\phi v - \cos\phi w) + A_x\frac{\partial^2 u}{\partial x^2} + A_y\frac{\partial^2 u}{\partial y^2} + A_z\frac{\partial^2 u}{\partial z^2} \qquad (3.0)$$

(acceleration) = - (pressure) + (horiz. Coriolis) - (vertical Coriolis) + (eddy viscosity)

$$\frac{Dv}{Dt} = -\frac{1}{\rho}\frac{\partial p}{\partial y} - 2\Omega\sin\phi u + A_x\frac{\partial^2 v}{\partial x^2} + A_y\frac{\partial^2 v}{\partial y^2} + A_z\frac{\partial^2 v}{\partial z^2} \qquad (3.1)$$

(acceleration) = - (pressure) - (horiz. Coriolis) + (eddy viscosity)

$$\frac{Dw}{Dt} = -\frac{1}{\rho}\frac{\partial p}{\partial z} + 2\Omega\cos\phi u - g + A_x\frac{\partial^2 w}{\partial x^2} + A_y\frac{\partial^2 w}{\partial y^2} + A_z\frac{\partial^2 w}{\partial z^2} \qquad (3.2)$$

(acceleration) = - (pressure) + (vertical Coriolis) - (gravity) + (eddy viscosity)

(1) x, y, and z are the Cartesian coordinates, east, north, and upwards from the sea surface.

(2) u, v, and w are the velocity components in the direction of x, y, and z.

(3) Ω is the angular velocity of rotation of the earth.

(4) ϕ is the latitude.

(5) ρ is the density of the fluid and "p" is the pressure.

(6) where $\frac{D}{Dt}$ is the material derivative

$$\frac{D}{Dt} = \frac{\partial}{\partial t} + u\frac{\partial}{\partial x} + v\frac{\partial}{\partial y} + w\frac{\partial}{\partial z}$$

(7) "g" is the gravitational acceleration with the effects of the earth's rotation included in it.

(8) A_x and A_y are the horizontal eddy viscosity coefficients and A_z is the vertical eddy viscosity coefficient.

The equations of motion are too complex to be solved directly. However, for the time and space scales of the motions, of particular interest in the Labrador Sea, the equations can be simplified by scaling the terms. Typical values for the offshore branch of the Labrador Current are:

$u = 0.3$ m/s

$v = 0.3$ m/s

$w = \frac{UH}{L} = 0.003$ m/s

$A_x = A_y = 10^3$ m^2/s

$A_z = 10^{-3}$ m^2/s

$\rho = 10^3$ kg/m^3

$\phi = 56.5°$

$H = 10^3$ m

$L = 10^5$ m

$T = 5\times10^5$ s (6 days)

$g = 10$ m/s^2

$2\Omega = 1.45\times10^{-4}$ s

Where the above values are inserted into Equations 3.0 and 3.1, the scale of the terms are:

$$6\times10^{-7} + 9\times10^{-7} + 9\times10^{-7} + 9\times10^{-7} =$$

(accleration)

$$-\frac{1}{\rho}\frac{\partial p}{\partial x} + 3.6\times10^{-5} - 2.4\times10^{-7} + (30. + 30. + 0.3)\times10^{-9} \tag{3.3}$$

+ (horiz. Coriolis) - (vertical Coriolis) + (eddy viscosity)

$$6\times10^{-7} + 9\times10^{-7} + 9\times10^{-7} + 9\times10^{-7} =$$

(acceleration)

$$-\frac{1}{\rho}\frac{\partial p}{\partial y} - 3.6\times10^{-5} + (30. + 30. + 0.3)\times10^{-9} \tag{3.4}$$

- (horiz. Coriolis) + (eddy viscosity)

The horizontal Coriolis terms are two orders of magnitude larger than the other scaled terms. Thus, the only terms available to balance the $0(10^{-5})$ Coriolis terms are the horizontal pressure gradients, and therefore Equations 3.0 and 3.1 can be reduced to the geostrophic relationship.

$$2\Omega \sin\phi v = \frac{1}{\rho}\frac{\partial p}{\partial x} \tag{3.5}$$

$$2\Omega \sin\phi u = -\frac{1}{\rho}\frac{\partial p}{\partial y} \tag{3.6}$$

The vertical equation of motion (Eq. 3.2) is scaled to:

$$6\times10^{-9} + 9\times10^{-9} + 9\times10^{-9} + 9\times10^{-9} =$$

(acceleration)

$$-\frac{1}{\rho}\frac{\partial p}{\partial z} + 3.6\times10^{-5} - 10 + (30. + 30. + 0.3)\times10^{-11} \tag{3.7}$$

(vertical Coriolis) - (gravity) + (eddy viscosity)

The gravity term is 5 orders of magnitude larger than the order scaled terms and therefore must be balanced by the vertical pressure gradient. This is the hydrostatic equation:

$$\frac{\partial p}{\partial z} = -\rho g \tag{3.8}$$

When the geostrophic equations (3.5) and (3.6) are differentiated with respect to z:

$$f \frac{\partial (v\rho)}{\partial z} = \frac{\partial}{\partial x} \frac{\partial p}{\partial z} \tag{3.9}$$

$$f \frac{\partial (u\rho)}{\partial z} = - \frac{\partial}{\partial y} \frac{\partial p}{\partial z} \tag{3.10}$$

where f is the Coriolis term, $(2\Omega \sin\phi)$,

and $-\rho g$ is substituted for $\partial p/\partial z$ by the hydrostatic equation, then:

$$f \left(v \frac{\partial \rho}{\partial z} + \rho \frac{\partial v}{\partial z}\right) = - g \frac{\partial \rho}{\partial x} \tag{3.11}$$

$$f \left(u \frac{\partial \rho}{\partial z} + \rho \frac{\partial u}{\partial z}\right) = -g \frac{\partial \rho}{\partial y} \tag{3.12}$$

The Boussinesq approximation allows 3.11 and 3.12 to be reduced to:

$$f \rho_o \frac{\partial v}{\partial z} = - g \frac{\partial \rho}{\partial x} \tag{3.13}$$

$$f \rho_o \frac{\partial u}{\partial z} = - g \frac{\partial \rho}{\partial y} \tag{3.14}$$

The essence of the Boussinesq approximation is (1) that the vertical variation in density is neglected because it is $0(10^{-3})$ smaller than the mean density, (2) density is considered as a constant when it appears as a coefficient, and (3) the horizontal variation to density is retained when it is multiplied by the large gravitational acceleration term, where density variation is dynamically significant. For further explanation of the Boussinesq approximation and its uses and limitations, see Veronis (1973) and Stern (1975).

Equations 3.13 and 3.14 relate the vertical variation of velocity to the horizontal density gradient. The average horizontal density gradient can be determined between two standard hydrographic stations. If Equation 3.13 is expressed in terms of pressure instead of depth through the hydrostatic equation and specific volume (α) instead of density then

$$f \frac{\partial v}{\partial p} = - \frac{\partial \alpha}{\partial x} \tag{3.15}$$

The velocity difference between two isobars is Equation 3.15 integrated with respect to pressure, with the horizontal gradient expressed as a finite difference.

$$v_1 - v_2 = \frac{1}{fL} \left(\int_{p_1}^{p_2} \delta_B \, dp - \int_{p_1}^{p_2} \delta_A \, dp \right) \tag{3.16}$$

where L is the station separation and δ is the specific volume anomaly (SVA). Because specific volume, $\delta_{S,T,P}$ can be considered as two separate quantities, a large invariant field, $\delta_{35,0,P}$ and a variable field, δ, it is necessary to only consider the difference between the variable fields when calculating the horizontal density (specific volume) gradient. The integration of specific volume anomaly between isobars is dynamic height, and therefore 3.16 can be expressed as the familiar equation for determining relative normal velocity between two hydrographic stations

$$v_1 - v_2 = \frac{1}{fL} (\Delta D_b - \Delta D_a) \qquad (3.17)$$

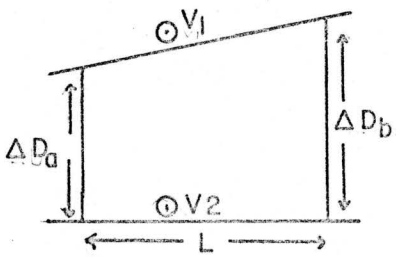

which was originally derived by H. Mohm in 1885 in a general formula, later expanded by Sandstrom and Helland-Hansen in 1903 (Sverdrup, et. al., 1942).

There are several restrictions to the application of the geostrophic method (Equation 3.17) when estimating the oceans' currents.

(1) This method relates only the geostrophic velocities to the pressure field. As the temporal (T) and horizontal length (L) scales in the horizontal equations of motions (Eqs. 3.3 and 3.4) decrease, the acceleration terms approach the size of the horizontal Coriolis terms. This change from an essentially geostrophic balance to a non-geostrophic balance occurs when $T \approx 2\pi/f$ or when the Rossby number, $R_o = \frac{U}{fL}$, is unity. $2\pi/f$ is the inertial period. More sophisticated investigations of the mutual adjustment of pressure and velocity fields by Rossby (1937, 1938), Cahn (1944), Bohin (1953), and Veronis (1956) demonstrated that the balance is essentially geostrophic at inertial periods and longer and non-geostrophic at shorter periods. Two major restrictions to the application of the geostrophic method arise due to the temporal scale of geostrophic motions.

Firstly, the pressure gradient is determined by calculating the dynamic height at two discretely sampled stations. If the time interval between the two stations is less than the inertial period, the dynamic height at the second station will not have changed significantly during the intervening period. Therefore, the difference between the two dynamic heights will accurately determine the average pressure gradient and therefore the average geostrophic velocity between the two stations. If, however, the time interval

between the two stations is greater than the inertial period, the dynamic height at the second station could have changed significantly during the intervening period. This can occur because the pressure field would have time to adjust to a changing geostrophic velocity field. Therefore, the dynamic height at the second station was determined in a pressure field different from the pressure field measured by the first station. Thus, the dynamic height difference between the two stations will not necessarily reflect the pressure gradient and the geostrophic velocity that did exist between the two stations. Just how much change could occur during the sampling interval is determined by the amount of variance in the pressure field in the region of the sampling period as compared to the longer-period (day and longer) variance in the pressure field.

Secondly, the motions at frequencies higher than f, i.e. internal waves, have pressure fluctuations associated with them. Since these pressure fluctuations are related to the velocities in a non-geostrophic manner, the individual estimates of dynamic height will be degraded, and therefore the estimates of the horizontal pressure gradient and the geostrophic velocities will be degraded.

(2) The pressure gradient determined by Equation 3.17 is the average gradient for the section. Therefore, the velocity calculated is a value averaged over the section and only the component normal to the section. This averaging, however, may be advantageous for it would smooth over the smaller scale motions which may not be of interest.

Equation 3.17 relates the pressure gradient to the velocity shear, thus a profile of relative velocities are determined and not absolute velocities.

(3) Navigational errors cause errors in the determination of relative positions between the stations, a d therefore causes errors in the measurement of L, the distance between stations. In the Labrador Sea, the Hudson had good relative positioning (within 100 m), but ship's drift due to wind and currents during the stations produced errors in L estimated as high as 5%.

Thus, the geostrophic method estimates from the pressure field, which contain contributions from non-geostrophic motions, a relative profile of velocities normal to the section, averaged over the stations' spatial separation and can be considered synoptic only if the stations were sampled at intervals less than the local inertial period.

Geostrophic velocities computed for a section are relative to a chosen reference level. The traditional pratice has been to assume a deep horizontal level of zero or constant velocity which extends across the entire section. From this "level of no motion" an absolute velocity profile can be established. With the advent of reliable current meters, the vertical shear between two or more current meters on the same mooring can be compared to the vertical shear estimated by the geostrophic method, thus providing a calibration of the geostrophic velocities. However, problems arise because direct current measurements and geostrophic current calculations are not directly comparable. Current meters measure absolute currents, both geostrophic and non-geostrophic, while geostrophic current calculations do not.

The high frequency variance due to the non-geostrophic motions in the current meters can be removed by low-pass filtering the velocity records. The velocities were resolved into components longitudinal and transverse to the hydrographic sections. Then the components were reduced to one-hour averages with a running mean filter. The data were then low-pass filtered using a digital filter which had a 50% power point at 1.2 cpd and a roll-off bandwidth of 0.6 cpd. The data were then decimated over eighteen points to achieve twelve-hour averages. The characteristics of the filter are shown in Figure 3.10. This filter removes almost all of the energy at the inertial frequency and higher, including the semi-diurnal tides, while allowing most of the energy at 0.5 cpd (2 days) and lower through. Thus, a velocity component from the current meter that is resolved in the same direction as those derived from the density field with a somewhat comparable temporal variance is achieved.

With the current meter measurements temporally filtered and averaged to obtain an equivalent time-average current as the geostrophic currents, the question of spatial equivalence remains. The point velocity of the current meter has to be spatially averaged over the horizontal separation of the station pair used to derive the geostrophic currents. When the horizontal spacing of the current meters is fine enough to resolve the scale of the velocity field, the spatial averaging of the current meters

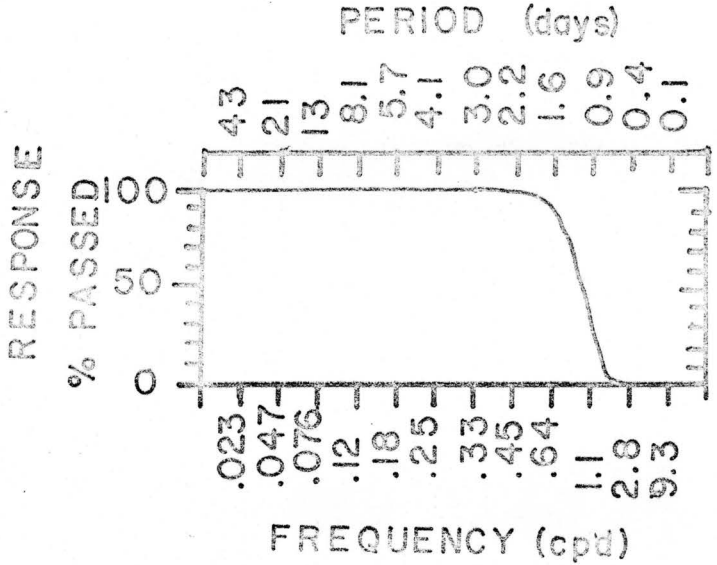

Figure 3.10 - Response characteristics of the low-pass filter used on the current meter records.

can be done accurately. Thus, for the station pairs which bracket a current meter, a reference velocity level is obtainable. However, in regions of narrow and intense currents the horizontal spacing of the current meters is often not fine enough to resolve the geostrophic velocity field. The velocity along the reference level has to be estimated.

Several schemes for estimating a reference level from current meter data for the purpose of comparing with geostrophic profiles have been used by investigators. Clarke and Reiniger (1973) used a linear interpolation scheme. The current meters' normal velocity components were linearly interpolated to establish a reference level for the station pairs that were between the current meters. For those station pairs at the ends of the mooring line which did not bracket a current meter, the end current meter's velocity was extrapolated. They used current meters 100 m off the bottom to reference the geostrophic velocities for the Gulf Stream. Warren and Volkmann (1968) avoided the problem by using a neutrally-buoyant float between each station pair. They, however, used an arbitrarily smoothed reference velocity along a common depth. Other schemes are possible in places where sharp horizontal velocity gradients exist over lengths comparable to the station separation. Since the current meter records at a point, it is likely in this case that it will be in either the region of high velocity or low velocity. Therefore it won't represent the average velocity that was derived from the geostrophic method, but an extreme for that interval. Thus, a more realistic current

profile should be determined that includes maximums and minimums which average to the original geostrophic values calculated. From this, a closer comparison can be achieved between the current meter velocity and the interpolated geostrophic profile.

The geostrophic velocity profiles for the five hydrographic sections were derived from the density fields. Three separate reference schemes were used to estimate the velocity profiles. The velocity was referenced to zero velocity at 1000 dbars, the current meters, as well as zero velocity at 1500 dbars for the deep sections. From the velocity profiles estimates of volume transports were made.

Two major sources of uncertainty arise in the construction of the velocity profiles adjusted to the current meters. The low-frequency variation in the current meter records is large at time scales comparable to the duration of the hydrographic sections. This makes the choosing of the appropriate reference velocity from the current meter difficult. Averaging over a slightly longer time period may reduce some of the uncertainty of the reference velocity. The error limits for a section were calculated using the extreme velocities that occurred during the hydrographic section. The second area where subjective interpretation introduces uncertainty into the velocity profiles is the choosing of an appropriate reference velocity for the station pairs which do not bracket a current meter. This problem is especially acute where the current widths are of the same magnitude as the station separation and therefore each station pair should be referenced separately. To minimize this

problem either of two simple schemes were used; linear interpolation and extrapolation when the current width was wider than the station separation, or the assumption of zero velocity at the reference level is left unaltered.

Geostrophic currents were calculated for the five longitudinal sections, Figure 2.8. The first section (stations 4-9) provided full depth coverage over the mooring array, but was done during the laying of the moorings, as a consequence the section took three days to complete. The next three sections (12-9, 19-17, and 19-21) were shallow (1000 m) casts just in the region of the two inshore moorings, 107 and 108. The last section (24-21, 25-30) included shallow stations in the region of the moorings and combined casts to the bottom at the stations from the outermost mooring, 109, to the center of the Labrador Sea. Table C shows the stations for each section, the distance between station pairs, the start time of the station, the time between start times of the stations, and the maximum common depth between the two stations for which geostrophic currents were calculated. The specific volume anomalies and the dynamic heights were derived at 10 dbar intervals for the CTD up traces and at 50 dbar intervals for the bottle casts. Where a station included a bottle cast, the dynamic height for the bottle cast was offset to match the dynamic height of the CTD trace at the depths where the two casts overlapped. This was to adjust the bottle cast integration from the surface down to the start of the bottle cast, which was near 2000 dbars. Geostrophic currents relative to the surface, and also adjusted relative to 1000 dbars, were calculated for each station pair, at 100 dbar intervals from the surface to 1000 dbars and every 200 dbars from 1000 dbars to the bottom of the cast. The estimated resolution of the geostrophic velocities is 10% when the velocity is greater than 1.0 cm/s and ±0.1 cm/s

TABLE C

HYDROGRAPHIC STATION PARAMETERS

STATION #	START TIME OF STATION (GMT) Dy Hr Mn	DISTANCE BETWEEN STATIONS km (±2 km)	TIME BETWEEN STATIONS hrs.	MAXIMUM DEPTH OF GEOSTROPHIC CURRENT CALCULATION dbars
Section 4-9				
4	63 01 45			
		21.6	4.4	1800
5	63 06 10			
		19.9	38.6	2500
6	64 20 48			
		24.6	6.0	2650
7	65 02 50			
		24.4	5.5	2650
8	65 08 20			
		25.3	11.7	2900
9	65 20 00			
Section 12-9				
12	66 09 00			
		32.6	3.0	1000
11	66 06 00			
		30.6	2.7	1000
10	66 03 20			
		70.1	7.3	1000
9	65 20 00			
Section 13-14				
13	66 11 30			
		33.1	3.1	1000
14	66 14 35			
Section 16-15				
16	66 20 23			
		35.9	3.0	1000
15	66 17 25			
Section 17-19				
17	66 23 00			
		32.1	2.9	1000
18	67 01 55			
		32.5	3.0	870
19	67 04 55			

STATION #	START TIME OF STATION (GMT) Dy Hr Mn	DISTANCE BETWEEN STATIONS km (±2 km)	TIME BETWEEN STATIONS hrs.	MAXIMUM DEPTH OF GEOSTROPHIC CURRENT CALCULATION dbars
Section 19-21				
19	67 04 55			870
		33.1	3.6	
20	67 08 28			1000
		31.3	3.2	
21	67 11 37			
Section 24-21, 25-30				
24	67 19 50			860
		15.5	2.5	
23	67 17 20			860
		32.8	3.0	
22	67 14 20			1000
		31.3	2.7	
21	67 11 37			1000
		69.0	19.0	
25	68 06 35			3000
		65.0	6.7	
26	68 13 20			3100
		63.8	7.2	
27	68 20 30			3350
		63.0	7.2	
28	69 03 45			3500
		62.1	6.4	
29	69 10 06			3500
		63.3	6.6	
30	69 16 45			

when the velocity is less than 1.0 cm/s. The 10% uncertainty in the horizontal separation, L, between the stations due to ship's drift is the major contribution to the error in the relative geostrophic velocities.

Section 4 - 9

Section 4-9 was the most complete section in terms of covering the entire depth range over the mooring line. It was, however, done over a period of three days concurrent with the laying of the current meter moorings. Thus, this section cannot be considered synoptic. The times of the current meter averages are the closest times to the station pair while not actually spanning the time interval between the taking of the stations.

Mooring 108 was laid two days after the two stations which would have bracketed it, 5 and 6. Mooring 109 was in place 18 hours after Stations 8 and 9. Stations 6 through 9 were combined CTD and bottle casts complete to the bottom, while Stations 4 and 5 were just CTD's to 1800 dbars. In order to reference the geostrophic velocities from Station Pair 5-6 to current meter 108,2480, Station 5 was extrapolated to the bottom. The cross section of specific volume anomalies, Fig. 3.11, was used for the extrapolation. The distance between contours of SVA were kept proportional to the spacing at Station 6. The upper bounds for the 0.000420 contour was the 0.000423 contour (not shown) from 5 to 6. The lower boundary was the bottom. This extrapolation scheme maintains the general change in the slope of the contours over the bottom 1000 m of the section. From the estimated values of SVA, the dynamic height was derived and a complete geostrophic velocity profile that bracketed 108,2480 was achieved.

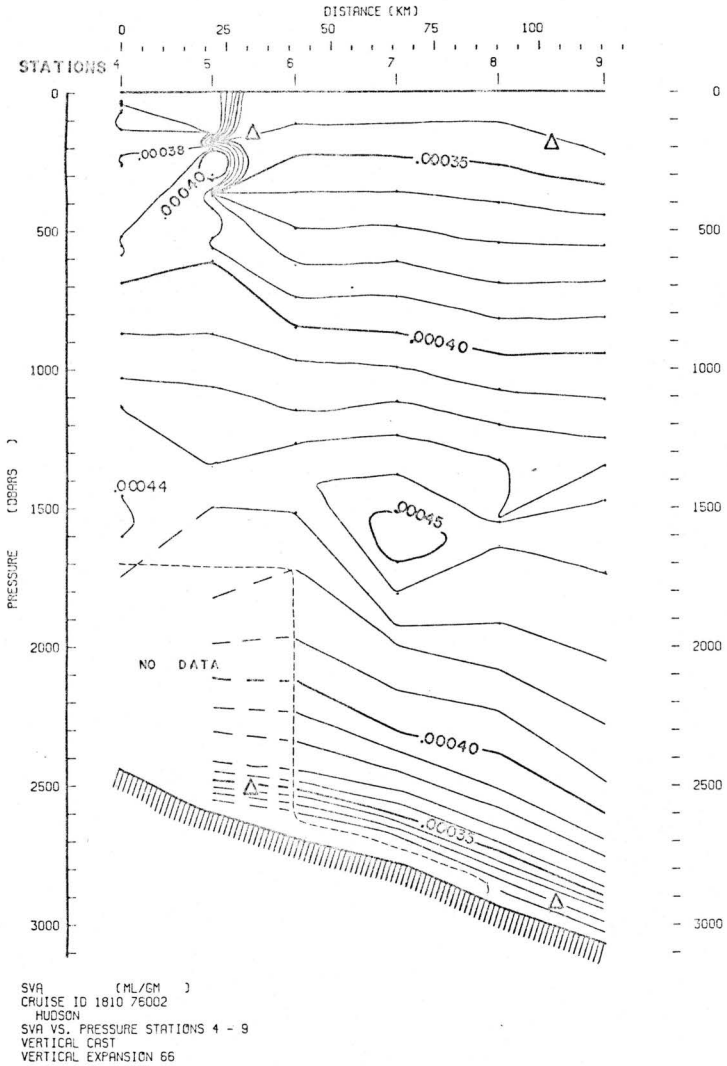

Figure 3.11 - Cross-section of specific volume anomalies for stations 4-9. Dashed contours are extrapolated values.

With the extension of Station 5 to the bottom, the two bottom current meters, 108,2480 and 109,2900 could be used to adjust the geostrophic velocities from this section. Station Pairs5-6 and 8-9 were adjusted directly to the 12-hour averages of the current meter velocity while Station Pairs 6-7-8 were adjusted to linearly interpolated values between 108,2480 and 109,2900. Station Pair 4-5 was adjusted at the deepest common level (1800 dbars) with Station Pair 5-6.

Twice in Section 4-9 the time interval between station pairs was approximately equal to (Sta. 8-9, 11.7 hrs.) or greater than (Sta. 5-6, 38.6 hrs.) the inertial period (14.4 hrs.). An estimate of variation in velocity due to geostrophic adjustments can be made from the low-frequency current meter energy. The temporal variance of low-frequency velocity at a current meter can be estimated from the frequency spectrum (Jenkins and Watts, 1968, p. 24) using Parseval's theorem,

$$\text{Variance} = E(\omega) = \int E \, d\omega$$

where ω is the frequency and E is the spectrum. The low-frequency variance of the velocity normal to the hydrographic sections between the inertial period (14.4 hrs.) and 100 hours is shown in Table D below.

TABLE D

THE LOW FREQUENCY VARIANCE AND VARIATION BETWEEN 1.52 CPD AND 0.244 CPD OF THE CURRENT METERS' VELOCITIES NORMAL TO THE HYDROGRAPHIC SECTION

CURRENT METER #	VARIANCE $E(\omega)$ (cm^2/s^2)	VARIATION $\sqrt{2E(\omega)}$ (cm/s)
108,160	237	22
108,2480	71	12
109,190	106	15
109,2900	16	6

TABLE E

THE COMPONENT OF VELOCITY NORMAL TO THE SECTION USED FOR REFERENCE OF THE GEOSTROPHIC VELOCITIES

STATION PAIR #	REFERENCE VELOCITY (CM/S) (ONSHORE) (OFFSHORE) MEAN MEAN	HIGH HIGH	LOW LOW	HIGH LOW	LOW HIGH	REFERENCE LEVEL (DBARS)
4-5	9.4	21.3	-2.7	21.3	-2.7	1800
5-6	10.1	22.0	-2.0	22.0	-2.0	2510 (108,2480)
6-7	9.3	19.5	-1.2	16.2	2.1	2650
7-8	8.1	16.3	-0.1	8.8	7.5	2790
8-9	7.0	13.0	1.0	1.0	13.0	2940 (109,2900)

The maximum and minimum reference velocities were based on the variation of the normal component of velocity between 16 hours and 4.1 days at 108,2480 and 109,2900, from Table D. Four combinations of maximum and minimum reference velocities are possible: high or low velocities occurring simultaneously at both onshore and offshore meters; or high velocities occurring onshore (offshore) in conjunction with low velocities offshore (onshore). The mean reference velocities were the low-pass 12-hour averages of the normal component of velocities from 108,2480 and 109,2900 nearest in time to the station pairs. These mean values were used in the construction of Fig. 3.12. The other station pairs not bracketing a current meter were interpolated, as before, from the two current meter values.

Figure 3.12

Geostrophic velocity (cm/s) for Section 4-9; adjusted to 10.1 cm/s at 108,2480 and 7.0 cm/s at 109,2900. The boxes contain the normal components of velocity (cm/s) from the current meters. Positive values are southward - out of the plane.

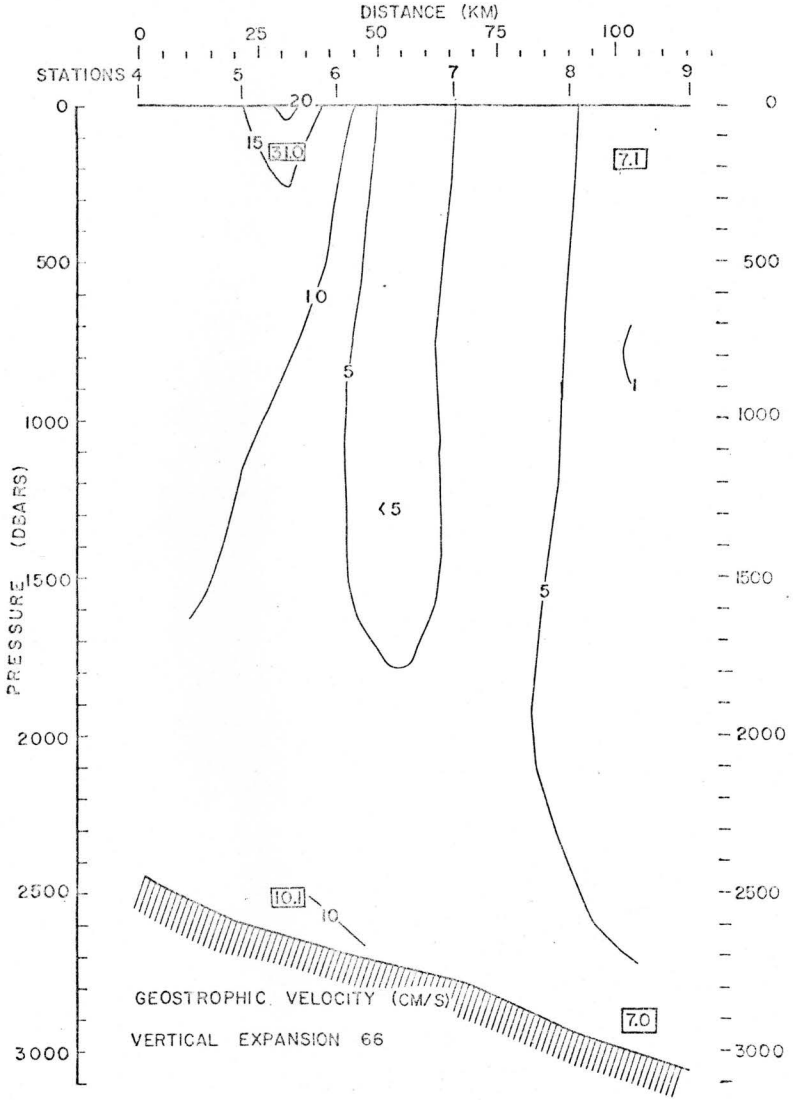
DISTANCE (KM)
0
25
50
75
100
STATIONS 4
5
6
7
8
9
0
500
1000
1500
2000
2500
3000
PRESSURE (DBARS)
20
15
5.1.0
7.1
10
5
<5
1
5
10.1
10
7.0
GEOSTROPHIC VELOCITY (CM/S)
VERTICAL EXPANSION 66

Transports for each station pair and for the section based on the different reference levels are shown in Table F. The first two reference levels were zero velocity at 1000 m and 1500 m, respectively. The last five columns are the transports based on the bottom current meters, 108,2480 and 109,2900 (see Fig. 3.12). The transports are based on the reference velocities given in Table E above.

The wide variation in the current meter velocities produces a very large range of possible transports. Despite the uncertainty, two points are evident (1) that the flow based on the current meters is considerably larger than the flow based on zero velocity at depth and (2) the flow has considerable variation over periods of a few days. This variation is investigated further in Section 3.5.

TABLE F

THE TRANSPORTS: SECTION 4-9

STATION PAIR	RANGE DBARS	SOUTHWARD TRANSPORTS (10^6 m^3/s) REFERENCE LEVELS							
		ZERO AT		CURRENT METERS					
		1000 DBAR	1500 DBAR	MEAN	HIGH	LOW	HIGH	LOW	108,2480 (INSHORE)
				MEAN	HIGH	LOW	LOW	HIGH	109,2900 (OFFSHORE)
4-5	0-1000	-0.06	0.13	2.5	5.0	-0.2	5.0	-0.2	
	1000-1800	-0.13	0.03	1.8	3.9	-0.2	3.9	-0.2	
	0-1500	--	0.21	3.7	7.5	-0.3	7.5	-0.3	
	1500-1800	-	-0.05	0.6	1.4	-0.1	1.4	-0.1	
	0-1800	-0.19	0.16	4.3	8.9	-0.4	8.9	-0.4	
5-6	0-1000	0.74	0.78	2.6	4.9	0.2	4.9	0.2	
	1000-2500	-0.02	0.04	2.8	6.3	-0.8	6.3	-0.8	
	0-1500	--	0.79	3.4	6.9	-0.2	6.9	-0.2	
	1500-2500	--	0.03	2.0	4.3	-0.4	4.3	-0.4	
	0-2500	0.72	0.82	5.4	11.2	-0.6	11.2	-0.6	

TABLE F (cont'd)

STATION PAIR	RANGE DBARS	SOUTHWARD TRANSPORTS (10^6 m^3/s) REFERENCE LEVELS ZERO AT 1000 DBAR	ZERO AT 1500 DBAR	CURRENT METERS MEAN	HIGH MEAN	LOW LOW	HIGH LOW	LOW HIGH	108,2480 (INSHORE) 109,2900 (OFFSHORE)
6-7	0-1000	0.01	-0.19	0.5	3.0	-2.1	2.2	-1.2	
	1000-2650	1.2	0.86	2.0	6.2	-2.2	4.7	-0.8	
	0-1500	--	-0.27	0.8	4.6	-3.0	3.3	-1.8	
	1500-2650	--	0.93	1.7	4.6	-1.3	3.6	-0.2	
	0-2650	1.2	0.66	2.5	9.2	-4.3	6.9	-2.0	
7-8	0-1000	0.16	0.53	2.1	4.1	0.1	2.3	2.0	
	1000-2650	-0.55	0.05	2.6	5.9	-0.6	2.9	2.3	
	0-1500	--	0.60	2.9	6.0	0.0	3.2	2.7	
	1500-2650	--	-0.02	1.8	4.0	-0.5	2.0	1.6	
	0-2650	-0.39	0.58	4.7	10.0	-0.5	5.2	4.3	
8-9	0-1000	0.08	0.05	0.4	1.9	-1.1	-1.1	1.9	
	1000-2900	0.49	0.42	1.1	4.0	-1.8	-1.8	4.0	
	0-1500	--	0.06	0.6	2.9	-1.7	-1.7	2.9	
	1500-2900	--	0.41	0.9	3.0	-1.2	-1.2	3.0	
	0-2900	0.57	0.47	1.5	5.9	-2.9	-2.9	5.9	
4-9	0-1000	0.92	1.30	8.1	18.9	-3.1	13.3	2.7	
	1000-bot	0.99	1.40	10.3	26.3	-5.6	16.0	4.5	
	0-1500	--	1.75	11.4	27.9	-5.2	19.2	3.3	
	1500-bot	--	1.30	7.0	17.3	-3.5	10.1	3.9	
	0-bot	1.92	2.69	18.4	-8.7	29.3	7.2	7.2	

Two regions of vertical shear occur in this section. The first region of vertical shear is between the cold, fresh water of the Labrador Current and the warmer (3.0°C and greater) offshore water. This can be seen between Stations 5 and 6 in the upper 500 m, see Fig. 3.11. The second region of vertical shear is in the bottom 200-300 meters. This is the southward flow of the core of the NWAB Water. The 2°C isotherm is a good indicator of the extent of this layer.

Section 4-9 was the only section which had a complete depth coverage in the region of the current meters for which a comparison can be made between the vertical shear of current meters, and the vertical shear of the geostrophic velocity profiles. However, the two station pairs (Sta. 5-6, 8-9) which bracketed the current meters had large sampling intervals, and in addition, the current meters were not in place until after the bracketing hydrographic stations were taken. Thus, a proper direct comparison is impossible, but a more general comparison is still possible.

The positive velocity difference (higher southward velocity at the surface than at the bottom) at Station Pair 5-6 was 6.7 cm/s between 160 and 2500 dbars. At Station Pair 8-9, the velocity difference in the geostrophic profile between 190 and 2900 dbars was -5.1 cm/s, see Fig. 3.12. The mean of the differences of the low-pass filtered 12-hour averages of velocity normal to the hydrographic sections between the entire records was 4.5 cm/s; std. dev. 18.3 cm/s for 108,160 and 108,2480. Between 109,190 and 109,2900 the mean was -11.3 cm/s, std. dev. 10.7 cm/s. Therefore, the geostrophic profiles had vertical shears that were consistent with the velocity differences between the current meters.

Section 12 - 9

This section was completed within 14 hours, and after the moorings were in place. The geostrophic velocity from Station Pair 11-10 was referenced at 160 dbars directly to the velocity at 108,160 of 24.0 cm/s. The interpolated value (12.7 cm/s) between 108,160 and 109,190 (7.1 cm/s) was used to reference Station Pair 10-9. Station Pair 12-11 was adjusted

at the greatest common depth (1000 dbars) with Station Pair 11-10. The volume transports above 1000 dbars on this section was (24 ± 10) x 10^6 m^3/s. The major source of uncertainty is in the low-frequency variation of the current meters. 108,160 ranged from a high of 31 cm/s to a low of 9.3 cm/s during the immediate preceeding and following 12-hour averages. In addition, the referencing of Station Pair 12-11 added still more uncertainty to this velocity section.

TABLE G

TRANSPORTS: SECTION 12-9

STATION PAIR	RANGE	SOUTHWARD TRANSPORT (10^6 m^3/s)	
	DBARS	1000 DBARS	CURRENT METERS
12-11	0-1000	0.09	7.1
11-10	0-1000	0.45	7.1
10-9	0-1000	0.27	10.0
Section 12-9	0-1000	0.81	24.2

Section 19-17

Station Pair 18-17 bracketed 108,160 so the twelve-hour and thirty-six-hour averages were used to adjust the geostrophic velocities. The normal component of the 12-hour averages of velocity from 108,160 was

9.3 cm/s just before this section, -12.3 during, and -7.4 following. The average over the thirty-six hours was -3.5 cm/s. Station Pair 19-18 was referenced to zero velocity at the bottom of the casts, 870 dbars. The resulting transport was $-0.8 \pm 3 \times 10^6$ m^3/s. based on the 36-hour average for the central value and the 12-hour averages for the limits.

Section 19-21

The twelve-hour average of the normal component of velocity at 108,160 was -7.4 cm/s during the time that this section was completed. The geostrophic velocity at 160 dbars from Station Pair 20-21 was -4.8 cm/s based on zero velocity at 1000 dbars. Thus there was good agreement between the geostrophic velocity and the current meter during this section. The preceeding (-12.3 cm/s) and following (-1.6 cm/s) twelve-hour averages from 108,610 were used to establish the error limits of the volume transports. The velocity profile for Station Pair 19-20 was based on zero velocity at the common bottom of the casts, 870 dbars. The resulting transport for this section was $(-1.1 \pm 2) \times 10^6$ m^3/s.

TABLE H

TRANSPORTS: SECTIONS 19-17 AND 19-21

STATION PAIR	RANGE	SOUTHWARD TRANSPORT (10^6 m^3/s)	
	DBARS	1000 DBARS	CURRENT METER
19-18	0-870	0.25 (870)	0.25
18-17	0-1000	-0.17	-1.0
Section 19-17	0-bot	0.08	-0.8

TABLE H (cont'd)

STATION PAIR	RANGE	SOUTHWARD TRANSPORT (10^6 m^3/s)	
	DBARS	1000 DBARS	CURRENT METER
Station Pair			
19-20	0-870	0.52 (870)	0.52
20-21	0-1000	-0.78	-1.6
Section			
19-21	0-bot	-0.26	-1.1

Section 24-21, 25-30

Section 21-30 was the last hydrographic section of the first phase of Hudson 76002. This section extended from the continental shelf break to the center of the Labrador Sea. The four inshore stations were shallow CTD casts along the mooring line. From Station 25, which corresponds in position with the outermost station of the first section - Station 9 to Station 30, the hydrographic casts were combined CTD and bottle casts to the bottom.

The basic method of referencing the velocity profiles was to zero the profiles at the bottom (1000 dbars) of the shallow stations and zero the profiles at 1500 dbars for the deep station pairs (Fig. 3.13). This scheme was in keeping with previous attempts at establishing velocity profiles in the Labrador Sea and with the idea of a mid-water velocity minimum. Three variations were tried from this basic scheme. The outermost station pairs were referenced to zero velocity at either 1000

dbars or 2000 dbars to check the sensitivity of the current profiles to the 'level of no motion'. In addition, the inshore stations were adjusted to the current meters from the basic reference scheme.

The offshore branch of the Labrador Current is evident in the velocity profiles at Stations 22-23-24, see Fig. 3.13. Smith, Soule, and Mosby (1937) noticed that the 1.0 cm/s contour extended as deep as 1500 dbars in some of their geostrophic sections. The limits for these station pairs were 0 to 2 cm/s at 870 dbars based on the assumption that the flow may have extended deeper than the bottom of the casts. Station Pair 22-21 bracketed 108,160. The agreement is quite good between the geostrophic velocity (-4.9 cm/s) at 160 dbars and the current meter velocity (-7.4 cm/s). When this section pair velocity is adjusted to -7.4 cm/s at 160 dbars the velocity at 1000 dbars is -2.5 cm/s. This northward flow is associated with the boundary between a parcel of Labrador Sea Water inshore of some Labrador Current Water, see Fig. 3.5. Offshore (Station Pair 21-25) a southward flow of Labrador Sea Water is reflected in both the geostrophic current and at 109,190.

In the offshore region a weak (<2 cm/s) northerly flow occurs in the surface waters. A deep bottom boundary southward current is also evident. The core (>4 cm/s) of this bottom current is water colder than 2.2°C (potential temperature) and fresher than 34.92 $^{o}/_{oo}$, see Figs. 3.5 and 3.6, which indicates that this deep southward flow is NWAB water. This agrees with the previous concepts of deep cyclonic circulation and is supported by the two deep current meters further inshore. The magnitude of these currents change very little (<1 cm/s) when the reference level is raised to 1000 dbars or lowered to 2000 dbars. This indicates that there is a relatively extensive mid-water minimum velocity shear layer associated with the NEAD water.

Figure 3.13

Geostrophic velocity (cm/s) for sections 24-21, 25-30; adjusted to zero velocity at 1000 dbars inshore (sta. 24-21-25) and 1500 dbars offshore (sta. 25-30). The boxes contain the normal components of velocity (cm/s) from the current meters. Positive values are southward - out of the plane.

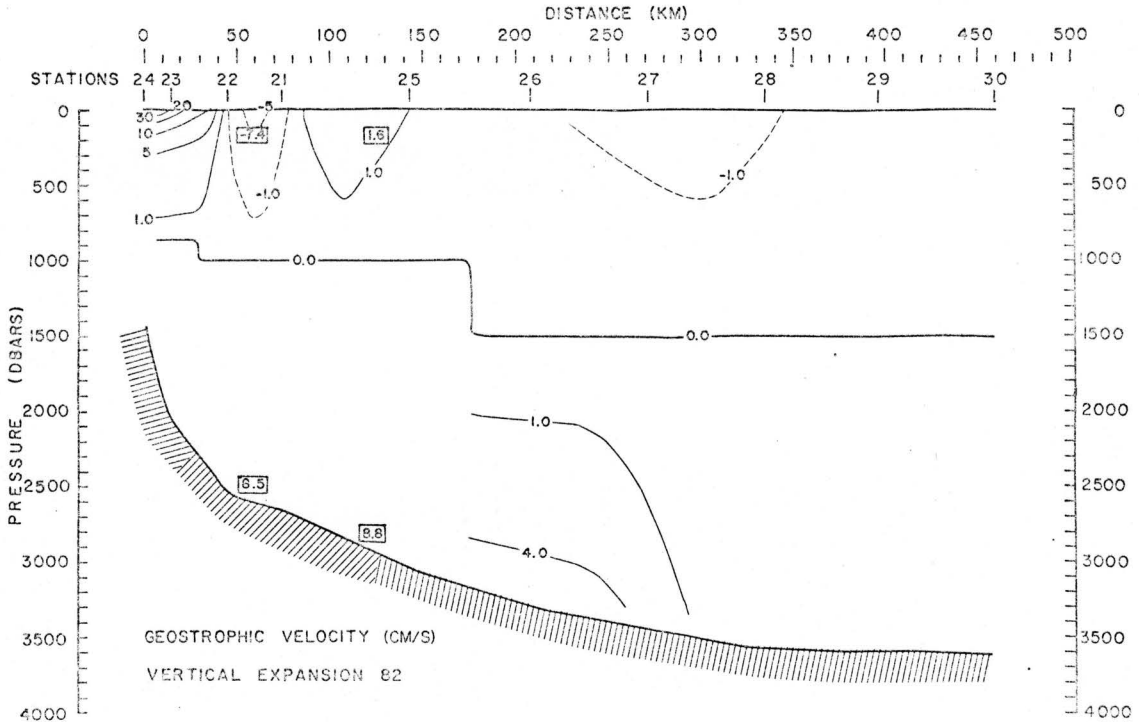
DISTANCE (KM)
0
50
100
150
200
250
300
350
400
450
500
STATIONS 24 23 22 21 25 26 27 28 29 30
PRESSURE (DBARS)
0
500
1000
1500
2000
2500
3000
3500
4000
30
20
10
5
-5
-7.4
1.6
1.0
-1.0
1.0
-1.0
0.0
0.0
1.0
4.0
6.5
9.8
GEOSTROPHIC VELOCITY (CM/S)
VERTICAL EXPANSION 82

The transport above 1500 dbars for 24-21-25 was 2.2±1 x 10^6 m^3/s. The offshore (Stations 25-30) transport above 1500 dbars was -0.5±0.3 x 10^6 m^3/s and below 1500 dbars 4.6±1 x 10^6 m^3/s.

TABLE I

TRANSPORTS: SECTION 24-21, 25-30

STATION PAIR	RANGE	SOUTHWARD TRANSPORT (10^6 m^3/s) REFERENCE LEVEL	
	DBARS	1000 DBARS	1500 DBARS
24-23	0- 860	0.88 (860)	--
23-22	0- 860	0.94 (860)	--
22-21	0-1000	-0.79	--
21-25	0-1000	1.18	--
25-26	0-1000	-0.02	0.04
	1000-3000	1.70	1.83
	0-1500	-0.02	0.07
	1500-3000	1.70	1.80
	0-3000	1.68	1.87
26-27	0-1000	-0.27	-0.53
	1000-3100	2.40	1.86
	0-1500	-0.20	-0.58
	1500-3100	2.33	1.91
	0-3100	2.13	1.33
27-28	0-1000	-0.43	-0.63
	1000-3350	0.47	-0.05
	0-1500	--	-0.67
	1500-3350	0.04	-0.68
28-29	0-1000	0.02	-0.24
	1000-3500	1.15	0.61
	0-1500	--	-0.30
	1500-3500	--	0.67
	0-3500	1.17	0.37
29-30	0-1000	0.19	0.22
	1000-3500	0.24	0.31
	0-1500	--	0.36
	1500-3500	--	0.17
	0-3500	0.43	0.53
24-25	0-1000	2.21	
25-30	0-1000	-0.51	-1.14
	1000-bot.	5.96	4.56
	0-1500	--	-1.12
	1500-bot.	--	4.54
	0-bot.	5.45	3.42
24-30	0-1000	1.70	

3.4 Comparison of Transports with Previous Estimates

Previous estimates of transport for the offshore branch of the Labrador Current have been based solely on geostrophic velocities. Virtually all of the previous work was done during the summer and early fall. From bottle casts, Smith, Soule, and Mosby (1937) calculated geostrophic velocities and transports relative to the 1500 dbar level. During July - August of 1928, 1931, and 1933 they did two sections perpendicular to the Labrador coast which were 40-80 km north (Section 'L') and 40 km south (Section 'M') of the hydrographic sections done by Hudson in 1976. They reported an average southward net transport for the Labrador Current for each of the five years. The net southward transport for the Labrador Current and the southward transport along the slope for Sections 'L' and 'M' are summarized below in Table J.

TABLE J

TRANSPORTS: MARION AND GENERAL GREENE'S SECTIONS "L" AND "M"

	SOUTHWARD TRANSPORT (10^6 m^3/s)			
YEAR	LABRADOR CURRENT	SECTION 'L'	SECTION 'M'	M:L
1928	5.06	4.66	4.24	0.91
1931	1.31	4.10	2.78	0.68
1933	7.60	2.79	6.70	2.18
1934	4.22			
1935	4.24			
ave.	4.57			

The ratio of transport of Section 'M' to Section 'L' indicates that there may exist a large variability in the calculated geostrophic transports for the Labrador Current over a distance of 80 to 120 km. The two sections were taken from one to three days apart, so the variability was either over the distance or short time scales.

From 1948 to 1969 the U.S. Coast Guard maintained a standard hydrographic section from South Wolf Island, Labrador to Cape Farewell, Greenland. The section was across the southern end of the Labrador Sea. The 22-year mean for the southward flow of the Labrador Current computed by the geostrophic method relative to zero velocity at 1500 dbars was 5.62 million m^3/s, with a standard deviation of 1.64 million m^3/s. The extrema were 2.74 and 10.22 million m^3/s, Moyniham and Anderson (1971). Most of the measurements were done in July and August.

Kuldo (1973) estimated a flow of 6.5 million m^3/s in November of 1971 along the South Wolf Island - Cape Farewell line for the Labrador Current above 1000 dbars.

The hydrographic section from the 1976 Hudson cruise that was most complete in terms of covering the area over the slope region was Section 4-9. The transport above 1500 dbars based on the 1500 dbar level was 1.8 million m^3/s. Section 24-25 geostrophic net southward transports above 1000 dbars based on 1000 dbar reference level was 2.2 million m^3/s. These transports are less than the previously published values which are in the 4 to 5 million m^3/s range. The most plausible explanation for the lower calculated transports is the lack of stations across the full width of the offshore branch of the Labrador Current. While velocities approaching the maximum values reported by Smith, Soule, and Mosby were calculated, stations were not taken on up the shelf. Thus, only a portion of the current was probably measured, resulting in the lower transports.

Swallow and Worthington (1969) tracked five neutrally buoyant floats in conjunction with a hydrographic survey in the Labrador Sea by the Erika Dan during March, 1962. They estimated a cyclonic circulation of 10 million m^3/s in the Labrador Sea below 1200 dbars. The range of southward transport on the Labrador side was from 5.4 to 15.6 million m^3/s. Transports from the Hudson 1976 cruise below 1500 dbars relative to 1500 dbar for the combined section of Stations 4-9 and 25-30 was 6×10^6 m^3/s, Tables F and I. The transport below 1000 dbars referenced to zero velocity at 1000 dbar was 7×10^6 m^3/s. Section 4-9 adjusted to the bottom current meters (108,2480; 109,2900) and combined with Section 25-30 with zero velocity at 1500 dbars the net southward transport below 1500 dbars was $12 \pm 6 \times 10^6$ m^3/s. These values agree with Swallow and Worthington's transport estimates for deep water.

3.5 Variability of the Volume Transports

In order to compare the volume transports between sections, a cross-section common to all five sections was used. This common section was from 0-1000 dbars and included just the three stations which bracketed Moorings 107 and 108. Sections 19-17 and 19-21 remained unchanged, while the other three sections consisted of stations: 4-6, 12-10, and 23-21. The volume transport above 1000 dbars based on the velocity profile adjusted to zero at 1000 dbars and to 108,160 is given below in Table K.

TABLE K

TRANSPORT: THE COMMON SECTION

SECTION	TRANSPORT (10^6 m^3/s)	
	0/1000	108,160
4-6	0.7±0.2	8±4
12-10	0.5±0.1	9±5
19-17	0.1±0.1	-2.5±1.5
19-21	-0.3±0.1	1±2
23-21	0.2±0.1	0±2

The variation in time of the transport from this common section is given in Figure 3.14.a. Despite the large error margins, it is evident that the total flow and the baroclinic portion of the flow was high during days 63-65 and fell to zero or a slightly reversed flow during Day 67. The peak-to-peak variation in the baroclinic transport for the common section is of the magnitude $1.0\pm0.2\times10^6$ m^3/s which is considerably smaller than the peak-to-peak variation in total transport of $10\pm5\times10^6$ m^3/s.

The variation in baroclinic velocity at the five station pairs which bracketed 108,160 showed changes in velocity at the surface of 20 cm/s and at 160 dbars of 12 cm/s. The variation in baroclinic velocity can be accounted for by a shifting of the horizontal distribution of baroclinic velocity. The velocity profiles typically show a decrease in southward baroclinic velocity offshore of approximately 0.4±0.2 cm/s·km at the surface and 0.2±0.1 cm/s·km at 160 dbars, e.g. see Fig. 3.12. The distance of the +5 cm/s isotach at the surface from the innermost station (24) ranged from 28±5 km to 77±10 km, Fig. 3.14.c. This indicates a

Figure 3.14

Variation with time of:

(a) The volume transports at the common section based on 108,160 - the crosses; the volume transports of the common section based on zero velocity at 1000 dbars, the horizontal lines. The vertical bars are the error margins and the horizontal bars incompass the time (stations) of the sections. Volume transports are in 10^6 m^3/s. Positive is southwards.

(b) The geostrophic velocity (cm/s) at the surface based on zero velocity at 1000 dbars for the station pairs which bracketed 108 - the open circles; and the 12-hour averages of low-passed filtered component of velocity normal to hydrographic section from 108,160 - the dots connected by lines. Positive values are southwards.

(c) The distance (km) offshore from Station 24 of the + 5 cm/s isotact at the surface based on the geostrophic velocities (zero velocity at 1000 dbars). The horizontal lines represent the time (and stations) over which the values were determined, and the vertical bars are the error margins.

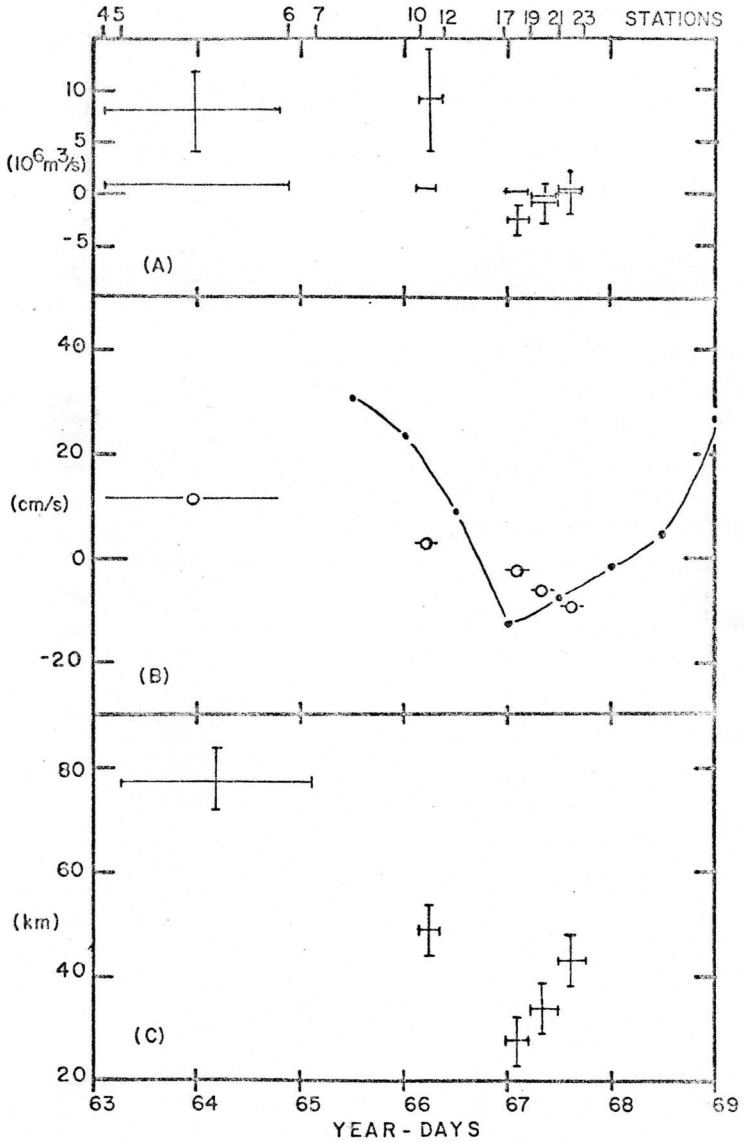
4 5
6 7
10 12
17 19 21 23
STATIONS
10
5
0
-5
($10^6 m^3/s$)
(A)
40
20
0
-20
(cm/s)
(B)
80
60
40
20
(km)
(C)
63
64
65
66
67
68
69
YEAR - DAYS

50±10 km horizontal shifting of the baroclinic velocity field over the period of the five hydrographic sections, (5 days). Thus, a displacement of 50±10 km on-offshore of the baroclinic velocity field would produce a 20±10 cm/s change in velocity at a fixed point on the surface, see Fig. 3.14.b, and 10±5 cm/s change at 160 dbars. This displacement could, therefore, account for the variation in baroclinic velocity observed at the station pairs which bracketed 108,160. In addition, the total velocity, as given by normal component of the 12-hour averages from 108,160, also varied widely over this same period and in phase with the baroclinic velocity. However, the variation in baroclinic velocity and transport could not account for all of the variation in total velocity and transport. Thus the rest of the variation must be due to barotropic variations in velocity and transport. The only other work in the Labrador Sea (Swallow and Worthington, 1969) which combined geostrophic velocity profiles with direct current measurements support the suggestion of a large barotropic component of flow (see their Fig. 7). Thus, a wide variation in transport over a few days' time is apparently real and due to the baroclinic velocity field and the barotropic velocity field varying approximately in phase.

CHAPTER 4 - VARIABILITY IN THE OFFSHORE CURRENTS

4.1 Introduction

Time-dependent variations occur over a large range of periods and spatial scales in the oceans. The scales range over twelve decades from fractions of a second to millennia. The oceanographic phenomena have spatial scales spanning nine decades from centimeters to tens of thousands of kilometers. The time and space scales observed are bounded by the instruments used to sample the system. Temporal variations with periods less than the Nyquist period, $2\Delta t$ where Δt is the sampling interval, are not resolved. The maximum resolvable variations are limited by the length of the record and the significance is determined by the noise level compared to the signal strength. The current meters recorded at 10-minute intervals for one month. Therefore, temporal variations between 20 minutes and approximately a fortnight were observable. The horizontal separation between current meter moorings and hydrographic stations will determine the resolution of horizontal spatial scales. The station separation was approximately 30 km and the coverage in the offshore direction extended 450 km. The repeated hydrographic sections gave an indication of variability over a period of several days.

The variations in the dynamic and thermodynamic states (currents and temperature and salinity) in the oceans are due to many different non-steady processes. These processes occur at different time and space scales. In general, larger temporal scales are associated with longer spatial scales. While the processes interact across all time and

space scales it is not possible to analyse all of the interactions. Some of the processes occur outside the limits of the observations, others are too weak and almost all are too complex to be understood completely. As a result, a major tool has been developed in the geophysical sciences; the conceptual model. This type of model attempts to reproduce the predominant characteristics of a distinctly identifiable phenomenon by simplifying the physics. While the conceptual model is incomplete dynamically, the distillation of observable phenomena by simple models into the basic physical processes is the first necessary step in understanding the system of interest.

The time scale of the features observed in March 1976 included internal waves, tidal and inertial motions, and low-frequency fluctuations. The separation of phenomena is by frequency. Internal waves occupy a time span between the maximum local buoyancy frequency, N, and the half-pendulum day, f. Tidal and inertial motions occur between 12 and 24 hrs. Below a day, low-frequency variability was observed. Two representative variance conserving spectra are presented in Fig. 4.1. Conceptual models were used to identify the processes responsible for the low-frequency fluctuations observed in the current meter records and hydrographic sections. Simple harmonic analysis was used to analyse the tidal and inertial motions. The internal wave motions were not investigated.

Figure 4.1

The variance conserving spectra (Frequency * Spectrum versus Frequency) for the north-south components of velocity from (a) 108,160 and (b) 108,2480. The spectra were determined by the standard spectral analysis package at the Bedford Institute (Dobson et al., 1974) which uses the fast Fourier transform technique. The 10-minute data were analyzed and filtered in 3 non-overlapping blocks of 1024 samples each and the spectral estimates were derived from averages of the Fourier coefficients over all three blocks. The vertical error bars are the standard deviations of the spectra estimates among the 3 blocks. The horizontal bars are the bandwidths. Note, that the ordinates have different scales. The abscissas are marked in frequency (cycles per day), period (day, hours, or minutes), and by the associated types of motions.

PERIOD
100.d
10.d
1.0day
1hr
20min
LOW-FREQUENCY MOTIONS
K_1 f M_2
N
INTERNAL WAVES
U(108, 160M)
FREQUENCY * SPECTRUM (CM²/S²)
500.
400.
300.
200.
100.
0.0
0.01
0.1
1.0
10
100
CPD
FREQUENCY
U(108, 248M)
FREQUENCY x SPECTRUM (CM²/S²)
200.
160.
120.
80.
40.
0.0

4.2 Tidal and Inertial Motions

The motions between 12 and 24 hours were dominated by surface (barotropic) and internal (baroclinic) tides, and inertial motions, see Fig. 4.1. The major semi-diurnal tidal component in the Labrador Sea is the principal lunar component, the M_2 tide, which has a period of 12.42 hours. The major diurnal tidal constituent is the luni-solar diurnal, the K_1, period 23.93 hours, (Godin, 1966). The tides along the Labrador Coast are principally semi-diurnal, (Dohler, 1966). The inertial period at the latitude of the mooring array is 14.4 hours.

The amplitudes and phases of the M_2 and K_1 tidal currents were derived over the entire records by the least-squares fit of sines and cosines at each frequency, see Fig. 4.2 and Table L. Two models are used to predict the barotropic tides and currents for comparison with the observed tidal currents. The first model is a simple continuity model of the onshore currents produced by the tide on the shelf co-oscillating with the deep ocean. The second model is Godin's (1966) two-dimensional numerical model of the tides of the Labrador Sea and Baffin Bay.

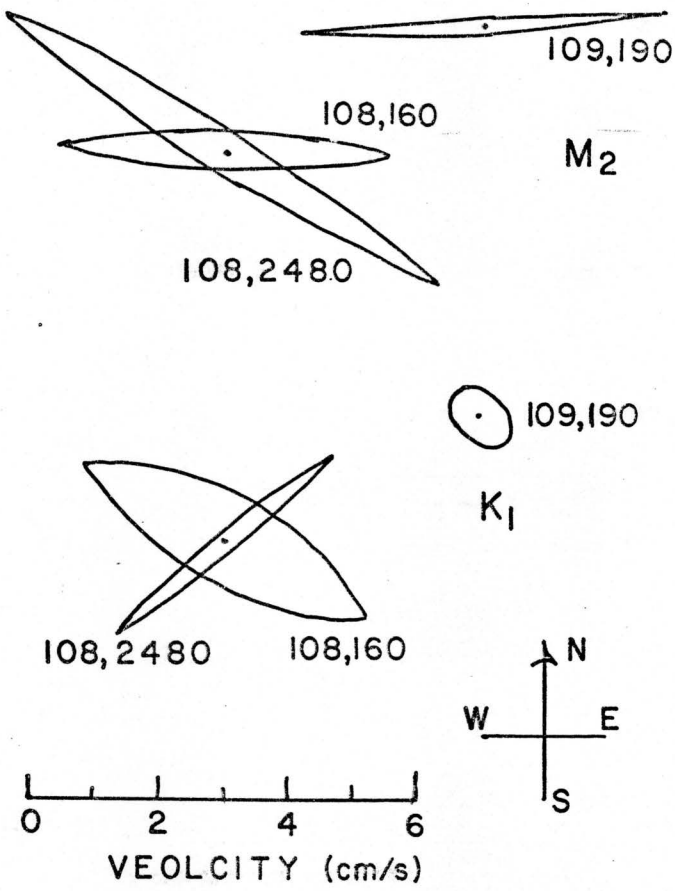

Figure 4.2 - The M_2 and K_1 tidal current amplitude ellipses for 108,160; 108,2480; and 109,190 derived from the entire records.

TABLE L

TIDAL AND INERTIAL ELLIPSES DERIVED FROM THE ENTIRE RECORD

The phase of the tide is the phase lag with respect to the equilibrium tide for the Greenwich Meridian. The phase for the inertial frequency is relative to the mid-point of the record.

	AMPLITUDE MAJOR (cm/s)	AMPLITUDE MINOR (cm/s)	PHASE OF MAJOR AXIS (Deg)	DIRECTION OF MAJOR AXIS (Deg)
108,2480				
M_2	4.1	0.3	235	301
K_1	2.3	0.2	351	230
Inertial	1.8	0.1	174	313
Length of record = 27.8 days centered at Day 78; 17.8 hr.				
108,160				
M_2	2.7	0.3	244	272
K_1	2.6	0.7	263	299
Inertial	1.2	0.9	109	304
Length of record = 27.8 days centered at Day 78; 17.4 hr.				
109,190				
M_2	2.9	0.1	264	266
K_1	0.5	0.4	217	172
Inertial	1.5	0.6	344	224
Length of record = 26.6 days centered at Day 79; 2.6 hr.				

Estimates of the amplitude of deep-ocean on-offshore barotropic tidal currents can be determined from the volume of water displaced on the shelf each tidal cycle, which equals a horizontal displacement in the deep ocean due to continuity. To estimate the volume of water displaced on the shelf, Defant's (1961) equation for a co-oscillating tide was used:

$$\eta = a_t \frac{\cos kX}{\cos kL} \cos \omega_t t \tag{4.0}$$

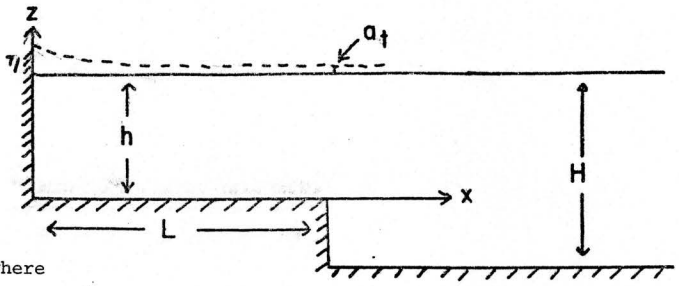

where

η = the deviation of sea level from the undisturbed sea surface

a_t = deviation from the undisturbed sea surface at the shelf break (X=L)

L = length of the shelf

h = depth of the water over the shelf

ω_t = $2\pi/T$ where T is the tidal period; the tidal frequency

k = $\omega_t/\sqrt{gh}$ the shallow water wavenumber

g = 982 cm/s^2

t = time

The volume of the tidal prism per unit width is:

$$Vol = \int_0^L \frac{a_t \cos kX}{\cos kL} \cos \omega_t t \, dx \tag{4.1}$$

$$= \frac{a_t \sin kL}{k \cos kL} \cos \omega_t t \tag{4.2}$$

The rate of change in volume over a tidal cycle is therefore:

$$\frac{d(Vol)}{dt} = \frac{-\omega_t a_t \sin kL \sin \omega_t t}{k \cos kL} \qquad (4.3)$$

which equals by mass conservation the deep ocean volume transport

$$= U H \sin \omega_t t \qquad (4.4)$$

Therefore,

$$U = \frac{-\omega_t a_t}{kH} \tan kL \qquad (4.5)$$

The Labrador Shelf in the area of Hopedale is 125±25 km wide and the water depth is 300±100 m. 'η' the amplitude of the tides at the coast was between 2.4 and 3.7 feet (0.73 to 1.13 m) for the semi-diurnal and 0.5 feet (0.16 m) for the diurnal tides. The tidal amplitudes and phases for Hopedale were obtained through MEDS, courtesy of D. Greenberg. The predicted barotropic currents due to the semi-diurnal tides are 0.4 to 0.9 cm/s at 108 and 0.3 to 0.8 cm/s at 109. The predicted diurnal barotropic tides are an order of magnitude less; 0.05 to 0.07 cm/s at 108 and 0.04 to 0.06 cm/s at 109.

The phase of the onshore currents at the shelf break will occur in phase with the change in volume (Eq. (4.5)). The phase will therefore be 90° before the high tide at the coast. Thus, the predicted phase of the barotropic currents at the shelf break relative to the equilibrium tide at GMT was 206° for the M_2 and 76° for the K_1.

The amplitudes and phases of the onshore (240°T) and alongshore (330°T) velocity components for four-day blocks and for the entire current meter records are shown in Table M. Four-day blocks were used to achieve one full cycle separation between the inertial and the tidal frequencies. When less than a cycle separates two frequencies, leakage of energy between the two occurs. The amplitudes of the M_2 onshore tidal currents ranged from 1.0 to 7.1 cm/s which are always greater than the predicted currents. However, the K_1 tidal currents were larger than the predicted currents. The phases of the tidal current also exhibited wide variations and were generally not in agreement with the predicted phases. This indicates that extrapolation of the tidal current in the far offshore from coastal tidal heights and phases is very unlikely to give a good indication of the offshore tidal currents. The wide variation in both the amplitudes and phases is likely due to the presence of baroclinic modes of the tides.

TABLE M

THE ALONGSHORE (NORTHWARDS) AND ONSHORE (WESTWARD) VELOCITY COMPONENTS OF THE M_2 AND K_1 TIDAL CURRENTS FOR FOUR-DAY BLOCKS AND FOR THE ENTIRE RECORDS

Amplitudes are in cm/s and phases are relative to the equilibrium tide at the Greenwich Meridian.

	M_2				K_1			
	ALONGSHORE (330°T)		ONSHORE (240°T)		ALONGSHORE (330°T)		ONSHORE (240°T)	
	AMP	PHASE	AMP	PHASE	AMP	PHASE	AMP	PHASE
108,2480	3.3	196	2.3	216	1.4	69	1.4	312
	0.9	31	1.0	346	0.8	332	3.0	329
4-day blocks	5.4	243	1.5	215	2.7	259	8.0	328
	7.6	223	3.3	223	1.3	111	2.7	108
	2.3	227	2.9	237	0.7	123	1.2	357
Entire	2.5	234	0.4	191	1.9	242	2.3	351

TABLE M (cont'd)

	M_2				K_1			
	ALONGSHORE (330°T)		ONSHORE (240°T)		ALONGSHORE (330°T)		ONSHORE (240°T)	
	AMP	PHASE	AMP	PHASE	AMP	PHASE	AMP	PHASE
108,160	2.2	226	2.2	144	3.0	191	4.6	312
4-day blocks	2.1	65	5.6	6	2.4	270	2.1	91
	4.2	265	2.8	301	2.0	185	2.4	300
	5.5	224	3.7	213	1.9	266	4.2	216
	2.2	248	6.6	236	6.5	237	6.9	196
	0.9	355	7.1	338	3.5	244	3.9	70
Entire	1.4	256	2.2	272	2.3	240	1.4	239
109,190	1.5	210	2.2	209	2.1	37	3.0	8.0
4-day blocks	3.6	270	5.6	319	3.4	245	0.8	187
	3.1	257	1.6	151	1.7	254	1.7	188
	1.5	123	1.7	200	5.4	274	2.1	300
	2.5	273	2.3	33	1.2	240	2.0	170
	2.0	345	2.7	113	2.5	271	2.3	276
Entire	1.4	267	0.6	6	2.5	259	0.5	207

Variation in the strength, phase, and direction of the baroclinic tides is due to several factors. Firstly, four-day blocks are not long enough to separate the principal lunar and solar constituents, therefore, a fortnightly modulation of the M_2 tide can be expected. Secondly, the barotropic tides force water up and down the sloping bottom everywhere. A generation site of the internal (baroclinic) tides occurs when the water is forced in a plane tangent to the ray path for internal waves at that frequency. This will occur only when the bottom slope and the density profile are just right. Changes in the water masses and currents will change the site of generation. In addition to changes in the site of generation, the ray paths of the internal waves will be refracted and

reflected by the density profile, velocity shears, as well as the surface and bottom. Changes in these factors will move the ray paths into and out of the region of the current meters. This will result in the variation of amplitude, phase, and direction of the tidal signal from the steady level of the barotropic tides. Clearly, this is what is shown.

Godin (1966) investigated the M_2 and K_1 tides of the Labrador Sea, Davis Strait, and Baffin Bay system. He estimated the cotidal lines and amplitudes based on coastal observations to compare with a barotropic model composed of three rectangular basins. From the model for the M_2 tide, he predicted cotidal lines and amplitudes, plus tidal currents and the phases of the currents. He was unable to obtain a solution for the K_1 tide, and considered that the K_1 currents were insignificant everywhere in the sea except in Davis Strait. At the equivalent position of the mooring, the M_2 currents were 3-7 cm/s back and forth parallel to the coast. The phase of the northward currents was 150-200°. The observed alongshore (330°T) M_2 velocities ranged from 0.9 to 7.6 cm/s with phases of 234-267° (Table M). This is in good agreement with Godin's prediction of velocity, but the observed currents lag Godin's currents by 50°-100°. The observed K_1 velocities ranged from 0.8 to 8.0 cm/s, which certainly was not insignificant. The K_1 tidal ellipses from the entire records of 108,160 and 109,190 were clockwise, while 108,2480 was rectilinear. The clockwise rotation of the current vectors is in agreement with simple Kelvin wave theory, which is what Godin used to model the tides. This suggests that the tides along the Labrador Slope contain portions from both models plus variations and effects due to the topography and baroclinic modes.

Inertial-period motions have been observed in a wide variety of places in the oceans (Webster, 1968). These motions are the balance between acceleration and the Coriolis term. Their period of 12 hr/sin (latitude), is the maximum period for internal waves. Inertial oscillations are transient phenomena thought to be generated by fluctuations in the winds or atmospheric pressure. The inertial period at the latitude of the mooring array is 14.4 hours. The currents at this period derived from four-day blocks of current meter data had amplitudes of 1-6 cm/s for the major axis and 0-2.5 cm/s for the minor axes. While there was energy at the inertial period, the currents were low and didn't constitute a major signal in the current records.

4.3 Features of the Low Frequency Fluctuations

In the spectra of alongshore velocity at the current meters on #108, Fig. 4.1, as well as the other spectra which are not shown, e.g. on-offshore velocity, temperature; the largest variance occurs at frequencies lower than 1.0 cpd. That the low-frequency motions dominated the spectra is a clear indication of their importance to the dynamics. But, before attempting to describe the dynamics, the features of the low-frequency motions are first investigated by three separate techniques.

4.3.1 Horizontal Hydrographic Sections

Four CTD stations were taken transverse to the mooring line and the other hydrographic lines to provide coverage of the temperature-salinity distribution along the slope. When these four stations (13 to 16) are combined either with the three stations measured immediately before (10 to 12) or the three stations measured immediately after (17 to 19), two equivalent two-dimensional spatial maps are possible; Section 'a' (Sta. 10-16) and Section 'b' (Sta. 13-19). The elapsed time between

a station in Section 10-12 and the station in the same position in Section 17-19 was 20 hours. Thus, the short-term variations in the horizontal distribution of temperature and salinity, along with the dynamic topography can be investigated.

A word of caution on contouring should be noted here. When four stations are located at the four corners of a square with two minimums and two maximums diagonal from each other, an ambiguity occurs. Either a depression can extend across the square and separate the two maximums or a ridge can separate the two minimums, as in the diagram below.

The result is a 90° shift of the direction of the contours, at the discretion of the person who did the contouring.

A ridge of relatively warm (>3.2°C), relatively saline (>34.82°/$_{oo}$) water extended NW-SE near Mooring 107 at 160 dbars, see Figures 4.3a and 4.3c. This same feature is present in the second section, Figures 4.3b and 4.3d, 10-15 km to the southwest near Station 19. Ten to fifteen kilometers northwest of Station 11 was water of the same T-S characteristics (3.25°C, 34.84-34.85°/$_{oo}$) as that found later at Station 18. Water with the same T-S characteristics as those at Station 17 were found early at Station 11. The displacement of the temperature-salinity field at 160 dbars suggested movement of water that was first to the northeast, then southeast, and then finally to the southwest. This suggested movement can be compared with the current observations at 108,160.

Figure 4.3

Horizontal sections of potential temperature at 160 dbars - a,b; salinity - c,d; and dynamic height - e,f; for sections 'a' stations 10-16 and 'b' stations 13-19. The potential temperature sections include the temperature from 108,160 adjusted to potential temperature from the nearby CTD profiles. The dynamic height (cm) is of the surface from 870 dbars. A conversion scale of dynamic height contour separation to geostrophic velocity is provided. The arrows on the dynamic height contour indicate the direction of flow provided zero velocity at 870 dbars. The progressive vector diagram of 108,160 from day 67:00 to day 68:00 is also shown. The scale of the PVD is equivalent to that of the section. The circles on the PVD correspond to the times of the CTD stations.

SECTION A SECTION B

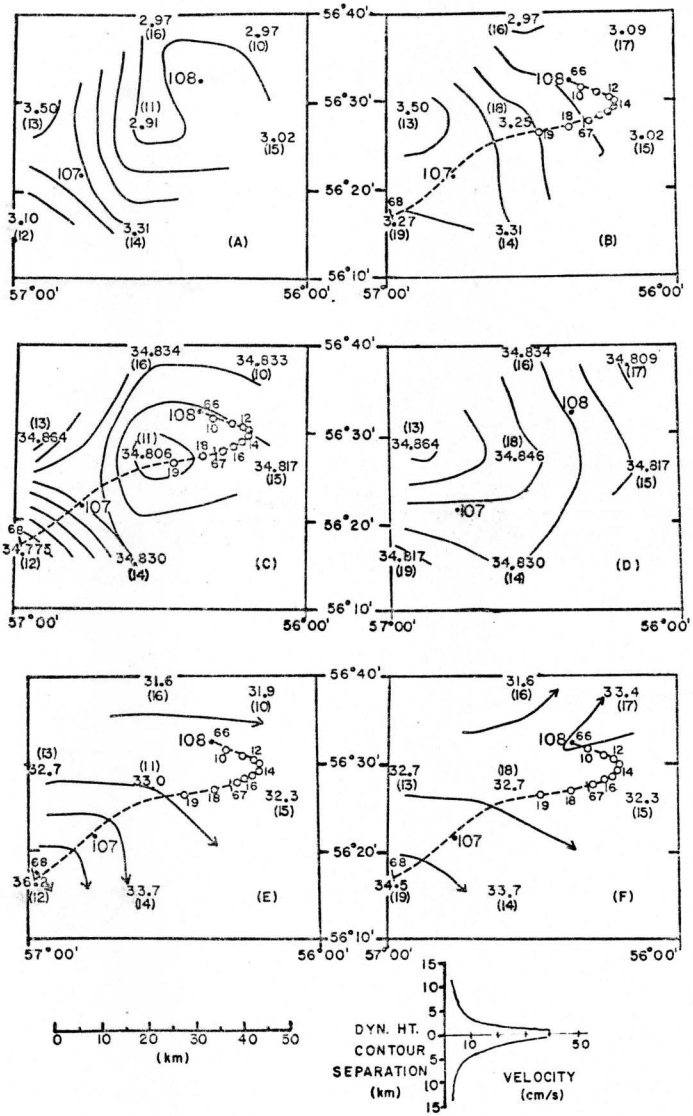

Current meter 108,160 velocity record indicated that before and during Section 'a', the flow was to the southeast and slowing. While the four transverse stations were being taken, the flow was quite low (15-25 cm/s) and was swinging 140° through south to westsouthwest. During and after section 'b', the direction of the flow was steady to the westsouthwest and accelerated up to speeds of 50-60 cm/s. The PVD (Fig. 3.5) from 108,160 plotted on the same scale for days 66 and 67, with the corresponding time of the stations marked, illustrated the displacement with time of the water at 108,160. PVD's can be thought of as the path of a water particle, if the horizontal velocity gradients are small.

The net displacement of the PVD from 108,160 during the time elapsed between Stations 11-12 and 18-19 was 10-15 km to the southwest. This indicates that the warm, saline ridge did indeed move from the region of 107 in Section 'a' to the region of Station 19 in Section 'b'. The net displacement between Stations 10 and 17 was 7-10 km to the southeast. It would appear that the source of water at Station 17 was from outside the immediate survey area. The PVD between the times of stations 11 and 18 suggested a movement of water from the northeast towards the central station. However, the nearest 2.25°C, 34.846 $^{\circ}/_{\circ\circ}$ water in Section 'a' to Station 11 was 10-15 to the northwest, not to the northeast. The temperature record from 108,160 peaked at 3.20°C during the time Station 14 was being taken. This was above the early and later levels of 3.06°C. The PVD indicated that the maximum southeastwards displacement occurred at the time of Station 14. This suggests that the warm (>3.1°C) water 15-20 km to the northwest of 108 moved first southeastwards reaching 108 at

the time of Station 14 and then moved southwestwards towards Station 18. This suggests that the temperature-salinity field was responding somewhat like a "slab" to the velocity field. The question remains as to how consistent the dynamic topography is with the currents observed at 108,160.

The dynamic topography for the two sections from the greatest common depth (870 dbars) to the surface is given in Figure 4.3e,f. The flow at 108,160 was along isobars in Section 'a'. The geostrophic velocity was 4±2 cm/s, while the observed velocity slowed from 30±5 cm/s to 15±2 cm/s during this time period. This indicates that the baroclinic portion of the flow was 10-30% of the total flow, or that baroclinic flow extended deeper than 870 dbars. With the 140° shift in the current direction between sections at 108,160, the dynamic topography in the region of #108 also reversed. Further, inshore (near #107) the gradient has lessened. The movement of the T-S distribution and the response of the dynamic topography suggest that the density field was responding to the velocity field at a time scale of 0(20 hr) or less and over spatial scales of at least 30-50 km. Thus, the dynamic topography was consistent with the currents at 108,160, but were lower. This indicates that the baroclinic currents extended deeper than 870 dbars and/or there was a barotropic component to the flow which was in phase with the baroclinic flow.

4.3.2 Cross-Correlation of Current Meter Records

Visual comparison of the PVD's, stick diagrams, and time series revealed potential correlations between the various components recorded

by the current meters. The PVD's, Fig. 3.7, suggested a strong correlation between velocity at the top and bottom current meters on Mooring 108. A comparison of the stick plots, Fig. 3.8, for 108,160 and 109,190 revealed a possible correlation of the north-south flows with a 30±5 hr. lag, (see Allen and Huntley, 1977). To quantify these and other possible correlations, a simple program was developed to determine the cross and auto-correlations of the various components.

The cross-correlation coefficient (after Jenkins and Watts, 1969) is:

$$\text{cross correlation} = \frac{\Sigma\, x'(t)\, y'(t+\Delta)}{(\Sigma(x'(t))^2)^{\frac{1}{2}}\,(\Sigma(y'(t+\Delta))^2)^{\frac{1}{2}}} \qquad (4.6)$$

where $x'(t)$ and $y'(t)$ are the two time series with their respective means removed, and Δ is the lag. When calculating an auto-correlation coefficient $x'(t) \equiv y'(t)$. The data were filtered as described in page 60 and decimated to eight-hour averages. The cross-correlation coefficients were calculated from -10 to +10 lags, each lag being eight hours.

Time series of oceanographic data often have features that persist over several sampling intervals and therefore will have high auto-correlation coefficients at non-zero lags. Since the significance levels are based on the number of independent events in the two time series being correlated, an estimate of the independent events must be made in each time series. With the correlation of time series with little or no auto-correlation, the total number of data points are simply used as the estimate of the independent events.

However, an auto-correlated time series, an estimate of "the effective number of independent observations", n*, was defined by Bayley and Hammersley (1946) for use in finding significant levels.

$$\frac{1}{n^*} = \frac{1}{n} + \frac{2}{n^2} \sum_{j=1}^{n-1} (n-j)(\rho(j\tau))^2 \qquad (4.7)$$

where 'n' is the total number of observations and $\rho(j\tau)$ is the auto-correlation of the j^{th} lag of period τ. 'j' was summed up to n/4 to avoid errors in calculation of $\rho(j\tau)$ due to a decrease in data points used in the calculations which had high 'j's. This value was suggested by Blackman and Tukey (1958). The n* values were stabilizing at n/4 values of 'j', thereby providing an estimate of n* that was not critically dependent on 'j'.

The determination of the significance levels were with (n*-2) degrees of freedom, df. Significance levels as defined by Panofsky and Brier (1968, p. 158) are:

$$\text{sign. level} = (1-P^{1/(df-1)})^{\frac{1}{2}} \qquad (4.8)$$

where 'P' is the probability level. The lower n* of the two series being correlated was used for determining the degrees of freedom. This procedure provides a significance level based on the number of independent events correlated and not the number of data points. For the degrees of freedom, 9-12 present in the velocity records, the 95% significance levels are 0.56 to 0.50.

The auto-correlation coefficient at zero lag is 1.0. The auto-correlation for a pure sinusoid falls off to zero at a lag of $\pi/2$, -1.0 at π and back to 1.0 at 2π. When the signal isn't a pure sinusoid, the auto-correlation will not be so well behaved. Nevertheless, the lags of the zero crossings, minimums, and maximums can be used to estimate the period of the major variability of the record. The auto-correlation for the U(east) and V(north) components of velocity are shown in Figure 4.4. The period of the major fluctuations estimated from the auto-correlations are given in Table N below.

TABLE N

PERIOD OF MAJOR FLUCTUATION BASED ON THE AUTO-CORRELATIONS

CURRENT METER	COMPONENT	PERIOD (DAYS)
109,190	U	3.0 ± 0.8
	V	6.2 ± 0.2
	TEMP	2.5 ± 0.4
108,160	U	3 or 15
	V	7.3 ± 0.3
	TEMP	5.1 ± 0.3
108,2480	U	4.8 ± 0.5
	V	9 ± 2
	TEMP	11 ± 1

The periods of the east-west motions were considerably shorter than the north-south motions. The bottom contours are approximately north-south at the mooring array, thus longer period (6-9 days) motions were alongslope and shorter period (3-5 days) motions were across-slope.

Of all the possible pairs of time series, significant cross-correlation coefficients were found for only two cases. Firstly, the cross-correlation coefficient of the V components from the top and bottom current meters on 108 resolved along 10°T to 20°T was greater than 0.7. This was above the 99% significant level. The V component of the top current meter lagged the bottom at a broad peak centered at 16 hr, see Fig. 4.4. This suggested strong variability in the longshore velocity which was transmitted up from the bottom to the surface layers. The auto-correlation suggested a period of 7-9 days for the major variability in the V components of velocity at both meters on 108. Therefore, a lag of 8-32 hr represents a phase lag of 15°-60° between the two current meters.

A second significant correlation existed; the U and V components of velocity from 108,2480 rotated relative to 330°T at lags of 8 hrs, plus or minus, but not at zero lag. This suggested rotational flow of either sense.

The correlation suggested by Allen and Huntley (1977) was strong southward flow at 108,160 preceding strong northward flow at 109,190 by 30±5 hr. based on visual offsetting, Fig. 3.8, the stick plots of current meters. The cross-correlation coefficient of V(108,160) at 0°T with V(109,190) at 15°T was -0.43 centered at 32±8 hrs. While the sense (negative) of the correlation and the lag was consistent with the Allen and Huntley suggestion, the correlation was only at the 80%

Figure 4.4

Auto and cross-correlations of the low-pass filtered current meter records. a,b,c are the auto-correlations of temperature (T), U, and V components of velocity from 108,160; 109,180; and 108,2480, respectively. d is the cross-correlation of UXV of 108,2480 rotated relative to 330°T, and for V(108,160) X V(108,2480). Positive lags indicate that the second component leads.

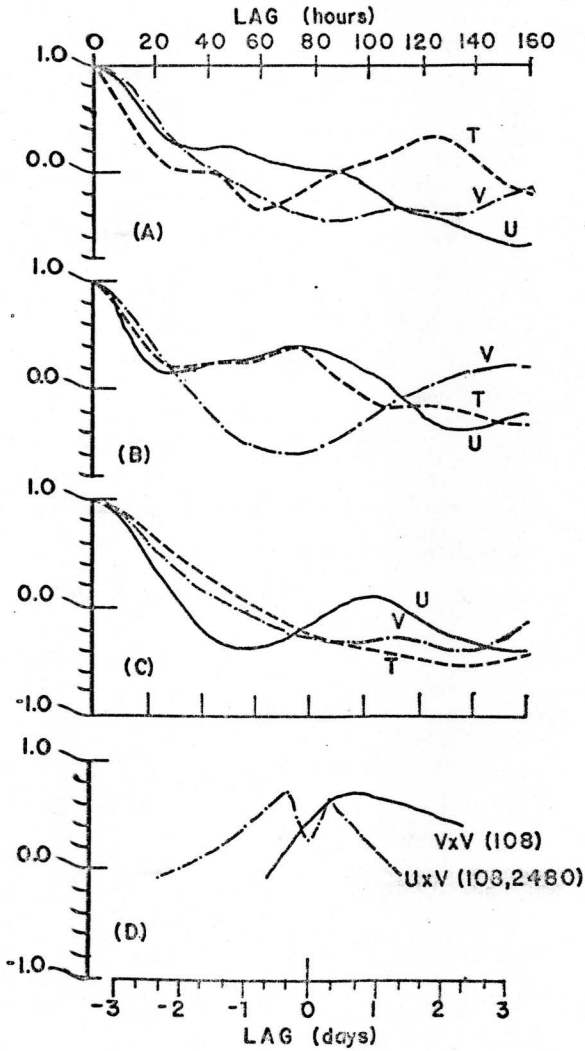
LAG (hours)
0
20
40
60
80
100
120
140
160
1.0
0.0
-1.0
T
V
U
(A)
(B)
(C)
(D)
VxV (108)
UxV (108,2480)
-3
-2
-1
0
1
2
3
LAG (days)

significance level. Because the time series were filtered to remove the variance higher than 2 days, the correlation that did exist must have been in a portion of the low-frequency spectrum. If the low-frequency motion had been dominated by a single frequency or an event or several events, then the cross-correlation of the various velocity components and temperatures would have revealed the major relationships. However, it appears that the low-frequency motions occurred over a broad band of frequencies. Therefore, it was necessary to investigate the relationships at separate frequencies. In order to determine at which frequency the correlations were present, the current amplitude ellipses at several low-frequencies were determined.

4.3.3 Current Ellipses

When the motions are characterized by periodicity at several frequencies, the current amplitudes and phase lags for each frequency can be estimated by the least-squared fit of sines and cosines curves:

$$H(t) = \sum_i A_i \cos(\sigma_i t - g_i) \qquad (4.9)$$

where A_i is the amplitude of frequency σ_i, and g_i is the phase lag relative to the center of the record. Current amplitude ellipses can be derived for each frequency when both velocity component constituents are known. This method of analyzing current meter data works best for currents which have distinct frequencies, e.g. tidal frequencies. For the range of frequencies considered here (4-12 days) the motions were not independent and individual frequency bands, but a blend of motions that varied with frequency. Thus the intent is to describe the change in the currents with frequency. The possible physical processes associated with these motions at the different frequency ranges will be dealt with in a later section.

The current amplitude ellipses were derived from the entire, unfiltered records from 108,2480, 108,160, and 109,190 at periods of 4, 6, 8, 9, 10, and 12 days. The ellipses from 108,2480 at 4, 6, and 8 days, Fig. 4.5a show a rotation to a more acute angle to the local isobaths with increasing period. The dashed line in Fig. 4.5a is the approximate (±10°) direction of the local isobaths averaged over 60 km from the Canadian Bathymetric Chart 814-A. Simple bottom-trapped topographic Rossby wave theory (Rhines, 1970) indicates that the frequency of the waves decrease when the angle of the motion to the bottom slope (the isobaths) decreases. This was precisely what was occurring at 108,2480 between 4 and 8 days.

At the longer periods of 8, 9, and 10 days the current ellipses are not rotated to the more acute angle with increasing period, Fig. 4.5b c, and d., suggesting that these longer period motions are not simple bottom-trapped topographic Rossby waves. The similarity between the amplitudes, direction, and phase at the three periods, Table O, suggested that similar processes were occurring throughout the band that extends from 8 to 10 days. The motions at 8-10 days didn't occur simultaneous at the three current meters. There was a lag of 22-33 hrs of the current at 108,160 from 108,2480. The lag from 108,160 to 109,190 was 108 to 120 hours. This suggested that the propagation of motion was upwards through the water column at 108, and had a component of propagation offshore in the direction of 109 from 108 (along 62°T, 72 km) of 17-19 cm/s. A complete analysis of these motions and those at 4-8 days in terms of the topographic Rossby wave theory will be presented in Section 4.4.

Figure 4.5

Current amplitude ellipses: at (a) 4, 6, and 8 day periods at 108,2480. The dotted line is the approximate orientation of the bottom contours averaged over 60 km; (b) 8, 9, and 10 day periods at 108,2480; (c) 8, 9, and 10 day periods at 108,160; and (d) 8, 9, and 10 day periods at 109,190.

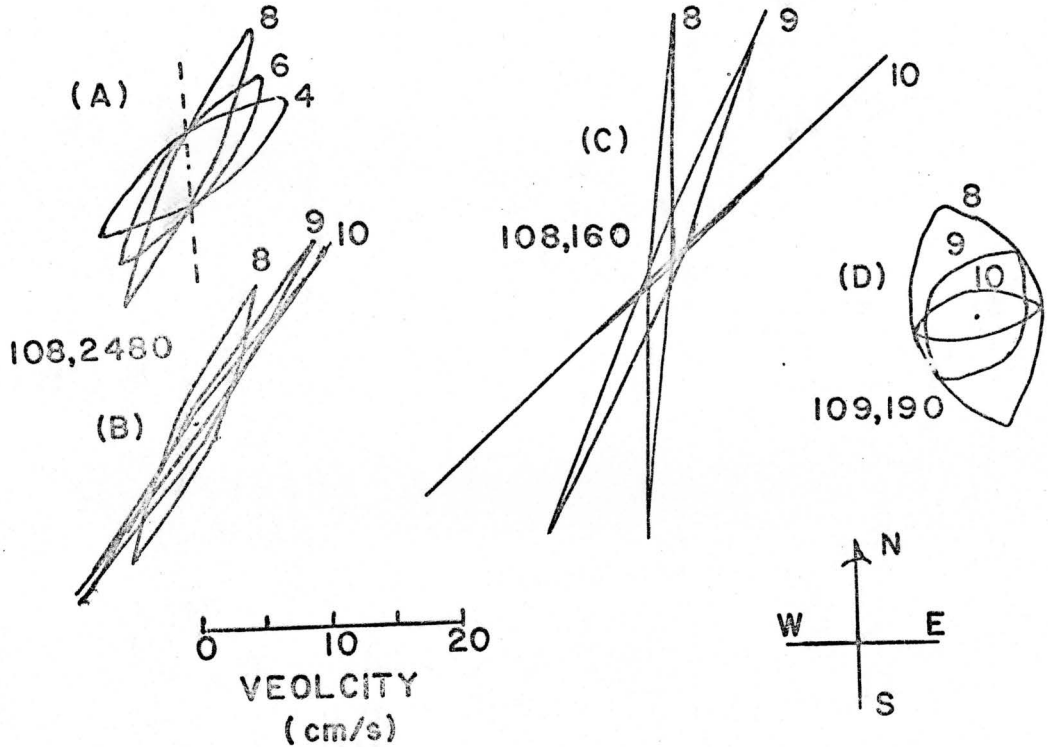
8
6
4
(A)
9
10
8
108,2480
(B)
8
9
10
(C)
108,160
8
9
10
(D)
109,190
N
W
E
S
0
10
20
VEOLCITY
(cm/s)

Allen and Huntley (1977) suggested that the southward velocity at 108,160 leads the northward velocity at 109,190 by 30±5 hrs. Subsequently checking their visual comparison, a weak negative cross-correlation coefficient between the northward velocity components was found, see Section 4.2.3. The strong north-south orientation of the 8-10 day current ellipses at 108,160 which lead the 8-10 day ellipses at 109,190 by 176°-203° is consistent with a weak negative correlation. With a change in the orientation of the velocity component at 109,190 from 0° to 45°T the lag of the maximum correlation with V(108,160) decreases from 40 to 0 hours. Perhaps a portion of the 30±5 hr (50±10°) lag was originally due to visual bias on Allen and Huntley's part and was later due to choice of wide orientations of velocity components that can be cross-correlated.

TABLE O

AMPLITUDE, PHASE, AND DIRECTION OF THE MAJOR AXIS OF THE CURRENT ELLIPSES AT 8-, 9-, AND 10-DAY PERIODS. LAGS BETWEEN 108,2480 AND 108,160; AND BETWEEN 108,160 AND 109,190. PHASE LAGS ARE RELATIVE TO DAY 78; 17.75 HRS; THE MID-POINT OF 108,2480

CURRENT METER #	PERIOD (days)	AMPLITUDE MAJOR (cm/s)	AMPLITUDE MINOR (cm/s)	PHASE OF MAJOR AXIS (deg)	DIR. (deg)
108,2480	8	12.2	1.7	339	206
	9	17.4	1.2	327	214
	10	17.3	0.4	322	217
108,160	8	20.9	1.0	22	185
	9	22.6	1.0	16	205
	10	25.1	0.2	13	228
109,190	8	8.7	5.1	225	166
	9	5.7	4.1	142	214
	10	5.3	1.8	194	264

LAGS (The first current meter leads)

PERIOD (days)	108,2480 (deg)	(hrs)	108,160 (deg)	109,190 (hrs)
8	43	22	203	108
9	49	29	176	106
10	51	34	181	120

4.4 Topographic Rossby Waves

Topographic Rossby waves are vorticity-conserving flows on a slope. The dispersion relation for topographic Rossby waves developed by Rhines (1970) and later expressed by Thompson and Luyten (1976) as:

$$\sigma = sN \sin\theta \coth(\sqrt{B}) \tag{4.10}$$

where σ is the frequency of the wave, s is the bottom slope assumed constant, N is the Brunt-Vaisala frequency (constant with depth), and θ is the angle between the wavenumber and the upslope direction. θ is also the angle between the velocity vectors and the bottom contours.

B, the Burger number, is the square of the ratio of the internal Rossby radius of deformation, r_i, to the horizontal length scale, L, of the wave.

$$B = (N^2H^2/f^2)/L^2 = r_i^2/L^2 \tag{4.11}$$

This expresses as a ratio the depth of the water (H) to the effective penetration depth (fL/N) of the wave off the bottom. L, however, is the inverse of the horizontal wavenumber, k_h.

$$L = \frac{1}{k_h} = \frac{1}{(k_1^2 + k_2^2)^{\frac{1}{2}}} \tag{4.12}$$

where k_2 is upslope and k_1 is alongslope to the right, facing upslope. This reduces the Burger number to the square of the ratio of the horizontal wavenumber to the inverse of the first internal mode of the Rossby radius of deformation, k_r

$$B = (k_h/k_r)^2 \tag{4.13}$$

When B>1, the wave is baroclinic and bottom trapped. In the limit B>>1,, $\coth\sqrt{B}$ goes to 1.0 and Equation 4.0 reduces to

$$\sigma = sN \sin\theta \tag{4.14}$$

which is the dispersion relation for bottom-trapped topographic Rossby waves. These motions are, therefore, buoyancy oscillations (N) along the bottom (s) at any angle from upslope (θ=90°) to alongshore (θ=0°). For a given constant slope and buoyancy frequency, the frequency of the waves is determined solely by the angle θ. The maximum frequency occurs when the motions are directly up and down the slope at θ = 90°, (Rhines, 1971).

As the wavelength increases, and therefore the penetration depth approaches the ocean depth, B approaches unity. With B≈1, Equation 4.10 cannot be simplified. Thus, Equation 4.10 is the dispersion relation for weakly bottom trapped topographic Rossby waves.

At long wavelengths, B<1, the penetration depth exceeds the ocean depth and Equation 4.10 again can be reduced, this time to the barotropic form of the dispersion relation:

$$\sigma = -\frac{s_f}{H}\frac{k_1}{k_1^2+k_2^2} \tag{4.15}$$

The variation of the horizontal velocity with depth for topographic Rossby waves is given by Rhines (1970) as:

$$V(z) = V_o \cosh(\sqrt{B}\, z/H) \tag{4.16}$$

where z is the depth, and H is the total water depth. When B>1, the velocity is bottom intensified, curve a in the diagram below, Profile b is the mixed or weakly-trapped form of topographic Rossby waves, Profile c is the barotropic (B<1) topographic Rossby wave.

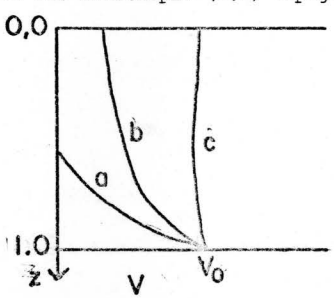

The current amplitude ellipses for 4, 6, and 8 days at 108,2480, Fig. 4.5a, suggest the presence of topographic Rossby waves, because the angle θ appears to be a function of σ. The appropriate dispersion relation is Equation 4.14 for bottom-trapped topographic Rossby waves. Before a comparison between the angle θ predicted by theory and the observed angle at each of the three frequencies can be made, the values for N, s, and the direction of the bottom contours must be determined.

The profiles of N, shown in Fig. 4.6, were calculated over 100 dbar intervals from interpolated (every 10 dbars) CTD values from the surface down to 2000 dbars, and over 200 dbar intervals thereafter from the bottle data.

The profiles of N are very smooth and slowly increasing towards the bottom. The value of N chosen for determining the frequency of topographic Rossby waves can either be a representative value for the whole water column (1.7±0.1 cph) or a representative bottom value (2.0±0.1 cph).

The appropriate values for the bottom slope and for the direction of the isobaths to use are even more nebulous (see Fig. 4.7). The bottom slope increases from 0.005 at the 2900 m isobath to 0.007 - 0.008 at the 2600 m isobath in a distance of 50 km. 40 km to the west the bottom shoals to 2000 - 2400 m and the slope steepens to 0.027-0.020. The slope steepens to 0.04 between the 1000 and 2000 m isobaths. The 1000 m isobath is located approximately 80 km from the site of Mooring 108. Canadian Bathymetric Chart 813 (1972) and 814-A (1978) were used to determine the bottom slopes. The models used are based on an assumption of a constant slope, or a slope that varies slowly over the wavelength of the wave. For large wavelengths (O(100 km) or greater) this assumption is a poor one, but at smaller horizontal scales (O(20 km) or less) the approximation of a constant bottom slope holds. A similar argument applies to the direction of the local topography to be used. The horizontal scale of the physical process determines the scale of the topographic features that will be averaged over. At 108 the direction of the

Figure 4.6

Profiles of the Brunt-Vaisala frequency (in cph) versus depth (meters); for stations 4-9, 25-30. Each profile is offset from the proceeding profile by 2.0 cph. One value of N was derived for each 100 dbar interval from the surface down to 2000 dbars and over 200 dbar intervals thereafter to the bottom.

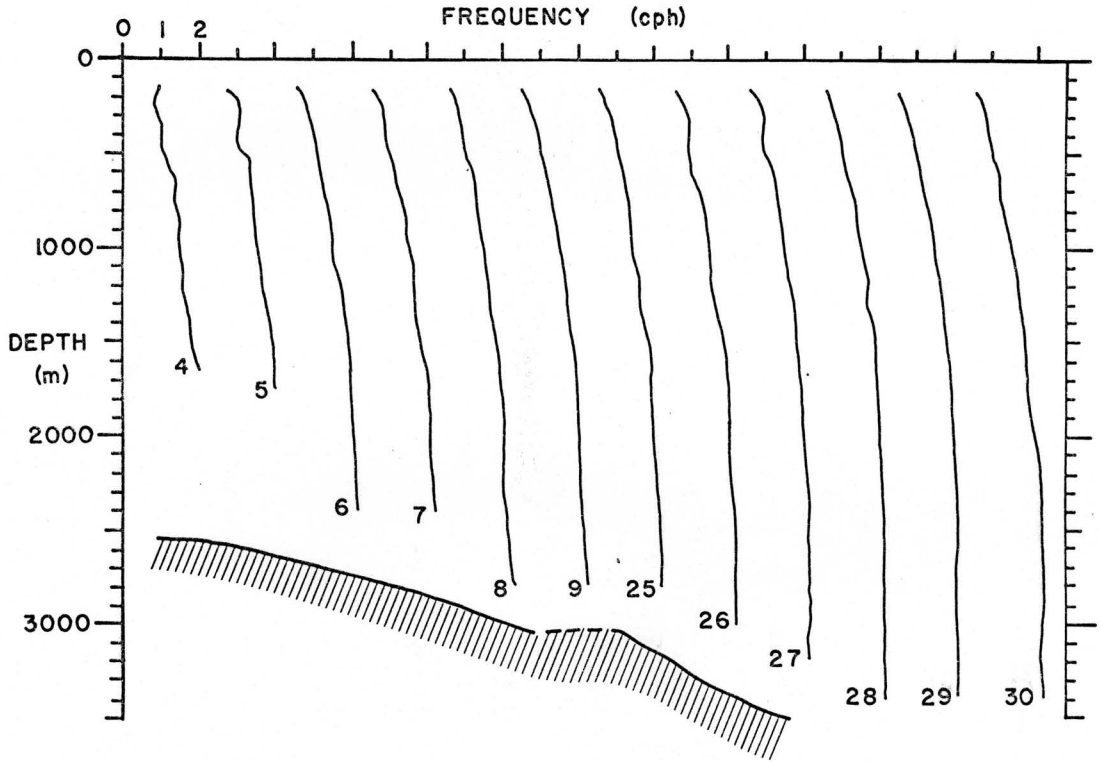
FREQUENCY (cph)
0
1
2
0
1000
2000
3000
DEPTH
(m)
4
5
6
7
8
9
25
26
27
28
29
30

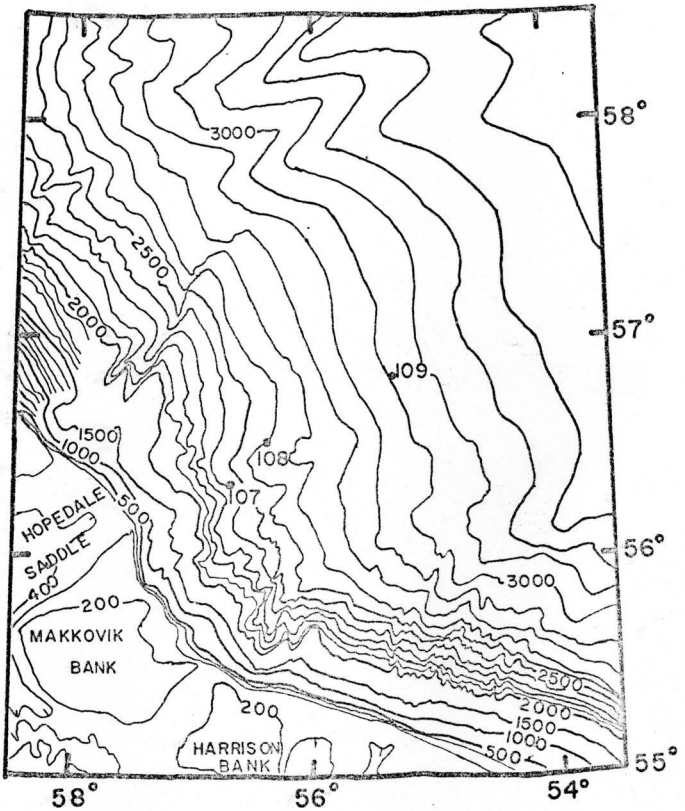

Figure 4.7 - The local topography in the mooring array region redrawn from Canadian Bathymetric Chart 814-A. Contour intervals are 100 m above 500 m and below 2000 m; the contour interval between 500 m and 2000 m is 500 m. Positions of current meter moorings 107, 108, and 109 are marked.

isobaths rotated counterclockwise from 60°T to 355°T when the area over which the contours were averaged was increased from 10 km to 50 km. At length scales of 50 km or more the average direction of the isobaths at 108 was 355°±10°.

A comparison of the theoretical values of θ and the observed values of θ from the current amplitude ellipses can be made. Rearrange Equation 4.14 to express the angle θ as a function of the physical parameters (N and s) and the frequency.

$$\theta = \sin^{-1}(\sigma/sN) \tag{4.17}$$

Table P below lists the predicted values of θ and the observed values as determined for N = 1.7±0.1 cph, s = 0.007 to 0.008, and the contours are along 355°±10°T.

TABLE P

THEORETICAL AND OBSERVED VALUES OF θ AS DETERMINED BY EQUATION 4.17 FOR BOTTOM-TRAPPED TOPOGRAPHIC ROSSBY WAVES

FREQUENCY ($days^{-1}$)	THEORETICAL θ (Deg)	OBSERVATIONAL θ (Deg ± 10°)
2π/3	75-90°	51°
2π/4	56±9°	60°
2π/6	33±5°	42°
2π/8	24±4°	31°
2π/9	21±3°	39°
2π/10	19±3°	42°

The comparisons between the predicted and observed values of θ were quite good at 4, 6, and 8 days. The predicted high-frequency cut-off was 2π/(2.7-3.7 days). The currents at 3 days apparently were above the cut-off frequency because the motions were at too small an angle to the bottom contours. At 9 and 10 days the motions are at too great an angle to the slope to be considered as bottom-trapped topographic Rossby waves.

Thompson (1971) and Thompson and Luyten (1976) have shown that the motions between one and two weeks at site D (39°10'N, 70°00'W) are dominated by weakly-trapped (baroclinic) bottom topographic Rossby waves. Thompson and Luyten (1976) pointed out that a correlation between the upslope velocity and the density (temperature) field should exist. The upslope velocity contains a component of upward vertical velocity which will bring denser (colder) water up the slope. For the coordinate system used here, V positive along the slope northwards, and U positive downslope-eastwards, the correlation should be positive U leading warmer water downslope by 90° and upslope velocity (-U) leading colder temperatures by 90°. Thus U and temperature should be in quadrature with U leading. Rhines (1970) described topographic Rossby waves as rectilinear motion. However, Thompson and Luyten (1976) show that the motions from real topographic Rossby waves between one and two weeks were ellipses which had the major axes in the orientation that Rhines predicted.

The motions at 4, 6, and 8 days suggested the presence of bottom-trapped topographic Rossby waves. The standard spectral analysis package at the Bedford Institute (Dobson et al., 1974) was used to check Thompson and Luyten's (1976) suggestion of an upslope and temperature correlation. The spectral band 3-5 days centered at 3.7 days was chosen for it was below the cut-off frequency (2 /(3.3±0.4 days) and within the range of periods (4-8 days) that appear to be bottom-trapped topographic Rossby waves. The cross-spectrum between upslope velocity (-U) and temperature for 108,2480 is shown in Fig. 4.8. At 3.7 days (0.272 cpd) the coherence

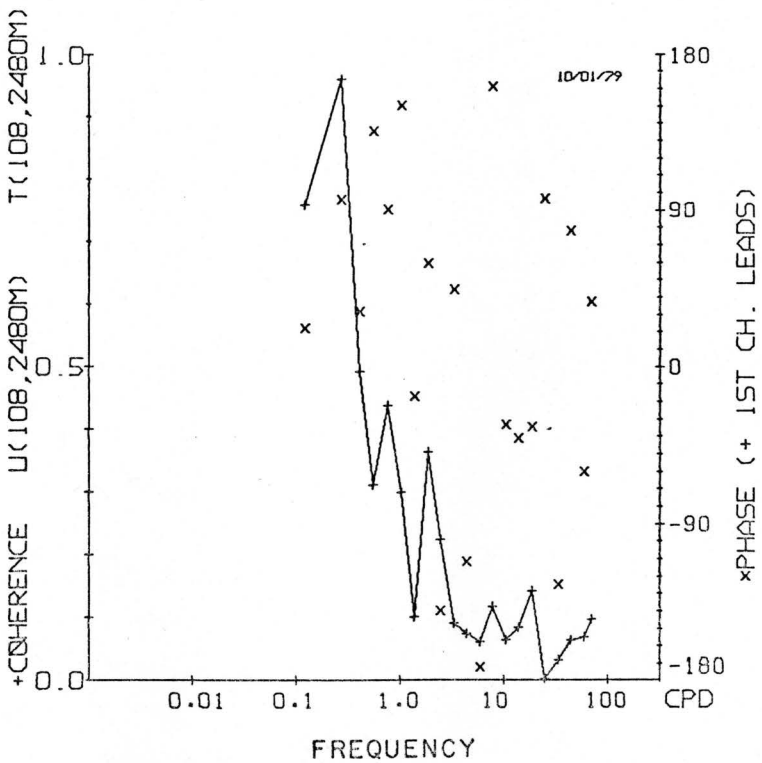

Figure 4.8 - Cross-spectrum between the down-slope velocity and the temperature at 108,2480.

between U and T was 0.96, with U leading T by 96°, error 15° determined from 3 blocks. Thus for the 3-5 day frequency band the upslope velocity was in quadrature with temperature with the velocity leading, just as Thompson and Luyten suggested they should be. This coherence fell off rapidly at 2.4 days (0.416 cpd) (band 2-3 days) which was above the predicted cut-off frequency (3.3±0.4 days). Thus, the motion between 4 and 8 days at 108,2480 were bottom-trapped topographic Rossby waves with the high-frequency cut-off between 3 and 4 days. The major fluctuations in temperature at 108,2480 and by association 107,2300 were probably due to the temperature gradient between the NWAB water and the NEAD water being swept up and down the slope by the bottom-trapped topographic Rossby waves.

The major fluctuation in the currents occurred at a period of 8-10 days. The similarity of the current amplitude ellipses at 8, 9, and 10 days between the top and bottom current meters on Mooring 108 suggested motion coherent over the water column. It has been shown that the motions between 4 and 8 days were most likely bottom-trapped topographic Rossby waves. With the transition to still longer periods and evidence of motion in the upper water column, suggesting a greater penetration depth, a transition from bottom-trapped ($B>1$) to weakly bottom-trapped ($B\approx1$) or barotropic ($B<1$) topographic Rossby waves can be expected. Thompson and Luyten (1976) were able to estimate directly the magnitude of the horizontal wavenumber and thereby determine B directly. They estimated wavenumbers from the ratios of the kinetic energy at different depths from a single current

meter mooring. Their upper current meter(s) were below the surface layer where other energetic motions would mask the topographic Rossby wave motions. Since 108,160 was in the active surface layer, this technique could not be used here to estimate the magnitude of the 8-10 day wavenumber at 108.

However, the wavenumber can be estimated. The on/offshore component of the wavenumber of the topographic Rossby wave was assumed to be responsible for constant phase lag of 108-120 hrs. from 108,160 to 109,190 at 8-10 days. 108-120 hours represents a phase speed of 16-19 cm/s and a wavenumber in the direction of 109 from 108 of 0.040 to 0.055 km^{-1}. In addition, the direction of the wavenumber can be estimated from the direction of the major axes of the current ellipses. Rhines (1971) predicted that the horizontal wavenumber is perpendicular to the water motion and is to the left facing upslope. In other words, the k_1 component of the horizontal wavenumber in the k_1, k_2 plane is negative. Therefore, the form of the topographic Rossby wave which had a wavenumber component in the direction of 109 capable of producing the observed phase lag and current ellipses was the form most likely to have been present.

From the dispersion relation, the locus of the horizontal wavenumber can be determined in wavenumber space, the k_1, k_2 plane. Longuet-Higgins (1964) showed that the center of the locus for a given frequency was $(-\gamma', 0)$ for the Rossby wave dispersion relation:

$$\sigma = - \frac{\beta k_1}{k_1^2 + k_2^2} \tag{4.18}$$

where $\gamma' = \beta/2\sigma$. For the Rossby wave case, k_1 is to the east and k_2 is to the north. For the topographic Rossby wave case, k_2 is upslope and k_1 is alongslope to the right, facing upslope. The corresponding γ' for barotropic Rossby waves is:

$$\gamma' = \frac{sf}{2H\sigma}. \tag{4.19}$$

Longuet-Higgins (1964) found that the group velocity vector, C_g, was from the horizontal wavenumber vector to the center of the wavenumber circle.

Substituting 4.11 and 4.12 into 4.10 and solving 4.10 for k_h, the locus of wavenumbers for weakly-bottom trapped topographic Rossby waves can be found:

$$k_h = \frac{f}{Ns} \coth^{-1} \left[\frac{\sigma}{Ns} \csc \theta\right] \tag{4.20}$$

for the limit: $\frac{\sigma}{Ns} \csc \theta \geq 1.0$

The loci of possible wavenumbers for the barotropic form is dependent on four known quantities; s, f, H, and σ. The weakly-trapped form is dependent on s, N, and σ which are known and on a limited range of θ.

The direction of the wavenumber estimated from the current ellipses for 8, 9, and 10 days from 108 was 95°-138°T. The direction of the local isobaths, which determined the axes of the k_1-k_2 plane was 355°±10°T, averaged over 60 km.

The limits of the loci of possible wavenumbers were determined from the values in Table Q below.

TABLE Q

TABLE OF PARAMETERS FOR DETERMINING TOPOGRAPHIC WAVENUMBERS

$f = 1.2 \times 10^{-4} s^{-1}$

$N = 1.6\text{-}1.8$ cph

$s = 0.007\text{-}0.008$

$H = 2600$ m

$\sigma = (7\text{-}9) \times 10^{-6} s^{-1}$ (T = 8-10 days)

$k_r = 0.045 \pm .005$ km-1 (wavenumber of the internal Rossby radius)

direction of $k_l = 355° \pm 10°T$

direction of $k_h = 95°\text{-}138°T$

direction of k_h component to 109 from $k_l = 67° \pm 10°$

k_h component to 109= $0.040\text{-}0.055$ km^{-1}

Figure 4.9 is the wavenumber loci for 8-10 days. Mooring 108 is at the origin. k_l lies along 355°T, thus north is to the right and west is at the top of the diagram. Circles marked A and B centered at (-.018,0) and (-.026,0) are the minimum and maximum limits of the locus of possible wavenumbers for the barotropic form of topographic Rossby

Figure 4.9

Horizontal wavenumber diagram for the 8-10 day topographic Rossby waves. Mooring 108 is centered at the origin, and K_1 points along slope to 355°T and K_2 is upslope. A and B are the barotropic dispersion locus limits. C and D are the weakly-bottom-trapped dispersion limits. E and F are the limits of the observed directions of k_h determined from the orientation of the current ellipses. Between G and H is the direction of 109 from 108 relative to the axes, which are known to ± 10°. I and J are the limits of wavenumber component in direction of 109 and L and M are the projections of those wavenumber components.

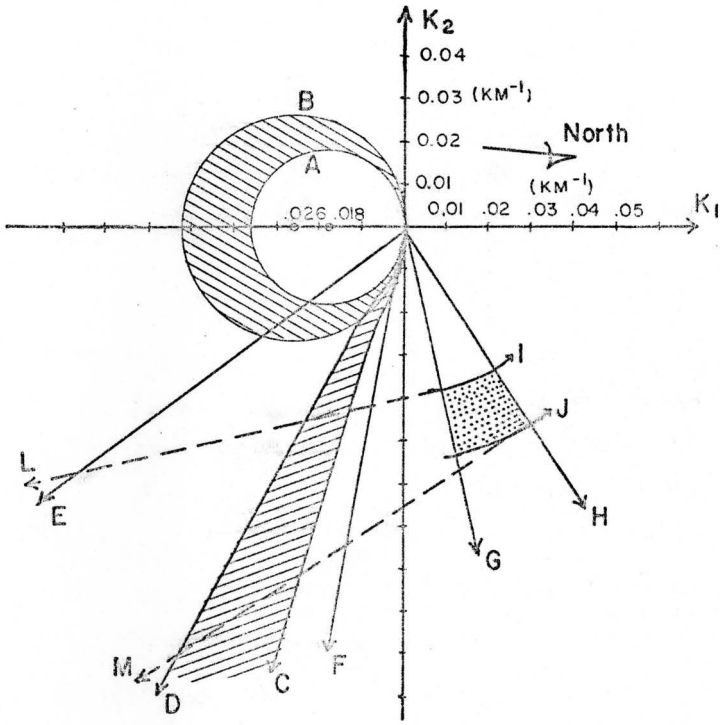
K2
0.04
0.03 (KM-1)
0.02
North
0.01
(KM-1)
0.01 .02 .03 .04 .05
K1
.026 .018
A
B
I
J
H
G
L
E
M
D
C
F

waves. Lines C and D are the limits of the locus of wavenumbers for weakly-bottom trapped (B≈1) form of the topographic Rossby waves. The limits of the loci of wavenumbers are based on extreme values of N, s, and σ as given in Table Q, as well as θ which was determined from the values of k_h and k_l, also given in Table Q. The direction of the horizontal wavenumber lies between lines E and F. The direction of 109 relative to the origin (108) is between lines G and H. The component of the wavenumber in that direction (0.040-0.055 km^{-1}) is shown by lines I and J. Therefore, the shaded area common to G-H and I-J represents the component of the wavenumber vector in the direction of 109 from 108. The limits of the possible wavenumbers capable of having a 0.040-0.055 km^{-1} wavenumber component in the direction of 109 are the dotted lines L and M. It is evident that the lines L and M lie outside the limits of barotropic (circles A and B) form of the topographic Rossby waves. However, the limits of the weakly-bottom trapped topographic Rossby waves (lines C and D) lie within the limits of direction of the wavenumbers (lines E and F) and are interesected by lines L and M; they are capable of producing the observed phase lag and current ellipses. Where lines L and M intersect C and D, the direction of the projected wavenumber is 101-113°T, with a magnitude of 0.05 to 0.09 km^{-1}. Thus, it is likely that the major fluctuations in the current meter records were caused by weakly bottom-trapped topographic Rossby waves and that the phase lag between 108 and 109 was due to the propagation of this 8-10 day wave to the westsouthwest.

Thus, a major feature of the observations, the phase lag of the major fluctuation between 108 and 109 could be explained by the presence of a weakly bottom-trapped topographic Rossby wave.

However, the next question is: were the magnitudes of the velocity fluctuations consistent with the fluctuations predicted by the topographic Rossby wave theory?

The variation of the horizontal velocity with depth is given by Equation 4.16. Figure 4.10 is the velocity profile based on a velocity of 15±2 cm/s at 2500 m from the current amplitude ellipses at 108,2480 for 8-10 days. B was assumed to be between 1 and 5. The velocity is shown to decay upwards but is still significant at the surface. The expected current amplitudes at 108,160 would be 4-10 cm/s.

The observed velocity at 108,160 for the 8-10 day period was 23±2 cm/s, was highly elliptical and led 108,2480 by 42°-50°. The presence of random motions not associated with the topographic Rossby waves could increase the current amplitudes of the major axes from the predicted values of 4-10 cm/s to the observed value of 23±2 cm/s. This would be, however, the addition of 16±3 cm/s to all directions at all phases, thereby increasing the minor axes as well. Since the minor axes are very small, O(1 cm/s), simple addition of random motions is unlikely. With this possibility ruled out, perhaps there was an interaction between the topographic Rossby waves and the surface currents which produced an enhancement of the current fluctuation and a lag of 42°-50° from the topographic Rossby wave motions.

Evidence of just such an interaction was found. The hydrographic section which was repeated several times showed variation in the surface

Figure 4.10

The velocity profiles of weakly-bottom-trapped topographic Rossby waves based on 15±2 cm/s at 2500 m. Profile A is based on a Burger No. of 1.0 and Profile B has a Burger No. of 5.0. The dotted lines represent the very extreme limits.

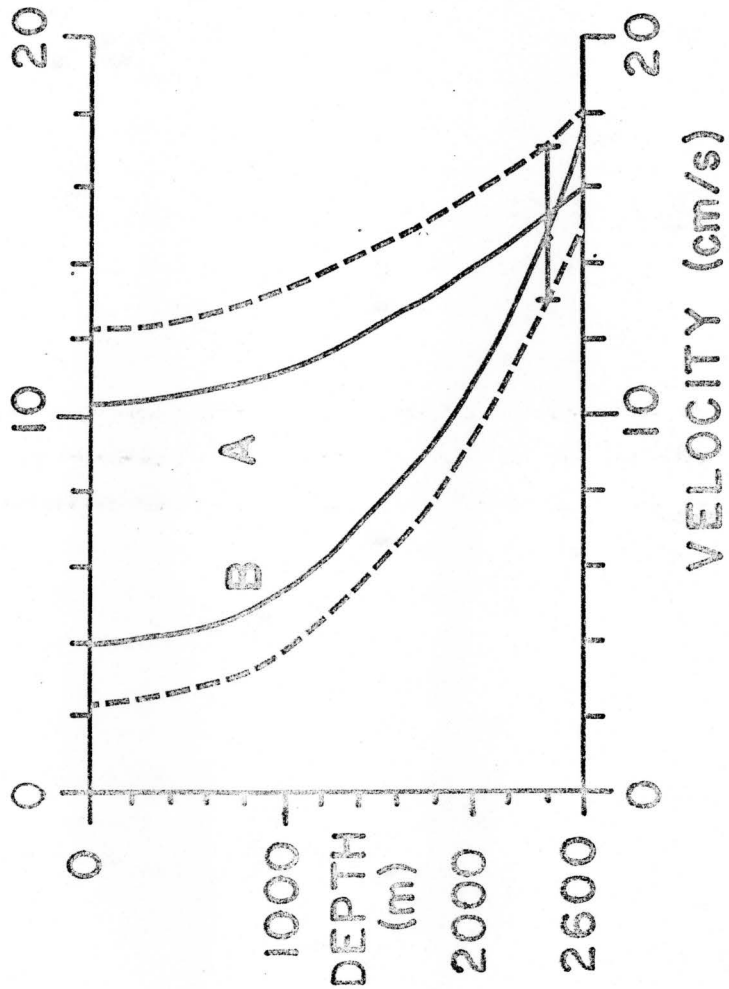
0
10
20
VELOCITY (cm/s)
0
1000
2000
2600
DEPTH (m)
A
B

baroclinic velocity field over a few days' time, see Section 3.5. If the additional 16±3 cm/s fluctuation in the current ellipses was due to variations in the surface baroclinic velocity field in the direction of the topographic Rossby wave motions, then the expected variation in the direction normal to the hydrographic section would be ±6 cm/s. The observed peak-to-peak variation in the baroclinic velocity field (normal to the hydrographic sections) was 12 cm/s, which is equivalent to an amplitude of 6 cm/s. This agrees very well with the expected variation, indicating that the additional 16±3 cm/s fluctuation in the surface current amplitude ellipses were probably due to variations in the baroclinic velocity field as it responded to the topographic Rossby wave motions.

Two simple models of interactions between the periodic motion of a topographic Rossby wave and the mean flow will be considered here in an attempt to establish the nature of the interaction. The displacement caused by the topographic Rossby wave could either shift the horizontal velocity gradients or modulate the mean flow.

The system can be modeled as follows. A_o is the amplitude of the topographic Rossby wave currents; which are rectilinear and form an angle θ with the positive y-axis. The y-axis is positive along the k_1 axis and the x-axis is positive offshore (along the k_2 axis).

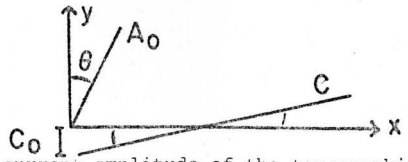

The current amplitude of the topographic Rossby wave varies in time as a sine curve.

$$A(t) = A_o \sin(\omega t) \tag{4.21}$$

The x and y projection of the current amplitudes vary as:

$$A_x(t) = A_o \sin\theta \sin(\omega t) \tag{4.22}$$

$$A_y(t) = A_o \cos\theta \sin(\omega t) \tag{4.23}$$

And the on-offshore (x) displacement of the topographic Rossby wave is:

$$D_x(t) = -\frac{A_o \sin\theta \cos(\omega t)}{\omega} \tag{4.24}$$

The mean current in the y-direction relative to an origin that is fixed to the water is assumed to linearly vary in the x-direction only:

$$C = C_o + \frac{dc}{dx}x \tag{4.25}$$

Therefore, the mean current velocity will vary in time dependent on the x-displacement of the topographic Rossby wave (Eq. 4.24).

$$C(t) = C_o - \frac{dc}{dx}\frac{A_o \sin\theta \cos(\omega t)}{\omega} \tag{4.26}$$

The total velocity in the y-direction is the mean velocity (Eq. 4.23) plus the topographic Rossby wave velocity (Eq. (4.26).

$$T_y(t) = A_o \cos\theta \left[\sin(\omega t) - \frac{dc}{dx}\frac{\tan\theta}{\omega}\cos(\omega t)\right] \tag{4.27}$$

This can be expressed as:

$$T_y(t) = G \sin(\omega t+\delta') \tag{4.28}$$

Therefore the y-phase correction is:

$$\delta' = \tan^{-1} \left(- \frac{dc}{dx} \frac{\tan\theta}{\omega}\right) \tag{4.29}$$

and the corrected y-amplitude is:

$$G = A_o\left(\cos^2\theta + \left(- \frac{dc}{dx}\right)^2 \frac{\sin^2\theta}{\omega^2}\right)^{\frac{1}{2}}$$

The resulting current ellipses can be determined from the two orthogonal components of motions, equations 4.22 and 4.28, by the method used by Doodson and Warburg (1941) for determining tidal current ellipses. θ' is the angle between the y axis and the major axis of the current ellipse. $A_{\theta'}$ is the magnitude of the major axis and $A_{\theta'+90}$ is the magnitude of the minor axis. ε and $\varepsilon+90$ are the phases of the major and minor axes of the current ellipses relative to the phase of the topographic Rossby wave motions.

$$\theta' = 1/2 \tan^{-1} \left[\frac{2 A_o \sin\theta/G}{1-A_o^2 \sin^2\theta/G} \cos -\delta'\right] \tag{4.30}$$

$$A_{\theta'} = [G^2 \cos^2\theta' + A_o^2 \sin^2\theta \sin^2\theta' + 2GA_o \sin\theta \sin\theta' \cos\theta' \cos-\delta']^{\frac{1}{2}} \tag{4.31}$$

$$\varepsilon+90 = - \tan^{-1} \left[\frac{G \sin ' \sin(90°-\delta) - A_o \sin\theta \cos\theta'}{G \sin\theta' \cos(90°-\delta)}\right] \tag{4.32}$$

$$A_{\theta'+90} = [G^2 \sin^2\theta' + A_o^2 \sin^2\theta \cos^2\theta' - 2\, G\, A_o \sin\theta \sin\theta' \cos\theta' \cos\text{-}\delta]^{\frac{1}{2}} \qquad (4.33)$$

$$\varepsilon = -\tan^{-1}\left[\frac{G \cos\theta' \sin(90°-\delta) + A_o \sin\theta \sin\theta'}{G \cos\theta' \cos(90°-\delta)}\right] \qquad (4.34)$$

To determine A_{θ}, and ε, values for A_o, θ, ω, and dc/dx were estimated. A_o, the current amplitude of the topographic Rossby wave near the surface was determined from the velocity profile, Fig. 4.10, to be 7±3 cm/s. θ, the angle of the motion to the mean current was 10°-50°. The frequency, ω, of the 8-10 day topographic Rossby waves was $(7\text{-}9)\times10^{-6}\,s^{-1}$. The horizontal velocity gradient (dc/dx) was estimated from the geostrophic velocity section, e.g. Fig. 3.13 and from the current meters. A typical southward flow of 40 cm/s at 108,160 and a northward flow of 20 cm/s at 109,190 is approximately 10^{-5} cm/s-cm. This agrees with the gradients found in the geostrophic velocity sections. From the above range of values, A_{θ}, was 1.0 to 2.0 times A_o and ε was 40°-80°. $A_{\theta'}$, the enhanced velocity amplitude, is rather sensitive to the dc/dx. If the current shear had occurred over a shorter distance, with a local value of 2×10^{-5} cm/s-cm, ε would then be 20°-70°

and A_{θ}', would have been 1.1-2.6 (A_o). The observed values of ε were 42°-50° and A_{θ}', was (2.0-2.6) (A_o). Therefore, when is 30°-50° and if dc/dx is sharper than expected, then this mechanism of shifting the local horizontal gradient in the surface current is quite capable of producing enhanced surface current ellipses which would lag the topographic Rossby wave ellipses.

The second possible interaction between topographic Rossby waves and the mean flow is based on the following assumptions. The offshore branch of the Labrador Current is assumed to have a constant dynamic height at the inshore boundary near the 1000 m isobath. The on-offshore displacement of water due to the topographic Rossby wave would change the sea surface and associated geostrophic velocity. The topographic Rossby waves are modeled by Equations 4.21 and 4.24. Since the mean Labrador Current is assumed to be in geostrophic balance:

$$C = -\frac{g}{f}\frac{H'}{L} \qquad (4.35)$$

where the z-axis is positive from the surface downwards (after Neumann and Pierson, 1963, p. 161).

H' is the difference in sea levels at the inshore boundary and the offshore edge of the current, the distance is L. L varies with time due to the displacement of current by the topographic Rossby waves.

$$D(t) = L_o - A_o \frac{\sin\theta \cos(\omega t)}{\omega} \tag{4.36}$$

Substituting 4.37 into 4.36 the mean velocity varies as:

$$C(t) = -\frac{gH'}{f}\left(L_o - A_o \frac{\sin\theta \cos(\omega t)}{\omega}\right)^{-1} \tag{4.37}$$

The total y-velocity is 4.23 plus 4.38

$$T_y(t) = A_o \cos\theta \sin(\omega t) - \frac{gH}{fL_o}\left(1 + \frac{A_o}{D_o} \sin\theta \cos(\omega t)\right) \tag{4.38}$$

Where $D_o >> \frac{A_o \sin\theta}{\omega}$; the total current half width is greater than the displacement of the topographic Rossby waves.

Following the same procedure as 4.27 through 4.30

$$\delta' = \tan^{-1}\left(-\frac{gH' \tan\theta}{fL_o^2 \omega}\right) \tag{4.39}$$

and

$$G = A_o \left(\cos^2\theta + \frac{g^2 H'^2 \sin^2\theta}{f^2 L_o^4 \omega^2}\right)^{\frac{1}{2}} \tag{4.40}$$

where A_θ, and ε are the same quantities as those defined by Equations 4.31 and 4.34, except that now G and δ' are defined by Equations 4.40 and 4.41.

Again, θ ranges from 10° to 50°, ω is $(7\text{-}9)\times10^{-6}s^{-1}$, A_o is 7±3 cm/s; and g equals 980 cm/s and f is $1.2\times10^{-4}s^{-1}$. A velocity of 30-40 cm/s at 108,160 assumes an H' of 40 to 50 cm 80 km inshore at x=0, near the 100 m isobath, when L is 100 km. L is the distance over which the sea surface responds to the topographic Rossby wave. L is assumed to be 100±20 km. A_θ, increased from $1.0(A_o)$ to $1.5(A_o)$ and ε decreased from 80° to 50° when the slope (H'/L) and θ were increased while ω was decreased.

While the second model produced only limited enhancement of the current ellipses, a modulation of the mean current and therefore the horizontal velocity gradient could be expected. This modulation would be roughly in phase with the current ellipses. Perhaps the process suggested in the second model is present to some extent and influences the interaction between the surface current and the topographic Rossby wave by modulating the local value of dc/dx in the first model. This would tend to increase the magnitude of the enhancement of the current ellipses.

The two models do offer explanations for the phase lag between the top and bottom current meters on 108 for the 8-10 day current ellipses. The apparent amplification of the topographic Rossby wave motion is probably due to an interaction with the surface velocity field. However,

the exact nature of this interaction is most likely much more complex than the two simple models used here for a first look.

When waves are in the presence of a steady flow, the frequency can be Doppler shifted. The frequency of a wave in the absence of any flow is

$$\omega = ck_h \tag{4.42}$$

where c is the phase speed. With a steady flow, v, the Doppler shifted frequency is:

$$\omega = (c+v\cos\theta)k_h \tag{4.43}$$

where θ is the angle between the wavenumber vector and v. The PVD's, Fig. 3.7 indicate that the flow at 108 was between 188° and 200°T with speeds of 12-15 cm/s. θ was 73°±12° and C eas estimated to be 16-19 cm/s. The resulting shift in the period of the 8-10 day topographic Rossby waves was less than a day, which is within the error limits. Therefore, Doppler shifting of the frequency of these waves was assumed to be minimal.

In summary, the current ellipses between 4 and 8 days at 108,2480 were due to bottom trapped topographic Rossby waves. The motions at higher frequencies were orientated at greater angles to the local isobaths. The cross-slope motion of the higher frequency topographic Rossby waves was responsible for the movement of the temperature gradient between the NEAD and NWAB waters. This caused large fluctuations in the temperature records of 108,2480 and 107,2300.

With the transition to longer periods the penetration depth of the topographic Rossby waves became comparable to the water depth (B approaches unity). This was the time scale (8-10 days) of the major fluctuations in the current regime at the offshore edge of the Labrador Current. While the 8-10 day topographic Rossby waves were weakly-bottom-trapped, there was still significant velocity at the surface (7±3 cm/s) to interact with baroclinic velocity field at the surface. This resulted in enhanced current fluctuations (23±2 cm/s) which lagged the topographic Rossby wave motion by 42° to 50°. The propagation of the 8-10 day topographic Rossby waves to the southeast had a component of propagation in the direction of 109 from 108 which was responsible for the 108-120 hour lag in the major current fluctuations between 108,160 and 109,190. Therefore, most of the features of the low-frequency fluctuations less than a month are explained by the presence of topographic Rossby waves.

Other low-frequency processes were also possibly present in the currents. The possibility of baroclinic instability in the bottom flow is discussed in the next section and the likelihood of continental shelf waves is investigated in Section 4.6.

4.5 Baroclinic Instability in the Bottom Flow

Current Meter 108,2480 was the only meter to return a full velocity record from the bottom flow of the NWAB water. Considerably variability in the velocity record existed between the predicted cut-off period for

topographic Rossby waves (2.9-3.7 days) and the tidal-inertial band (12-24 hrs). This variability was located at 1.8-2.9 days, separated by a valley from the tidal-inertial motions, see Fig. 4.1b.

The motions of the highest frequency topographic Rossby waves are directly across the contours. This peak in variability at 108,240 was along the contours at 2.1-2.9 days, which completely rules out the possibility that this motion was due to topographic Rossby waves. The 2-3 day variability was, however, similar to that observed by Smith (1976) in the Denmark Strait overflow. He successfully showed that the variability was due to baroclinic instabilities in the bottom flow.

There exist some basic similarities between the Denmark Strait overflow system and the bottom flow of the NWAB water. The first connection between the two systems is that the NWAB water in the Labrador Sea is of Denmark Strait overflow origins, Worthington (1976). Thus both are part of the same deep circulation. Second, spectral diagrams from the current meters which were placed in the Denmark Strait overflow and the NWAB water flow reveal a peak in energy close to two days. Smith showed that baroclinic instability in the mean flow of the Denmark Strait overflow produced unstable waves with a period of 2 days. Third, the hydrographies of the two systems are basically the same, a strong bottom current flowing along a bottom slope of $O(10^{-2})$. To determine the possibility of baroclinic instability as the physical process occurring in the NWAB water flow, the dispersion relation from P. Smith's (1976, Equation 3.8) model was used.

Baroclinic instability (Orlanski and Cox, 1973) is the transfer of potential energy to kinetic energy. When a horizontal density gradient exists as shown below

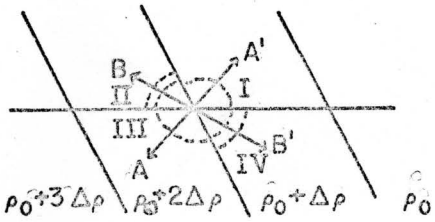

motions can exist in any direction. If a particle is displaced from A to A' then the particle will be in a region of lighter water, gravity will act on it to restore it to its original position. Conversely, a particle forced from A' to A will be restored by buoyancy. Motions between Sections I and III are internal gravity waves. However, if a particle is displaced from B to B' gravity will act to accelerate the particle as would buoyancy accelerate a particle moving from B' to B. Motions between Sections II and IV are, therefore, amplified by the gravity-buoyancy forces. This will result in a transfer of potential energy to kinetic energy, the net result being an increase in the velocity field at the expense of the horizontal density gradient. This is baroclinic instability.

The bottom prevents motions normal to its slope and by conservation of mass increases motions parallel to the slope. If a bottom slope lies along A-A' in the above figure, motions are prevented along B-B' and the system is stabilized. However, if the slope is along B-B', the motions are directed along B'-B and the system is destabilized, increasing the possibility of baroclinic instabilities occurring in the bottom flow.

Several investigators have developed models for baroclinically unstable flows, along a bottom slope (e.g. Smith, 1976; Mysak, 1977; and Mysak and Schott, 1977). Briefly, the models incorporate the following characteristics: The hydrography is a two-layer geostrophic flow in a channel with a sloping bottom. Mysak's model includes one wall of the channel as the upper continental slope. Smith uses two artificial vertical walls to define the system, which simplifies the boundary conditions (Pedlosky, 1964, 1974). The current is assumed to have negligible horizontal shear. This assumption eliminates from consideration the possibility of either barotropic or combined barotropic-baroclinic instabilities. To investigate the combined instability in ocean currents due to the presence of both horizontal and vertical shear, Orlanski (1969) had to use a numerical model. Lastly, the bottom slope is of the $0(10^{-2})$, thus the variation in Coriolis force with latitude, the β-effect can be neglected. LeBlond and Mysak (1978) demonstrate this as a reasonable assumption when the bottom slope is of $0(10^{-2})$ or greater and are comparable effects when the slope is of $0(10^{-3})$. Therefore, the models are on a constant f-plane with a sloping bottom.

The basic source of instability in the models of Smith and Mysak is the vertical shear between the two layers and the bottom slope. As a result the critical criterion for instability in the models is the interface slope exceeding the bottom slope. Figures 3.3; 3.5 of the temperature fields is rather inconclusive as to whether this criterion was met or not. Thus the dispersion relation from Smith's model was used to establish whether baroclinic waves were possible in the NWAB water flow.

The dispersion relation (Equation 3.8) from Smith (1976) is:

$$ac^2 + bc + d = 0 \tag{4.44}$$

where

$$a = \alpha(\alpha+\gamma+1)$$

$$b = q_1(\alpha+1) + q_2(\alpha+\gamma) - \alpha(U_1+1)(\alpha+\gamma+1)$$

$$d = q_1q_2 - q_1(\alpha+1) - U_1q_2(\alpha+\gamma) + U_1\alpha(\alpha+\gamma+1)$$

and

$$\alpha = (k^2+m^2\pi^2)/F$$

$$q_1 = \beta-\alpha(1-U)$$

$$q_2 = \beta-B + (1-U) + i\,\frac{r\alpha}{k}$$

The solution to Eq. 4.44 is

$$C = C_r + ic_i = -\frac{b}{2a} \pm \frac{1}{2a}\,[b^2-4ad]^{\frac{1}{2}} \tag{4.45}$$

where

k = downstream wavenumber

m = mode

B' = bottom slope parameter

F = internal Froude number

U = U_1/U_2

r = friction parameter

β_y = y-projection of the variation of the Coriolis parameter

γ = layer depth ratio

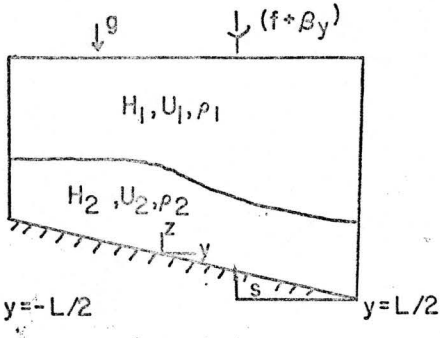

For a wave to become unstable and grow the roots of the dispersion relation must be imaginary, for it is the imaginary portion of the roots of the equation which are the growth terms, while the real part represents the phase speed of the wave. Only the maximum growing wave would overcome the dissipative forces and generate a dominant signal in the current system. Therefore, if the dispersion relation for the NWAB water system has maximum imaginary roots at a period of 2-3 days, baroclinic instability is the possible source of the 2-3 day variability. The physical and dimensionless parameters from Smith (1976) and for the NWAB water flow are contained in Table R below.

TABLE R

PHYSICAL AND DIMENSIONLESS PARAMETERS FOR THE LABRADOR SEA AND DENMARK STRAIT OVERFLOW

PARAMETER	NWAB LABRADOR SEA	DENMARK STRAIT (SMITH (1976))
H_1 (m)	2000-2600	400
H_2 (m)	300-800	150
L (km)	50-150	100
U_1 (cm/s)	2; 20-35	0
U_2 (cm/s)	10; 30-40	60
s	.01	0.01
f (s^{-1})	1.2×10^{-4}	1.3×10^{-4}

PARAMETER	NWAB LABRADOR SEA	DENMARK STRAIT (SMITH (1976))
$\beta_y (cm^{-1}s^{-1})$	0	-0.5×10^{-13}
ν $(cm^2 s^{-1})$	0	0
$g_r = g(\rho_2 - \rho_1)$	= .05	0.45
$\gamma = H_2/H_1$	= .11-.40	0.375
$F = f^2L^2/g_r H_2$	= 90-2300	250
$R_o = U_2/fL$	= .01±005; .03±.01	0.05
$B' = g_r \alpha / fU_2$	= .42; .10-.014	0.346
$E = \nu/fH_2^2$	= 0	0
$r = E^{\frac{1}{2}}/2R_o$	= 0	0

In Smith's two-layer model, the critical parameter is the shear between the two layers. Because the perturbations occurred in the bottom flow, the important interface was believed to be between the NWAB waters and the NEAD waters. Thus, the values in Table R were determined from typical NEAD and NWAB water values. The surface currents and water masses were therefore assumed not entering into the dynamics and were considered to be part of the upper layer. Figure 3.12 suggests that the bottom velocity layer was 50 to 150 km wide and from 300 to 800 m thick. Two sets of parameter ranges were used for the velocities. A low set corresponding to the period of weak highly variable flow and a high range corresponding to the period of strong southward flow. The measured shear between the two layers was 0-10 cm/s over the bottom 500-1500 m. For the low range of velocity and for some of high range, this level of shear was maintained. Higher shears were also considered possible when the higher velocities were present and therefore were also tested.

The dispersion relations for the possible combination of parameters were determined for mode 1 (m=1). The period of the maximally unstable wave was dependent mostly on the lower layer velocity, U_2. The growth rate (expressed inversely in terms of the inertial periods to e-fold;

$\tau_i = f/(\sigma_i U_2/L))$ was dependent on the vertical shear (U_2-U_1) and to a lesser extent on L and the bottom layer velocity. Increasing the shear, H_1 and U_2 all increase the growth rate. Smith noted that higher modes decreased the growth rates, therefore only mode 1 was considered here. For the parameter range that would occur during the strong-steady southward flows, the period of maximally unstable waves was 2.0-2.5 days with e-folding times of 13-33 inertial periods (5-20 days). The wavelengths were between 40 and 70 km. When the velocities were reduced to the levels that occurred during the periods of low velocity (U_1 = 2 cm/s; U_2 = 10 cm/s) the period of the maximally unstable waves increased to 10-11 days. The growth rates decreased (τ_i = 35-42 inertial periods), while the wavelengths were centered at 65 km. This indicates that the occurrence of the 2-3 day unstable wave would have been transitory, dependent on the phase of the (8-10 day) topographic Rossby waves.

Pedlosky (1976) illustrated that a current which is marginally unstable and varies in the downstream direction will develop disturbances in the locally unstable regions. The waves will not substantially diminish when they enter the locally stable region of the current, if the dissipative time scale is long compared to the advective time scale. Thus, it is possible that the 2-3 day waves were produced during the periods of strong-steady currents when the growth rates were fastest and the system unstable while not being dissipated significantly during the periods of relative stability. It should, however, be noted that while baroclinic instabilities in the bottom flow may be responsible for the 2-3 day fluctuation found there, it's not conclusively shown so, only that it is possible.

4.6 Continental Shelf Waves

Topographic Rossby wave theory describes motions which are attributable to a local balance between potential vorticity and the bottom slope, while continental shelf wave theory describes motions which are the results of the balance of the general potential vorticity structure over the entire width of the continental shelf and slope, with the generalized shelf topography. In Section 4.4, the nature of the observed motions was demonstrated to be topographic Rossby waves. In this section, continental shelf wave theory is explored briefly in an attempt to determine what, if any, low-frequency motions (specifically the observed motions) could arise due to the presence (and growth) of continental shelf waves on the Labrador Shelf.

Continental shelf waves can be described as barotropic low-frequency oscillations of the sea surface trapped to the continental shelf by Coriolis force. Non-barometric responses at continental tide gauges have been attributed to continental shelf waves off both Australian coasts by Hamon (1966); off Oregon by Mooers and Smith (1968); and off North Carolina by Mysak (1969). Typical periods were of the order 10 days. The theory for barotropic low-frequency oscillations which are trapped to the continental shelf by the Coriolis force was first developed by Robinson (1964). The dispersion relation for a variety of continental shelf waves has appeared in the literature in attempts to account for the non-barometric sea surface signals propagating along continental coasts, (e.g. Mysak (1967), Rhines (1969)). The model developed by Niiler and Mysak (1971) is used here because it uses a western boundary current over the shelf edge to produce the potential

vorticity structure. Thus the essential characteristics of the Labrador Current can be incorporated into the model.

The dispersion relation of Niiler and Mysak model is determined by the potential vorticity structure P(x) of the mean current over the shelf topography which varies only in the x direction offshore.

$$P(x) = (f+\xi)h^{-1} \qquad (4.46)$$

Where f is the Coriolis force, ξ is the relative vorticity, and h is the water depth.

In dimensionless form the potential vorticity structure is

$$P(x) = (1+Vo')h^{-1} \qquad (4.47)$$

where Vo' is the northward current scaled by f and l (the shelf width or half width of the current) and h is the depth scaled by the maximum depth (H). The current configuration of model 'a' of Niiler and Mysak and the corresponding potential vorticity distribution for the northward flowing Gulf Stream at the region of the Blake Plateau is shown below, (from Niiler and Mysak (1971) Fig. 3a)

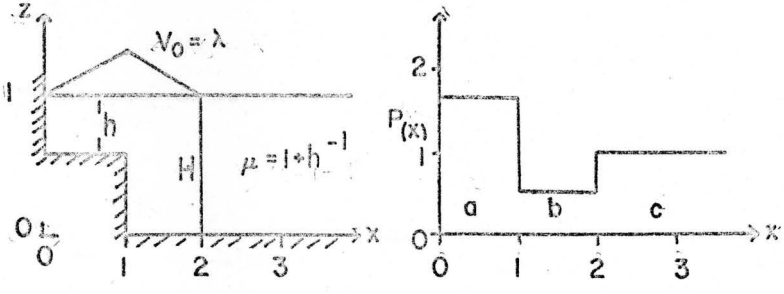

λ is the Rossby number of the current defined as dVo'/dx and $\mu = 1+h/H$ is a topographic parameter. The potential vorticity is

a. $(1+\lambda)\ (\mu-1)$

b. $(1-\lambda)/1$

c. $(1+0)/1$

The dispersion relation relating the frequency, σ, to the wave-number, k, as a function of the above potential vorticity structure was given in Niiler and Mysak's Equation 7 as

$$\sigma^2(\mu \exp(|k|) \cosh k - 1) \qquad (4.48)$$
$$+ \sigma[\mu\lambda \cosh \sinh k + \mu\lambda \exp(|k|)$$
$$(k \cosh k - \sinh k) - \lambda k + (2-\mu)$$
$$\exp(|k| \sinh k)$$
$$+ \lambda \sinh k[\mu\lambda(k \cosh - \sinh k) + (2-\mu) \sinh k] = 0$$

Table S contains the values for the Labrador Current estimated from Figure 3.13 and from Smith, Soule, and Mosby (1937) for Niiler and Mysak's model 'a' configuration.

TABLE S

CONTINENTAL SHELF WAVE PARAMETERS FOR THE LABRADOR CURRENT

f = $1.2 \times 10^{-4}\ s^{-1}$

L = 125±25 km

Vo = -50±10 cm/s

h = 300±100 m

H = 3000±200 m

λ = -.03 range (-.02 to -.05)

μ = 11 range (8 to 17)

The corresponding potential vorticity structure for the Labrador Current is shown below based on the mean values of Table S.

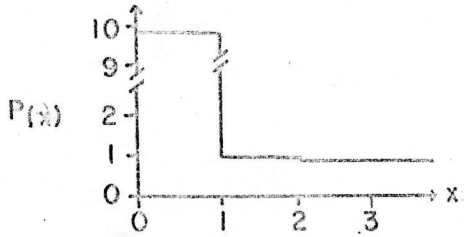

There are two modes for the continental shelf waves. One travels on the horizontal shear of the current and the other is a shelf wave. The shelf waves are modified by the shear flow and the shear waves are modified by the topography. In Niiler and Mysak's model of the Gulf Stream, the shear wave propagates northwards and the shelf wave propagates southwards at low wavenumbers but is modified enough at higher wavenumbers to propagate northwards. Thus, the two modes were able to coalesce and produce unstable growing waves. Figure 4.11 is the dispersion relation determined for the Labrador Current from the mean values in Table S. The upper curve is the shear mode and the lower is the shelf mode. Both are southward travelling waves. Because the Labrador Current flows in the opposite sense to the Gulf Stream, thereby making $V_0(x)$ negative, the modifying effects on the two modes were not present. Thus, the two modes didn't coalesce, and therefore no continental shelf waves which would grow would be present. This does not, however, rule out the possibility of neutral shelf waves. The range of periods would be 24-60 days, dependent on the Rossby number, the longer periods being associated with the lower Rossby numbers. If

Fig. 4.11

Dispersion relations for continental shelf waves on the Labrador Shelf determined by Niiler and Mysak's (1971) model 'a' for various values of μ (shelf topography) and λ (Rossby number).

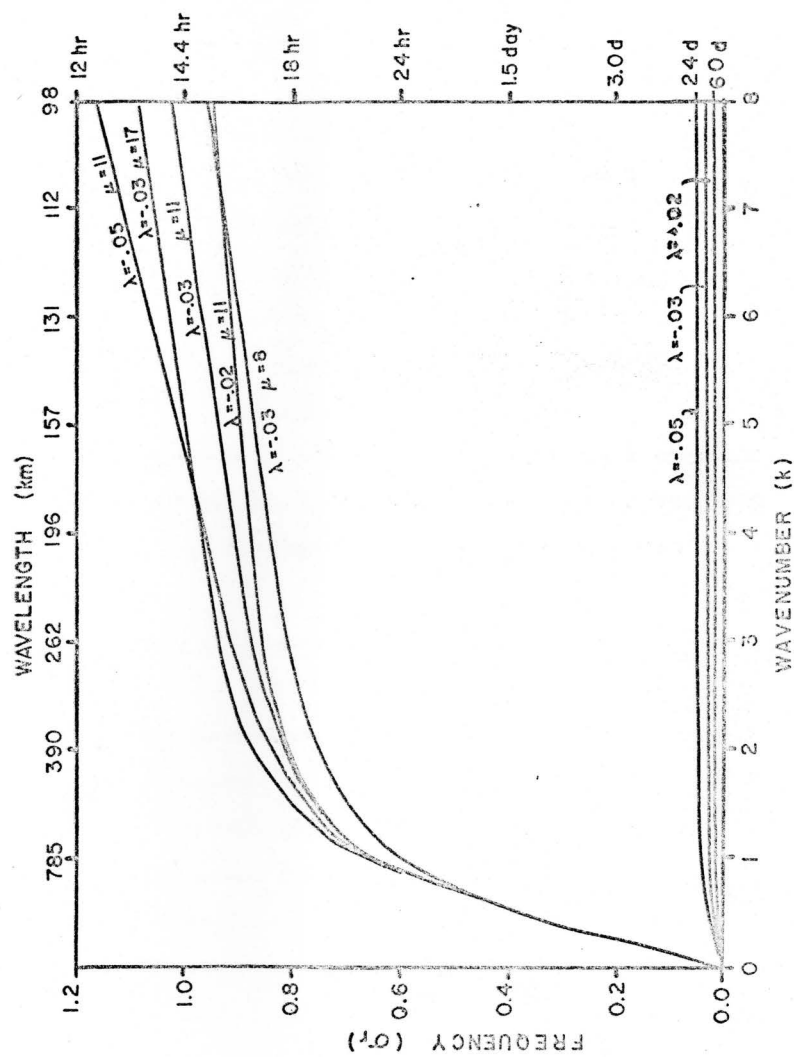
WAVELENGTH (km)
785
390
262
196
157
131
112
98
12 hr
14.4 hr
18 hr
24 hr
1.5 day
3.0d
24d
60d
FREQUENCY (σr)
1.2
1.0
0.8
0.6
0.4
0.2
0.0
0
1
2
3
4
5
6
7
8
WAVENUMBER (k)
λ=-.05 μ=11
λ=-.03 μ=17
λ=-.03 μ=11
λ=-.02 μ=11
λ=-.03 μ=8
λ=-.05
λ=-.03
λ=-.02

there is an external source causing perturbations near this period range at the northern end of the Labrador Current, fluctuations in the current could be the results of a continental shelf wave propagating southward along the coast. There is a possible source of perturbations at the northern end of the Labrador Current. The dynamic topography diagrams of Smith, Soule, and Mosby (1937) and Lazier (1973) show eddy-meander like features in the northern end of the Labrador Sea. These features are part of the extension of the West Greenland Current as it passes across the northern end of the Labrador Sea. Perhaps the impingement of eddy-meanders on the Labrador slope excite continental shelf waves. The expected period of these waves would be of O(24-60 days). Longer current meter records on the slope and shelf or simultaneous tide gauge records from the coast of Labrador might reveal the presence of southward propagating continental shelf waves.

4.7 Summary of the Low-Frequency Variability

At the bottom current meter on the inshore mooring (108,2480), bottom-trapped topographic Rossby waves were present. The motion with periods between four and eight days were ellipses with axis oriented to the bottom contours almost precisely as predicted by theory. The expected correlation between the density (temperature) field and the velocity field was also observed. This physical connection resulted in the large fluctuations in the temperature gradient between the NWAB water and NEAD water.

Simple topographic Rossby wave theory was able to account for the phase lag of the major fluctuations between the moorings. However, a phase lag between the bottom currents and the surface currents could only be explained by a positive interaction between the baroclinic surface currents and the topographic Rossby wave motion. A simple model of the interaction was able to reproduce the observed phase lag, but not the full magnitude of the enhancement of the surface current fluctuation. Evidence of a positive interaction was shown in the repeated hydrographic sections. The presence of weakly-bottom trapped topographic Rossby waves and the interaction with the surface currents accounted for the major fluctuation in the current regime. The interaction with the geostrophic currents caused significant changes in the calculated volume transport over the period of a week.

Because the variability in the flow of the Labrador Current is significant on time scales of a few days, the investigation of year-to-year variability based on a single standard section is rather tenuous. The U.S. Coast Guard (Moyniham and Anderson, 1971) in an attempt to monitor the year-to-year variability in the southward transport of icebergs by the Labrador Current maintained a standard hydrographic section across the southern end of the Labrador Sea. This section was done once a year during July - August from 1948 to 1969. Volume transports were based on the geostrophic method with a zero velocity at 1500 dbars. Moyniham and Anderson could not find a correlation between the flow based on the geostrophic sections and the severity of the iceberg season. Dinsmore and Moyniham (1972) also noted the large random fluctuations in the Labrador Current transports from year-to-year. They suggested

that short-term meteorological events might be responsible for some of the variation and that the year-to-year fluctuations masked any multi-year cycles. Two Soviet investigators (Treskinkov and Baranov (1977)) proposed water budgets based on the Arctic Ocean, Labrador Sea, and Baffin Bay based on the annual U.S. Coast Guard sections, and found multi-year cycles. What is indicated here in this work is that the short-term variability is significant, and most likely greater than the year-to-year variability. Therefore, a single estimate of transport simply cannot be used to estimate the transport for the entire year or season. This would be the reason why Moyniham and Anderson did not find a correlation between flow and seasonal iceberg transports, for the flow was only correct for time scales of the major fluctuations, which are of the order of a few days.

At frequencies higher than the highest possible topographic Rossby wave, there were along-slope fluctuations of 2-3 day periods in the bottom flow. These fluctuations were similar to fluctuations observed by Smith (1976) in the Denmark Strait overflow. His model of baroclinic instatilities in a two-layer system was used to model the bottom flow of NWAB water. Unstable growing waves at 2-3 days were predicted by Smith's model for the Labrador case, but only during the periods of strong, steady, southward flow. Thus, it was possible that the 2-3 day fluctuations were due to baroclinic instabilities, if the dissipation during the periods of weak, highly-variable flows was not significant.

Continental shelf waves have been observed with periods of 0 (10 days) on other shelves. Niiler and Mysak's (1971) model of continental shelf waves in the presence of a strong boundary current was used to predict the possible frequency of shelf waves on the Labrador shelf. Their model indicates that only stable, neutral waves could exist which would propagate southward with periods of the 0 (24-60 days); which is longer than what could have been observed by a record only one month long.

In addition to the low-frequency variability, there were fluctuations at the diurnal and semi-diurnal tidal periods and at the inertial period (14.4 hrs). The currents associated with these motions were low (1-6 cm/s). The tidal currents were in general agreement with Godin's (1965) numerical model of the M_2 and K_1 tides of Baffin Bay and the Labrador Sea.

Ocean currents continue to prove to be variable. Here the variability characteristic of the offshore branch of the Labrador Current and the deep flow of the NWAB water during March 1976 has been investigated to determine the physical processes behind the fluctuations observed. That variability is important in interpreting oceanographic data that is dependent on the Labrador Current and the NWAB water flow.

CHAPTER 5 - CONCLUSIONS

The data collected in winter 1976 has revealed several important features concerning the Labrador Current system. These include the following:

a. The current meters and hydrographic sections indicated a southward flow at the offshore edge of the Labrador Current of Labrador Sea Water and Atlantic Water remnants which was higher than the previous estimates based solely on geostrophic sections. The transports contained considerable variability at periods of a few days. Further offshore, a rather persistent northward surface flow was found.

b. Bottom-trapped topographic Rossby waves produced pronounced cross-slope motions between four and eight day periods in the bottom flow. Large fluctuations in the temperature field were associated with these motions.

c. At slightly longer periods (8-10 days), the topographic Rossby waves extended throughout the entire water column. There was sufficient motion at the surface associated with the weakly bottom-trapped topographic Rossby waves to have positively interacted with the baroclinic surface currents. This interaction produced the major fluctuations in the currents. This resulted in periods of strong, steady flow interspersed with periods of weak, highly variable flow which often contained complete reversals in direction, which propagated offshore with the 8-10 day topographic Rossby waves.

d. Also present in the bottom flow were alongslope variations in velocity at 2-3 day periods. Baroclinic instabilities might have been occurring during the periods of strong, steady flow generated by the 8-10 day topographic Rossby waves.

The existence of such large amplitude variability is important to our understanding of the system because it (1) is central to the dynamics, (2) may determine the extent of mixing, and (3) will produce the extremes. Historically, physical oceanographers have been concerned with the determination of the water mass budgets. With the realization of the importance of the time-dependent motions in the oceanic systems, the emphasis has shifted to determining the dynamics of the system. Thus, the formulation of an accurate model of the Labrador Sea system will depend on a full understanding of the dynamics of the system. On the Labrador Slope, the most energetic motions were associated with the topographic Rossby waves and the permanent boundary currents, and therefore their relationships constitute an important portion of the dynamics of the Labrador Current and Sea.

The supply of nutrients to the shelf and mixing and exchange of waters along the offshore edge of the Labrador Current are critical parameters needed to model the biology of the Labrador shelf and slope. The role that large, short-term fluctuations in the Labrador Current play in determining the mechanisms by which water, heat, salt, nutrients, momentum and plankton are mixed and exchanged along the Labrador shelf and slope

are yet unresolved. But surely, the shear associated with these large amplitude current variations will have some affect on the mixing and exchange mechanisms.

That the amplitude of the fluctuations can exceed the mean currents indicates that the synoptic current regime is largely determined by the low-frequency variability. Thus, short-term, local prognostic models of currents sea ice drift or iceberg trajectories will require a knowledge of the synoptic current regime. The presence of large short-term fluctuations in the currents will also tend to mask any long-period variations (e.g. seasonal, year-to-year, multi-year) that might exist in the permanent currents. It has been shown here that the calculated volume transport through a section varies widely on the same time scale as the short-term current fluctuations and are also dependent on the scheme used to calculate the transport. Therefore, only long-term (months to years) continuously recording current meters will be able to provide the measurements on the temporal variability that is needed to separate the long-term variations in flow from the short-term fluctuations in currents; and the use of lone hydrographic sections for establishing flows should be used with caution. The presence of extreme values rather than mean values are important to other processes; e.g., the sensitivity and response of plankton and fish to rapid temperature fluctuations and synoptic current variations; the loading on offshore structures by peak currents; and the role of strong bottom currents in sediment transportation and distribution.

The design of the Bedford Institute's 1977-78 current meter was based largely on the results from the March, 1976 array. The spacing between moorings and current meters was chosen to resolve the low-frequency variability. The 1977-78 array was extended inshore and included moorings in the alongshore direction in order to measure the spatial variation over the shelf and slope of the low-frequency variability. A mooring was placed on the lower continental slope to check for the presence of a northward flow offshore similar to that observed in March, 1976. Current meters were also added to the moorings at 1000 m depth to obtain direct measurements in the mid-depth minimum velocity zone. Other physical oceanographic studies are continuing on the Labrador Current. These and future studies, whether primarily interested in higher frequency motions or longer period variations in the current must also adequately measure the energetic low-frequency variability in order to properly interpret their results, for it has been shown here that the low-frequency variability is an important and integral part of the dynamics of the Labrador Current.

REFERENCES

Allen, A.A. and D.A. Huntley (1977) Currents at the Offshore Edge of the Labrador Current. Proc. POAC 77, Memorial Univ. of Newfoundland, 11 pp.

Bayley, G.V. and J.M. Hammersly (1946) The "Effective Number of Independent Observations" in an Autocorrelated Series. J. Roy. Stat. Soc., Lond. 8(1-B), 184-197.

Bennett, A.S. (1976) Conversion of In Situ Measurements of Conductivity to Salinity. Deep-Sea Res. 23, p. 157-165.

Bialek, E.L. (1966) Handbook of Oceanographic Tables. U.S. Naval Oceanographic Office, Washington, D.C. SP-68, 427 pp.

Blackman, R.B. and J.W. Tukey (1958) The Measurement of Power Spectra. Dover, New York.

Bolin, B. (1953) The Adjustment of a Non-Balanced Velocity Field Towards Geostrophic Equilibrium in a Stratified Fluid. Tellus, 5(3) 273-285.

Cahn, A. (1945) An Investigation of the Free Oscillations in a Simple Current System. J. Meteorol., 2(2), 113-119.

Campbell, N.J. (1958) The Oceanography of Hudson Strait. F.R.B. Man. Rept. Ser. No. 12, 60 pp.

Clarke, R.A. and R.F. Reiniger (1973) The Gulf Stream at 49°30'W. Deep-Sea Res. 20, 627-641.

Defant, A. (1961) Physical Oceanography. Oxford, New York, Pergamon Press.

Dinsmore, R.P. and M.J. Moyniham (1972) On the Interchange of Labrador Sea and North Atlantic Ocean Waters, ICES Symposium on "Physical Variability in the North Atlantic", Dublin, 1969. p. 206-212.

Dobson, D. and F. Jordon (1978) The Labrador Sea - A Bibliography of Physical Oceanography, Bedford Institute Data Series D-78-5, 1-25.

Dobson, F., E.F. Brown, and D.R. Chang (1974) A set of programs for analysis of time series data including fast Fourier transform spectral analysis. Rept. BI-C-74-2 Bedford Institute.

Dohler, G. (1964) Tides in Canadian Waters, Can. Hydrogr. Ser. Dept. of Mines and Tech. Surveys (now Dept. of the Environment), Ottawa, 14 pp.

Doodson, A.T. and H.D. Warburg (1941) Admiralty Manual of Tides, Hydrographic Dept., Admiralty, London. p. 181.

Dunbar, M.J. (1951) Eastern Arctic Waters. F.R.B. Canada. Bull. 88, 131 pp.

Fofonoff, N.P. and C. Froese (1958) Program for Oceanographic Computations and Data Processing on the Electronic Digital Computer ALWAC III-E. PSW-1 Programs for Properties of Sea Water. P.O.G. Manuscript Report Series, No. 27, 41 p.

Fofonoff, N.P. and S. Tabata (1958) Program for Oceanographic Computations and Data Processing on the Electronic Digital Computer ALWAC III-E. DP-1 Oceanographic Station Data Program. P.O.G. Manuscript Report Series, No. 25, 40 p.

Godin, G. (1966) Tides, Labrador Sea, Davis Strait and Baffin Bay. Marine Science Branch. MRS. No. 2, 156 pp.

Grant, A.B. (1968) Atlas of Oceanographic Sections. North Atlantic Ocean, Atlantic Oceanographic Lab., Bedford Institute, Rep. B.I. 68-5.

Gould, W.S. and E. Sambuco (1975) The Effects of Mooring Type on Measured Values of Ocean Currents. Deep-Sea Res. 22, 55-62.

Hamon, B.V. (1966) Continental Shelf Waves and the Effects of Atmospheric Pressure and Wind Stress on Sea Level. J. Geophys. Res. 71(12), 2883-2893.

Hendry, R.M. and A.J. Hartling (1979) A Pressure-Induced Direction Error in Nickel-Coated Aanderaa Current Meters. Deep-Sea Res. 26, 327-335.

Jenkins, G.M. and D.G. Watts (1969) Spectral Analysis and its Applications. Holden-Day, San Francisco 1-525.

Kollmeyer, R.C., D.A. McGill, and N. Corwin (1967) Oceanography of the Labrador Sea in the Vicinity of Hudson Strait in 1965. Bull. U.S. Cst. Guard, 19, 1-34.

Kudlo, B.P., (1973) Water Circulation in the ICNAF Area in 1971-1972. ICNAF Res. Doc. 73/42.

Lazier, J.R.N. (1973) The Renewal of Labrador Sea Water. Deep-Sea Res. 20, 341-353.

LeBlond, P.H. and L.A. Mysak (1978) Waves in the Ocean. Elsevier.

Lee, A. and D. Ellett (1965) On the Contribution of Overflow Water from the Norwegian Sea to the Hydrographic Structure of the North Atlantic Ocean. Deep-Sea Res. 12, 129-142.

Lee, A. and D. Ellett (1967) On the Water Masses of the Northwest Atlantic Ocean. Deep-Sea Res., 14, 183-190.

Longuet-Higgins, M.S. (1964) On Group Velocity and Energy Flux in Planetary Wave Motions. Deep-Sea Res. 11, 35-42.

Matthews, D.J. (1939) Tables of the Velocity of Sound in Pure Water and Sea Water for Use in Echo-Sounding and Sound-Ranging. Hydrographic Dept. London. 52 pp.

Mooers, C. and R.L. Smith (1968) Continental Shelf Waves off Oregon. J. Geophys. Res. 73, 340-357.

Moyniham, M.J. and M.S. Anderson (1971) Oceanography of the Grand Banks Region and the Labrador Sea - April-June, August, and October, 1969. U.S. Cst. Guard Rep. No. 48 CG 378-48, 1-259 pp.

Mysak, L.A. (1967) On the Very Low Frequency Spectrum of the Sea Level on a Continental Shelf. J. Geophys. Res. 72(12) 3043-3047.

Mysak, L.A. (1969) Low-Frequency Sea Level Behavior and Continental Shelf Waves Off North Carolina. J. Geophys. Res. 74(6) 1397-1405.

Mysak, L.A. (1977) On the Stability of the California Undercurrent Off Vancouver Island. J. Phys. Ocean. 7, 904-917.

Mysak, L.A. and F. Schott (1977) Evidence for Baroclinic Instability of the Norwegian Current. J. Geophys. Res. 82, 2087-2095.

Neumann, G. and W.J. Pierson, Jr. (1966) Principles of Physical Oceanography. Prentice-Hall, Englewood Cliffs.

Niiler, P.P. and L.A. Mysak (1971) Barotropic Waves Along an Eastern Continental Shelf. Geophys. Fluid Dynamics 2, 273-288.

NOIC (1975) Models RCM-4 and RCM-5. Aanderaa Recording Current Meters. National Oceanographic Instrumentation Center, Instrument Fact Sheet, No. 75002, 12 pp.

Orlanski, I. and M.D. Cox (1973) Baroclinic Instability in Ocean Currents. Geophys. Fluid Dyn. 4, 297-332.

Panicker, N.N., S. Schultz, and D. Schmidt (1974) Analysis of Surface Mooring Dynamics. Proc. of sixth Annual Offshore Technology Conf. Houston, Texas.

Panofsky, H.A. and G.R. Brier (1968) Some Applications of Statistics to Meteorology. Pennsylvania State Univ. 224 pp.

Pedlosky, J. (1964) The Stability of Currents in the Atmosphere and the Ocean. Part 1. J. Atmos. Sci. 21, 201-219.

Pedlosky, J. (1974) Longshore Currents, Upwelling and Bottom Topography. J. Phys. Oceanogr. 4, 214-226.

Pedlosky, P. (1976) Finite-Amplitude Barcclinic Disturbances in Downstream Varying Currents. J. Phys. Oceanogr. 6, 335-344.

Pond, S. and G.L. Pickard (1978) Introductory Dynamic Oceanography. Pergamon of Canada, Ltd. 241 pp.

Rhines, P. (1969) Flow Oscillations in an Ocean of Varying Depth - I. Abrupt Topography. J. Fluid Mech., 37(1), 161-189.

Rhines, P. (1970) Edge-, Bottom-, and Rossby Waves in a Rotating Stratified Fluid. Geophysical Fluid Dynamics, il, 273-302.

Rhines, P. (1971) A Note on Long-Period Motions at Site D. Deep-Sea Res. 18, 21-26.

Robinson, A.R. (1964) Continental Shelf Waves and the Response of Sea Level to Weather Systems. J. Geophys. Res. 69(2) 367-368.

Rossby, C.G. (1937) On the Mutual Adjustment of Pressure and Velocity Distributions in Certain Simple Current Systems. J. Mar. Res 1(1), 15-28.

Rossby, C.G. (1938) On the Mutual Adjustment of Pressure and Velocity Distribution in Certain Simple Current Systems, II. J. Mar. Res., 1(3), 239-263.

Saunders, P.M. (1976) Near-Surface Current Measurements, Deep-Sea Res. 23, 249-257.

Smith, E.H., F.M. Soule, and O. Mosby (1937) The Marion and General Greene Expeditions to Davis Strait and Labrador Sea. Bull. U.S. Cst. Guard, 19, 1-259.

Smith, P.C. (1976) Baroclinic Instability in the Denmark Strait Overflow. J. Physical Oceanography 6(3), 355-371.

Smith, P.C., T.R. Foote, and R. Boyce (1978) In Situ Calibrations of Temperature and Salinity for the Aanderaa RCM-5 Current Meter Bedford Inst. Report Ser. BI-R-78.

Stern, M.E. (1975) Ocean Circulation Physics. Academic Press, New York, 246 pp.

Sverdrup, H.U., M.W. Johnson, and R.H. Fleming (1946) The Oceans, Their Physics, Chemistry, and General Biology. Prentice-Hall, Englewood Cliffs.

Swallow, J.C. and L.V. Worthington (1969) Deep Currents in the Labrador Sea. Deep-Sea Res., 16, 77-84.

Thompson, R. (1971) Topographic Rossby Waves at a Site North of the Gulf Stream. Deep-Sea Res., 18, 1-19.

Thompson, R. and J.R. Luyten (1976) Evidence for Bottom-Trapped Topographic Rossby Waves from Single Moorings. Deep-Sea Res., 23, 629-635.

Treshinikov, A.F. and G.I. Baranov (1977). The Structure of the Circulation and Budget Dynamics of the Waters of the North Polar Region. Polar Oceans, ed. M.J. Dunbar, p. 33-44.

Veronis, G. (1956) Partition of Energy Between Geostrophic and Non-Geostrophic Oceanic Motions. Deep-Sea Res. 3, 157-177.

Veronis, G. (1973) Large-Scale Ocean Circulation Adv. Applied Mechanics, 13, 1-93.

Warren, B.A. and G.H. Volkmann (1968) Measurement of Volume Transport of the Gulf Stream South of New England. J. Mar. Res. 26(2), 110-126.

Webster, F. (1968) Observation of Inertial-Period Motions in the Deep Sea. Rev. of Geophysics 6(4), 473-490.

Worthington, L.V. (1976) On the North Atlantic Circuation. The John Hopkins University Press, p. 1-110.

Worthington, L.V. and W.G. Metcalf (1961) The Relationship Between Potential Temperature and Salinity in Deep Atlantic Water. Rapp. P-V Reun. Cons. Perm. Int. Explor. Mer., 149, 122-128.

Worthington, L.V. and W.R. Wright (1970) North Atlantic Ocean Atlas of Potential Temperature and Salinity in the Deep Water Including Temperature, Salinity, and Oxygen Profiles from the Erika Dan Cruise of 1962. Woods Hole Oceanographic Institution Atlas Series, 2, 58 plates.